7-DEHYDROCHOLESTEROL ENCAPSULATED NANOPARTICLES TO ENHANCE RADIOTHERAPY

by

IAN MICHAEL DELAHUNTY

(Under the Direction of Jin Xie)

ABSTRACT

Radiation therapy remains a mainstay treatment modality for cancer, but its dose and efficacy are limited by normal tissue toxicity. Pro-drugs that can be selectively activated under radiation to enhance radiotherapy are desirable. Even more desirable is the ability to deliver these pro-drugs directly to the site of disease. Upon delivery, the ideal drug would become activated, thus only enhancing radiation therapy in the desired tissues, and potentially eliminating off-target effects and normal tissue toxicity. Herein, we investigate the potential of 7-dehydrocholesterol (7-DHC), a cholesterol analog and precursor, as a pro-drug for radiosensitization. 7-DHC is highly susceptible to radical oxidization, and has the highest propagation rate for free radical chain oxidation among known lipid molecules. As reviewed in chapter 1, 7-DHC can react with free radicals generated during radiation, undergoing autoxidation and catalyzing the oxidation of other biomolecules, in turn amplifying radiation-induced cell damage. Chapter 2 describes, in length, *in vitro* studies with CT26 cells confirming this postulation, finding significantly elevated oxidative stress, lipid peroxidation, DNA damage, and mitochondrial depolarization in treated cancer cells. This results in increased cancer cell viability drop

and reduced clonogenicity, indicating effective radiosensitization. For efficient delivery, 7-DHC was encapsulated into poly(lactide-co-glycolic)-block-poly(ethylene glycol) nanoparticles or 7-DHC@PLGA NPs. When tested *in vivo*, chapter 3 shows that 7-DHC@PLGA NPs significantly enhanced radiotherapy, resulting in 40% eradication of the tumors after one round of treatment. Importantly, the nanoparticles caused no detectable tissue or hematological toxicities, nor hypercalcemia. Our studies suggest the promise of 7-DHC as an efficient, safe, and activatable radiosensitizer.

INDEX WORDS: radiation therapy, radiosensitizer, Smith Lemli Opitz Syndrome, PLGA, vitamin D, 7-dehydrocholesterol, colon carcinoma

7-DEHYDROCHOLESTEROL ENCAPSULATED NANOPARTICLES TO ENHANCE RADIOTHERAPY

by

IAN MICHAEL DELAHUNTY

BS, Denison University, 2016

A Dissertation Submitted to the Graduate Faculty of The University of Georgia in Partial Fulfillment of the Requirements for the Degree

DOCTOR OF PHILOSOPHY

ATHENS, GEORGIA

2021

7-DEHYDROCHOLESTEROL ENCAPSULATED NANOPARTICLES TO ENHANCE RADIOTHERAPY

by

IAN MICHAEL DELAHUNTY

Major Professor:	Jin Xie
Committee:	Jeffrey Urbauer
	Sergiy Minko

Electronic Version Approved:

Ron Walcott
Dean of the Graduate School
The University of Georgia
May 2021

TABLE OF CONTENTS

Page

LIST OF TABLES

Page

LIST OF FIGURES

Page

CHAPTER 1

INTRODUCTION AND LITERATURE REVIEW: VITAMIN D, OXIDATIVE STRESS, AND IMPLICATIONS IN CANCER THERAPY

Background and biological significance of vitamin D

The biologically active form of vitamin D (VD) is a fat-soluble vitamin obtained in large part from the diet. Traditionally known as simply an essential nutrient, VD has more recently been recognized as a seco-steroidal prohormone produced in the epidermis of the skin by ultraviolet B radiation (UVB, 290–320 nm). Photolysis by UVB radiation produces pre-vitamin D_3, which is then metabolized in the liver and kidney to generate the biologically active form, 25-hydroxyvitamin D, or calcitriol, which binds to the vitamin D receptor (VDR) to enable its diverse physiological functions. In this classic metabolic pathway, VD begins as 7-dehydrocholesterol in the skin, which as previously mentioned, undergoes UVB-induced photolysis to pre-vitamin D_3. In this 2-step reaction, the B ring of 7-dehydrocholesterol becomes opened, followed by rapid isomerization at body temperature. This pre-drug then binds to the vitamin D binding protein (VDBP) and is first delivered to the liver, where it is metabolized by two cytochrome P450 $(CYP)_4$-containing enzymes, vitamin D 25-hydroxylase CYP2R1 and CYP27A1 to calcidiol, which is the major circulating form of VD. Calcidiol is further metabolized in the proximal tubule of the kidney by CYP27B1 to the biologically active form, calcitriol. Once in circulation, calcitriol can be delivered to target tissues where it is known to regulate upwards of 200 genes[1-3] including those involved in renin production in the kidney, insulin production in the pancreas, release of cytokines from lymphocytes, production of

cathelicidin in macrophages, and growth and proliferation of vascular smooth muscle cells and cardiomyocytes.[4]

However, the renal synthesis of calcitriol is tightly regulated by two counter-acting hormones, with up-regulation via parathyroid hormone (PTH) and down-regulation via fibroblast-like growth factor-23 (FGF23).[5, 6] Low serum phosphorus levels stimulate calcitriol synthesis, whereas high serum phosphorus levels inhibit it. Following its synthesis in the kidney, calcitriol binds to VDBP to be transported to target organs. As previously mentioned, this regulation occurs predominantly through the nuclear hormone receptor known as VD receptor (VDR). This receptor is a transcription factor that regulates gene expression that mediates hormone biological activity. Recently, however, VDR has also been found in tissues not involved in maintaining calcium homeostasis and bone health. This presents an interesting conundrum in that VDR's presence in these tissues suggest that VD could be involved in a much wider spectrum of biological processes as I will discuss in future sections of this review. Figure 1.1 depicts the metabolic pathway of VD.

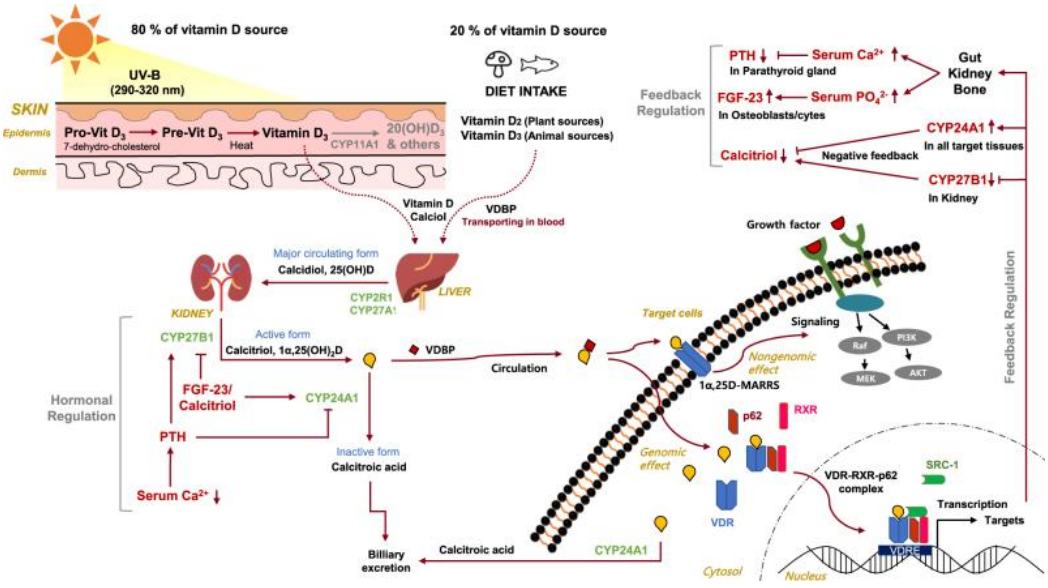

Figure 1.1. Overview of vitamin D metabolism and gene regulation. Reprinted with permission.[7]

As stated, the classical role of vitamin D is to regulate metabolism of calcium and phosphate, which is essential for bone remodeling. However, extensive research over the past decades has suggested that low sunlight exposure and vitamin D deficiency are also associated with the increased risk of many other extra-skeletal diseases such as cancer.[8-13] In fact, this phenomenon was first cited 80 years ago in 1941.[14] Since then, exhaustive research has revealed a much broader picture, extending this hypothesis to over 18 different types of cancer; all studies suggesting a correlation between UVB radiation exposure, serum vitamin D levels, and cancer incidence.[15] It is even more interesting to note that VDR is widely distributed among tumor cells, further adding to this aforementioned hypothesis. Such tumors include those of colon, prostate, breast, and ovarian, among others. The presence of VDR indicates a potential role of calcitriol in the regulation of tumor growth. This has been very well studied over the years, and there are predominantly five mechanisms by which calcitriol appears to regulate tumorigenesis: (1) inhibition of tumor cell growth;[16, 17] (2) inhibition of angiogenesis;[18-21] (3) triggering apoptosis;[22] (4) enhancing "traditional" anti-cancer agents;[23] (i.e. chemotherapeutics, external beam radiation, etc.) (5) anti-inflammatory effects.[24]

Due to this overwhelming evidence suggesting the role of vitamin D in tumorigenesis regulation, numerous studies have investigated using calcitriol as a cancer therapeutic. However, because of calcitriol's part in serum calcium regulation, severe hypercalcemia has, to this point, limited its clinical therapeutic applications. Hypercalcemia, to a large extent inevitably leads to calcification of soft tissues such as the intestines, kidney, and heart, leading to organ failure and in some cases, death. In addition, it has also been shown that some tumors employ several mechanisms that reduce cellular calcitriol levels, as well as diminish its function to protect themselves from the antitumorigenic effects of vitamin D.[25, 26] Furthermore, although tumor cells

express VDR, studies comparing VDR expression levels in normal, benign, and malignant tissues of skin, breast, ovary, and prostate revealed a negative correlation between VDR expression and tumor malignancy.[27-32] In addition to diminished VDR expression in certain tumors, the enzyme CYP24A1, which degrades calcitriol has been found to be upregulated in various malignancies. Consistently, research has found that CYP24A1 expression is correlated with advanced stages of colon, prostate, breast, and lung cancers, inducing resistance to vitamin D-based therapy.[30, 33-36]

Given the upside that there seems to be a therapeutic benefit of utilizing vitamin D, and the downside that tumors have evolutionarily developed methods to block its therapeutic pathways, the development of more creative and innovative ways to exploit vitamin D cannot be understated. In this review, I seek to explore the effects of vitamin D, its analogues and its precursors on disease progression and therapy. In particular, I focus on pulmonary fibrosis, cancer associated fibroblasts within the tumor microenvironment, and cancer in general, with the aim of unraveling the role these drugs, in particular 7-dehydrocholesterol, play in cellular oxidative stress and tumorigenesis.

Role of vitamin D and its analogues in disease progression

Pulmonary Fibrosis

Pulmonary fibrosis describes a progressive and irreversible lung disease, with a mean life expectancy of only 3-5 years. This disease is a result of a dysregulated wound healing response caused by lung injury and infection.[37] Chronic exposure to injury factors such as radiation leads to this dysregulated wound healing response, as well as overlapping inflammation. This disease is characterized by 4 distinct stages: a clotting and coagulation phase, an inflammatory phase, a

fibroblast migration/proliferation/activation phase, and a tissue remodeling and resolution phase. Figure 1.2 outlines this process, as well as therapeutic modalities and drugs that have been utilized in the past to treat idiopathic pulmonary fibrosis (IPF) at the various stages of progression. It is worth mentioning that two drugs, Pirfenidone and Nintedanib, were approved by the FDA in 2014 to treat IPF. Despite their approval however, these drugs were *not* recommended to be given to patients due to problems with accurate diagnoses and high mortality rates.

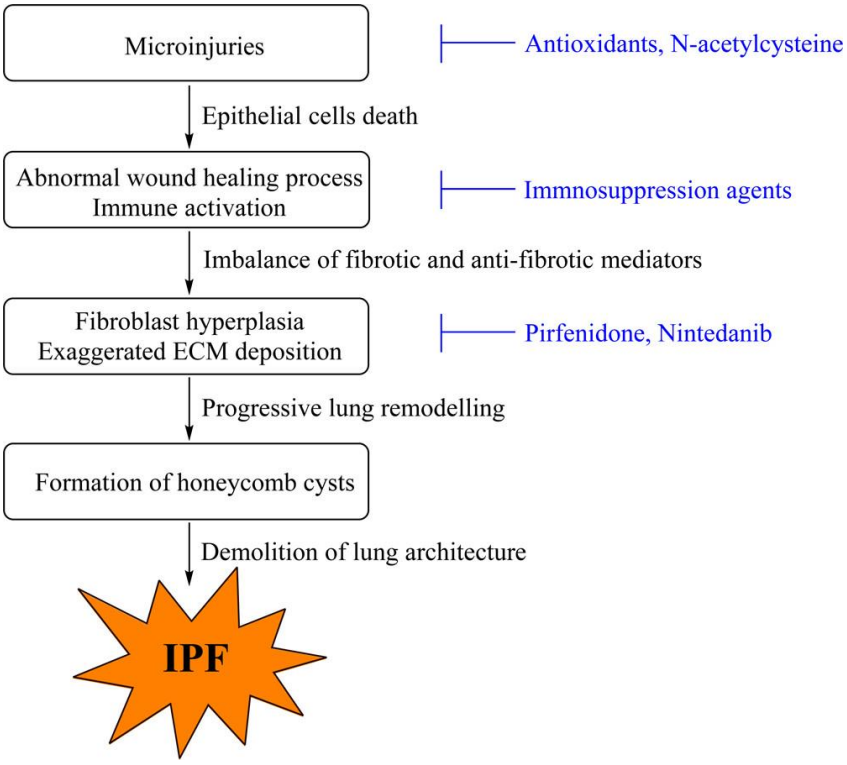

Figure 1.2: Pathogenesis of pulmonary fibrosis.[38] Reprinted with permission from Liu, Y.-M. et al. Journal of Medicinal Chemistry 2017, 60 (2), 527-553. Copyright (2021) American Chemical Society.

As stated earlier in this review, vitamin D has long been regarded as a key player in calcium homeostasis, bone health, electrolyte and blood pressure regulation and immune response. In addition, vast amounts of research have also demonstrated vitamin D's role in the

treatment of fibrosis. For instance, in the first stage of fibrosis as epithelial cells are stimulated by injury factors such as external beam radiation, they release inflammatory mediators. These mediators in turn activate an antifibrinolytic coagulation cascade. The primary mediator of this cascade is a complex called TF/FVIIa which is comprised of tissue factor (TF) and activated factor VIIa (FVIIa). It is worth mentioning that this signaling cascade is also implicated with the proliferation and migration of colon cancer.[39, 40] With this in mind, much research has been done to explore the effects of vitamin D on this first stage of fibrosis. Indeed, Martinez-Moreno and colleagues discovered that the addition of vitamin D blunted the tumor necrosis factor-α (TNF-α)-induced TF expression and activity in aortic VSMC cells,[41] showing that vitamin D can exert anticoagulant properties, and it does so in two predominant ways: suppressing TF expression by TNF-α, and the activation of a protease inhibitor, TFPI.

The next phase of wound healing is inflammation: the injured epithelial or endothelial cells release excessive inflammatory mediators such as macrophages. These macrophages can release cytokines IL-13 and IL-1, as well as large amounts of growth factors such as active transforming growth factor β (TGF-β), platelet-derived growth factor (PDGF), fibroblast growth factor (FGF) and TNF-α, which promote the inflammatory response and fibrosis.[38] Similar to the first stage described above, vitamin D has been shown to be an effective agent against the inflammation stage as well. Prior research has demonstrated that vitamin D can cause a decrease in inflammatory cytokine levels such as IL-13, -17, -1, -6, and -8, as well as TNF-α. Further, it has been shown to directly act upon $CD4^+$ T-cells to promote an IL-10-secreting T-reg population.[42-45]

The final major phase prior to the onset of fibrosis occurs where fibroblast hyperplasia and exaggerated ECM deposition is initiated. Upon injury, the release of inflammatory mediators

by the epithelial cells in steps 1 and 2 start the antifibrinolytic-coagulation cascade that triggers clotting and creates an interim extracellular matrix (ECM). This ECM triggers the next phase, where myofibroblasts are converted via the epithelial-mesenchymal transition (EMT), which is activated by TGF-β that was released from macrophage cells, as well as induced by proinflammatory cytokines in prior steps.[46] TGF-β then attaches to cell surface serine/threonine receptor kinases leading to phosphorylation of SMAD2 and SMAD3.[47, 48] In this regard, it has long been postulated that TGF-β is one of the key drivers of fibrosis,[49, 50] and therefore a main target of vitamin D. In parallel, the activation of renin-angiotensin system (RAS) has been shown to induce lung fibrosis.[51-53]

Studies have revealed that Vitamin D can both downregulate the RAS systems,[54] as well as inhibit the TGF-β-SMAD signaling pathway.[55] In this latter process, vitamin D binds a complex with VDR, then the complex directly interacts with SMAD3, resulting in decreased binding of SMAD3 to DNA, finally culminating in the inhibition of the TGF-β-SMAD signal transduction.[56] In this study, investigators reported that paricalcitol, a synthetic VDR ligand, inhibited fibrogenesis induced by SMAD3 transcriptional gene activation via the binding of VDR to phosphorylated SMAD3. This in turn reduced the propensity of TGF-β to release collagen and inhibited the differentiation of myofibroblasts.[57] While all of the various mechanisms of VDR-SMAD are thoroughly understood, all studies up to this point ultimately lead to an identical final result: vitamin D down-regulates TGF-β-induced nuclear SMAD3 transcriptional activity, consequently blunting TGF-β signaling, thus reducing the onset of fibrosis.

Fibroblast Targeting

Cancer associated fibroblasts (CAFs) are a cell type within the tumor microenvironment (TME) that promotes tumorigenic features by initiating the remodeling of the extracellular matrix or by secreting cytokines. Traditionally thought of as quiescent bystanders in the TME, recent evidence has shown that as neoplasia proceeds, fibroblasts engage in cross-talk with adjacent cancer cells to foster their growth and transformation as activated fibroblasts, non-transformed but pro-tumorigenic cells. The step that allows normal fibroblasts to acquire a CAF phenotype is the trans-differentiation to neoplastic-myofibroblasts.[58] Put simply, CAFs are cells that are negative for epithelial, endothelial and leukocyte markers with an elongated morphology and lacking the mutations found within cancer cells.[59]

Due to the evidence described earlier regarding vitamin D's ability to interact with the TGF-β-SMAD signal transduction pathway and inhibit fibrosis in non-neoplastic myofibroblasts, it is postulated that a similar mechanism is employed when utilizing vitamin D to target the neoplastic phenotype, i.e. CAFs. Indeed, a study by Ferrer-Mayorga, *et al*. revealed that an increased expression of VDR within primary colorectal tumors expressing fibroblast markers (vimentin and α-smooth muscle actin, α-SMA), and not expressing epithelial proteins (cytokeratin-18 and E-cadherin), led to increased overall patient survival.[60] The association of VDR on longer overall survival prompted these researchers to examine the action of calcitriol on the tumors. They found that, through global gene expression analysis, several chemokines and ECM proteins with immune cell chemoattractant potential are among calcitriol's target genes in CAFs.

In another hallmark study, Shermann and colleagues showed that calcitriol, previously shown to induce quiescence in pancreatic stellate cells, the precursors of pancreatic

myofibroblasts, reprograms the stromal phenotype to one that is not inflammatory and quiescent.[61] These two findings help add to the body of evidence, as well as the hypothesis that vitamin D can in addition to the non-neoplastic myofibroblasts, act on neoplastic fibroblasts and increase survival in certain cancer types.

Cancer

While we've seen that vitamin D can aid in the therapy of fibrosis as well as promote the transition of CAFs back to their quiescent state via its interactions with the VDR, it is also worth exploring the other numerous anticancer properties of vitamin D. The inhibiting effects of vitamin D on tumor cell growth were first described by Colston *et al.* in 1981 who showed for the first time a dose-dependent decrease of cell proliferation in melanoma cells treated with calcitriol.[62] The growth inhibiting activity of this molecule was subsequently observed in other tumor cell lines including breast, prostate, and colon cancer cells.[63] Since then, the mechanisms of this inhibition have been extensively studied. Unsurprisingly, as seen with fibrosis and CAFs, vitamin D seems to act upon TGF-β to illicit its anti-tumoral properties. TGF-β is a member of a superfamily of growth factors which is implicated in the regulation of several important biological processes such as cell proliferation, differentiation, motility, adhesion, organization, and programmed cell death. TGF-β inhibits cell proliferation by regulating cell cycle progression and inducing apoptosis.[64] It is further is known to inhibit the proliferation of normal epithelial cells and the early steps of carcinogenesis while it fosters the later steps of cancer progression, e.g., cell motility, invasion, and metastasis.[65] Experimental data over the years have found that, according to the cell type, vitamin D may increase the expression levels of TGF-β and that of its receptors, or its secretion.[66-70] Yang *et al.* found that even short term exposures of less than 12 h

to calcitriol results in an increased expression of TGF-β and/or TGF-β receptors in breast cancer cells.[71] In all these studies, increased levels of TGF-β have all led to decreased cancer cell proliferation. In addition, it has even been suggested that vitamin D can regulate the entire process of tumorigenesis, from initiation and cell differentiation, to metastasis and cell microenvironment interactions.[72] Some additional key properties of vitamin D that allow it to modulate tumorigenesis include those controlling inflammation, proliferation, and the induction of apoptosis. These three concepts will be highlighted below.

Vitamin D inhibits inflammation

Chronic inflammation is a prolonged inflammatory response resulting in progressive destruction and regeneration of tissues by reactive oxygen species (ROS) and cytokines secreted at the site of inflammation. Connections between inflammation and incidence of cancer were first established in the 1800s. Since then, the connections have been well studied, and the mechanisms, either intrinsic or extrinsic, by which inflammation drives tumorigenesis are well established, and outlined in Figure 1.3. It is now well-accepted that chronic inflammation is one of the main contributors to the initiation of tumorigenesis.[73] Regardless of the pathway, the downstream effects appear to remain consistent. Transcription factors such as NFκB, STAT3, and HIF1α become activated in tumor cells, which trigger the production of various chemokines and cytokines within those cells. These cytokines in turn recruit inflammatory cells such as macrophage and myeloid-derived suppressor cells (MDSCs), which create an auto-regulatory feedback loop, culminating in cancer-related inflammation that ultimately

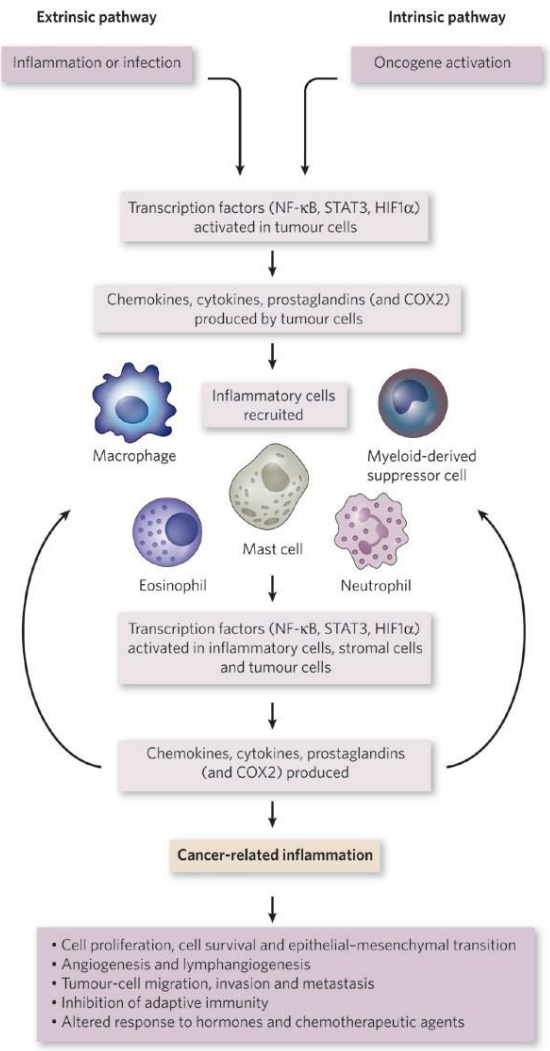

Figure 1.3. Pathways that connect inflammation and cancer.[73] Reprinted with permission from Springer: *Nature*. Mantovani, A., et al. Cancer-related inflammation, 2008.

drives cell proliferation and survival, epithelial-mesenchymal transitions, angiogenesis, and tumor cell migration, invasion and metastasis.

Unsurprisingly, it has been shown that vitamin D can inhibit these inflammatory processes at all of the aforementioned stages: it can inhibit cytokine secretion as well as transcription factor expression and activation. For example, it has been demonstrated that

vitamin D inhibits IL-6, a pro-inflammatory cytokine crucial in colorectal cancer progression. VD does so by inducing the expression of MAPK phosphatase-5 (MKP-5), which prevents the phosphorylation and activation of p38 MAPK.[74] Similarly, vitamin D reduces the production of IL-8, which has been found to be an important angiogenic factor.[75] Additionally, vitamin D can also inhibit the transcription factor NFκB signaling pathway. Vitamin D suppresses the phosphorylation of both AKT and its downstream target I kappa Bα (IκBα) in macrophages through upregulation of thioesterase superfamily member 4 (THEM4), an AKT modulator protein leading to the inhibition of NFκB and COX-2 expression.[76] Another transcription factor, STAT3, which is known to be constitutively active in large granular lymphocyte leukemia was shown by Olson, K.C., *et al*. to be inhibited by vitamin D.[77]

Taking these data as a whole, we can see that vitamin D can inhibit inflammation leading to tumorigenesis through two main mechanisms: Transcription factor and cytokine inhibition. It is important to note that this is not an exhaustive list, and for further mechanisms, readers should be directed to additional reviews on this topic.[78, 79] Transcription factors such as STAT3 and NFκB become activated in tumor cells, and thus secrete cytokines such as IL-6 and -8 in order to recruit immune inflammatory cells. Inhibiting these two crucial steps stops the feedback loop responsible for recruiting the inflammatory cells, and can thus modulate the onset and progression of tumorigenesis in this manner.

Vitamin D inhibits tumor cell proliferation

As is becoming evident, vitamin D has pleiotropic effects that go beyond its traditional role in calcium homeostasis.[80] Underlying many of the noncalcemic actions of vitamin D, including effects on carcinogenesis is the ability of vitamin D secosteroids to inhibit cellular

proliferation.[81-88] Hundreds of genes with vitamin D receptor response elements (VDREs) either directly or indirectly influence the cell cycle and proliferation, as well as differentiation. Further, vitamin D can also affect cell function in a non-genomic manner such as to influence pathological cell growth and carcinogenesis, among others.[89-91]

Genomically however, the anti-proliferative properties of vitamin D are mediated by several mechanisms including the regulation of growth factors, cell cycle, and several other well-cited signaling pathways. For example, vitamin D increases the expression of insulin-like growth factor (IGF)-binding protein 3 and the cyclin-dependent kinase (CDK) inhibitors, p21 and p27. Doing so downregulates the expression of CDK2, leading to inhibition of cell proliferation and cell cycle progression.[92] In addition, calcitriol inhibits the Wnt/β-catenin signaling pathway,[93, 94] as well as activating transcription factors forkhead box O3/4 (FoxO3/4),[95] all inducing either cell cycle arrest, or otherwise inhibiting downstream cell proliferation.

In an effort to narrow down its vast array of antiproliferative properties, I will be focusing on two very specific, and often overlooked, mechanisms by which vitamin D, specifically calcitriol, inhibits tumor cell proliferation: induction of cystatin D and modulation of matrix metalloproteases. In a hallmark study, Álvarez-Díaz and coworkers, through a transcriptomic analysis on SW480-ADH colon cancer cells, discovered that cystatin D was a candidate calcitriol target gene.[96] Cystatin D is an inhibitor of several cysteine proteases of the cathepsin family. However, its inhibitory profile is only linked to cathepsin S, H and L, but not B. In their work, they subsequently discovered that by upregulating cystatin D in the presence of vitamin D, colon cancer cells showed decreased proliferation, migration and invasiveness, as well as increased differentiation and apoptosis. Figure 1.4 illustrates the mechanism by which calcitriol induces cystatin D expression and the resulting effects on cell proliferation.

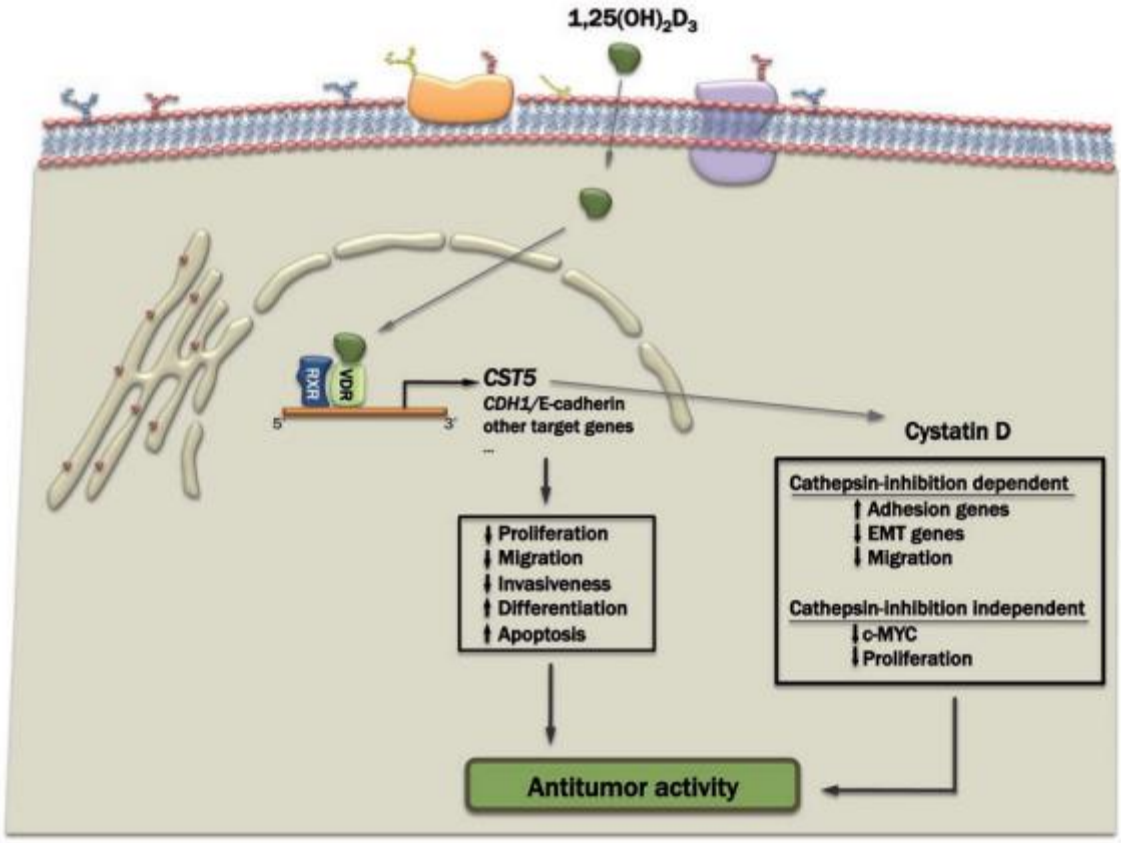

Figure 1.4. Calcitriol promotes the transcription of CST5 gene, leading to the expression of Cystatin D and various antitumor properties. Reprinted with permission.[96]

In addition to inhibiting cell proliferation through the upregulation of cystatin D, vitamin D has also been shown to act upon matrix metalloproteases (MMPs). MMPs are a family of zinc-dependent proteases capable of degrading components of the ECM, and are tightly regulated by tissue inhibitors of metalloproteases (TIMPs). Frequently, both TIMPs and MMPs are disrupted in cancer, thus promoting cancer cell migration. Over the years, numerous studies have shown that vitamin D plays a vital role in the regulation of both MMPs and TIMPs.[97] Koli and

coworkers showed that in breast cancer cells, MMP-9 and TIMP-1 expression are decreased in the presence of vitamin D, thus inhibiting proliferation in those cells.[98] Bao *et al*. showed a similar mechanism in prostate cancer cells.[99]

Vitamin D induces apoptosis

As a final step in modulating tumorigenesis, after controlling inflammation and cancer cell proliferation, vitamin D causes the induction of apoptosis. Vitamin D can induce apoptosis in cancer cells through a variety of different mechanisms. Predominantly, VD induces intrinsic, or mitochondrial cell death by downregulating anti-apoptotic proteins Bcl-2 and Bcl-XL, and upregulating pro-apoptotic proteins Bax, Bak, and Bad.[100] This mitochondrial pathway is of upmost importance in Chapter 2, so will thus be the focus of this section.

The Bcl family of proteins play an important role in mitochondrial-induced apoptosis. In general, this family of proteins regulates the release of other proteins from intermembrane space in the mitochondria. Once released, these proteins activate caspase proteases that dismantle cells and signal phagocytosis.[101] Divided into two classes, the Bcl family of proteins can be either anti-apoptotic (Bcl-2 and Bcl-XL) or pro-apoptotic (Bax, Bak, and Bad).[102] In particular, Bcl-2 plays an important role in blocking the release of cytochrome C into the intermembrane space. It turns out, that not only is cytochrome C an essential component of the mitochondrial electron transport chain, it was also identified as one of the three apoptotic protease activating factors (Apafs) for caspase activation.[103] By downregulating Bcl-2, vitamin D in turn triggers the release of cytochrome C. Cytochrome C, once released into the cytosol can interact with oligomerized APAF1, forming the apoptosome. This apoptosome activates a cascade of caspase proteases, the

terminal effector caspase being caspase 3/7. Thus, VD ultimately activates intrinsic cell death via the activation of caspase proteases 3/7.

7-dehydrocholesterol and Smith Lemli Opitz Syndrome

As is evident, vitamin D has implications in a wide range of pathological conditions, with the most prominent being cancer. However, up to this point our discussion has been limited primarily to calcitriol, the biologically active form of vitamin D. What remains to be described are the diverse range of activities that the precursor of vitamin D can have. In this section I will describe the role of one particular precursor, 7-dehydrocholesterol (7-DHC), and its implications in Smith-Lemli-Opitz syndrome. Biologically speaking, 7-DHC is a zoosterol that functions in the serum as a cholesterol precursor, and is photochemically converted to vitamin D3 in the skin, therefore functioning as provitamin-D_3. As will become apparent in future chapters, 7-DHC plays a major role in the remainder of this Dissertation.

Smith-Lemli-Opitz syndrome (SLOS) is a congenital disorder, as well as an autosomal recessive disorder that was first identified in 1964.[104] SLOS is caused by an inborn error in cholesterol metabolism resulting from a deficiency in the enzyme 7-dehydrocholesterol reductase (DHCR7).[105] It is characterized by prenatal and postnatal growth restriction, microcephaly, moderate-to-severe intellectual disabilities, and multiple major and minor physical and internal malformations. The malformations include distinctive facial features, cleft palate, cardiac defects, underdeveloped external genitalia in males, postaxial polydactyly, and 2-3 syndactyly of the toes. Due to the malformation of DHCR7, which is responsible for the reduction of 7-DHC to cholesterol, SLOS patients show decreased levels of cholesterol and increased levels of 7-DHC and its isomer 8-dehydrocholesterol (8-DHC, cholesta-5,8(9)-dien-3β-ol) in serum and tissues,

particularly in the cortex and midbrain.[106, 107] The large accumulation of 7-DHC in the brain yields a variety of consequences for SLOS patients. 7-DHC is an excellent H-atom donor, and highly susceptible to free radical oxidation. In fact, 7-DHC has the highest known propagation rate constant towards free radical chain oxidation among lipid molecules (2260 $M^{-1}s^{-1}$, compared to 11 $M^{-1}s^{-1}$ for cholesterol). As a result, 7-DHC can become oxidized, giving rise to a number of metabolites, namely oxysterols.[108-112] These oxysterols can be highly toxic, and the large accumulation in the brain results in the variety of cognitive abnormalities just described.

7-DHC oxidation and oxysterols in SLOS

Oxysterols are 27-carbon derivatives of cholesterol created by enzymatic or radical oxidation.[113] For purposes of this discussion, I will focus only on radical oxidation, and the implications this oxidation has in diseases such as SLOS. The pro-apoptotic effect of oxysterols is primarily connected to overproduction of reactive oxygen species (ROS).[114] Interestingly, it are these ROS that can initially cause the oxidation of 7-DHC to these oxysterols, so it is not surprising that ROS production mediates their apoptotic effects. Oxysterol-induced apoptosis in a variety of malignancies is well cited,[115-126] and is mediated by both intrinsic mitochondrial pathways[115, 127] and an extrinsic death receptor-dependent pathway.[128]

As mentioned above, both cancer and SLOS show high levels of ROS. With these species present, one can postulate that 7-DHC can undergo free radical chain oxidation reactions to yield oxysterols. In fact, Xu, *et al.* has suggested that the mechanism of free radical chain oxidation of 7-DHC involves abstraction of hydrogen atoms at the C-9 and/or C-14 position of the sterol.[129] Extending from this is the fact that a lot of lipids, including 7-DHC and polyunsaturated fatty acids (PUFAs) are prone to undergo reactions with molecular oxygen by free radical

mechanisms known as lipid peroxidation.[130, 131] This concept, mechanism, and reaction end products will be discussed heavily in the next section, as well as for the rest of this dissertation.

Lipid radical propagation and oxidative stress on cellular function, metabolism, and tumorigenesis

As aforementioned, the polyunsaturated fatty acids that comprise the lipid membranes of cells as well as organelles such as the mitochondria are highly susceptible to free radical oxidation in a process known as lipid peroxidation. As such, a body of evidence over the last several years has shown that oxidative stress and resulting lipid peroxidation are involved in various and numerous pathological states including inflammation, atherosclerosis, neurodegenerative diseases, and cancer.[132] Again, for the purposes of this review I will focus only on lipid peroxidation and oxidative stress as it relates to cancer and tumorigenesis. The term "oxidative stress" is frequently used to describe the imbalances in redox couples such as those reduced to oxidized glutathione (GSH/GSSG) or NADPH/NADP+ ratios. These imbalances primarily result from the overproduction of ROS, and are responsible for the alteration of macromolecules.

In cells, ROS are generated naturally as byproducts of cellular metabolism, and include species such as superoxide anion ($O_2^{-\bullet}$), perhydroxyl radical ($HO_2^{\bullet}$), hydroxyl radical ($^{\bullet}OH$), nitric oxide (NO), and other species such as hydrogen peroxide (H_2O_2), singlet oxygen ($^1O_2$), hypochlorous acid (HOCl), and peroxynitrite ($ONOO^-$).[133] Under ordinary circumstances, cells have highly efficient methods of clearing these ROS in order to prevent damage to the cell. For instance, several antioxidant enzymes such as superoxide dismutases MnSOD and Cu/ZnSOD, which are located in the mitochondria and the cytosol, respectively, convert superoxide into

hydrogen peroxide. Catalase can then further decompose hydrogen peroxide into water and molecular oxygen.[134]

However, in cases of severe cellular disruption such as cancer, the normal mechanisms by which cells can protect themselves from ROS damage become aberrant and intracellular ROS levels rise. The relative levels to which this oxidative stress reaches determines the fate of the cell. On one hand, very high levels of ROS and oxidative stress result in cell death. However, lower levels of ROS have been implicated in tumor metastasis which is a complicated processes including epithelial-mesenchymal transition (EMT), migration, invasion of the tumor cells and angiogenesis around the tumor lesion.[135] This complex interplay between cellular oxidative stress and antioxidant defense has, over the years, led to the development of potential therapeutics to selectively raise the ROS and oxidative stress levels in cells beyond a toxic threshold, leading to cell death. These lipid peroxidation byproducts that cause this toxicity will be discussed below.

Implications of lipid peroxidation on cell function and tumorigenesis

Of the many stimuli that can cause an increase in intracellular ROS, ionizing radiation (IR) is by far the most prominent, and is therefore the leading treatment modality for most (~50%) cancers.[136] The mechanism by which IR induces cell damage is two-fold. On one hand, IR can directly interact with the DNA in the nuclei of the cancer cells causing both single and double strand DNA breaks. On the other hand, IR can hydrolyze water inside the cell, leading to the generation of ROS in extracellular environments to generate, primarily, hydroxyl radicals.[137] Figure 1.5 illustrates the effects of IR on cells.

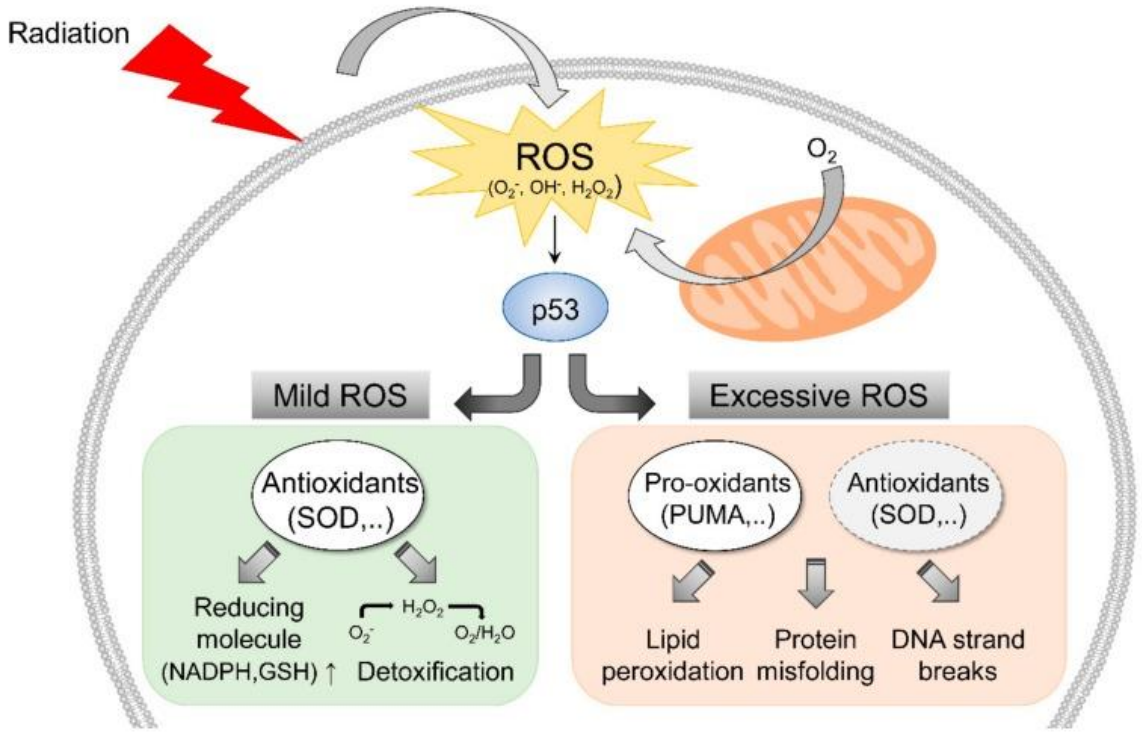

Figure 1.5. Effects of IR on cancer cells via the production of ROS, and activation of the p53 pathway. Reprinted with permission.[138]

When ROS levels are "excessive," many downstream processes occur that ultimately lead to cellular apoptosis. Lipid peroxidation is one such process, and will be the sole focus of this section. In lipid peroxidation, the ROS generated from IR attacks lipids containing carbon-carbon double bond(s), especially polyunsaturated fatty acids (PUFAs) in the cell membrane, as well as membranes of the mitochondria. This process typically involves hydrogen abstraction from a carbon, with oxygen insertion resulting in lipid peroxyl radicals and hydroperoxides.[139] These radicals can then be propagated throughout the membrane, initiating a chain reaction, damaging more lipids, generating more radicals, and so on.

Secondary to these lipid hydroperoxides are a class of aldehyde species that are highly toxic and even mutagenic. Among the many different aldehydes which can be formed during

lipid peroxidation, malondialdehyde (MDA), and 4-hydroxy-2-nonenal (4-HNE) have been extensively studied by Esterbauer and his colleagues in the 1980s.[140-146] MDA appears to be the most mutagenic product of lipid peroxidation, and is an end-product generated by decomposition of arachidonic acid and larger PUFAs.[147] Additionally, MDA is used most often as a convenient biomarker for lipid peroxidation as will be discussed in Chapter 2.

MDA elicits its pH-dependent, mutagenic action by forming adducts with proteins and DNA following its formation. This high reactivity is primarily based on its being highly electrophilic, making it strongly reactive toward basic, nucleophilic amino acids. Initial reactions between MDA and free amino acids generate Schiff-base adducts[147-149] which are referred to as advanced lipid peroxidation end-products (ALEs). MDA adducts can also participate in secondary deleterious reactions by promoting intramolecular or intermolecular protein/DNA crosslinking that can induce profound alterations in proteins and DNA. On this note, it has been shown that MDA can react physiologically with several nucleosides to form adducts to deoxyguanosine and deoxyadenosine, eventually leading to extensive DNA damage.[150, 151] To summarize, lipid peroxidation plays an important role in cell death. Upon the addition of ionizing radiation, ROS are generated and propagated through the lipid membrane, oxidizing many PUFAs and generating lipid hydroperoxides and toxic aldehyde species such as MDA. These end products lead to extensive protein and DNA damage, all culminating in cell death.

On the note of DNA damage, ROS-induced DNA damage can result in base modification, deoxyribose modification, DNA cross-linking, and single and double strand breaks. The most common oxidative DNA lesion is 8-hydroxy-guanine (8OHdG). Numerous studies have shown increased levels of 8OHdG in animal tumor models and various human

cancers.[152, 153] If this damage is not repaired prior to replication, DNA mutation and cell death are likely to occur.

While it may seem obvious that increasing ROS levels in cancer cells will provide a beneficial and efficient therapeutic, it should not come as a surprise that, as with other therapeutic modalities, tumors have developed methods to evade increased oxidative stress. Cancer cells comprising late stage disease for example, have become highly adapted to intrinsic oxidative stress with upregulated antioxidant capacity. This redox adaptation not only enables the cancer cells to survive under increased ROS stress, but also provides a mechanism of resistance to many anticancer agents and radiation therapy described above.[154] This adaptive resistance is primarily mediated through the upregulation and activation of two pro-survival pathways: NE-E2-related factor 2 (Nrf2)[155] and increased glutathione (GSH) levels.[156]

Future Prospective

This review has demonstrated the vast array of biological effects of vitamin D as well as its precursors. In particular, in addition to its classical role in regulation of serum calcium and phosphate levels, vitamin D has been implicated in the regulation of fibrosis through its inhibition of TGF-β, as well as targeting CAFs in colon cancer and reversing the EMT. Interestingly, along the lines of cancer inhibition are the anti-inflammatory and antiproliferative properties of vitamin D as well as its ability to induce apoptosis in certain cancer cells though the downregulation of antiapoptotic genes such as Bcl-2 and Bcl-xl, and the upregulation of proapoptotic genes such as Bax, Bak, and Bad.

Despite all the advances in research into the mechanisms by which vitamin D can inhibit cancer progression, there is not a single, current therapeutic based on vitamin D that is FDA

approved. It is for this reason that I turned my attention, and the focus of this review, to the biological precursor to vitamin D, 7-Dehydrocholesterol. Serving 2 purposes in the body, 7-DHC acts in the serum as the direct precursor to cholesterol via reduction by the DHCR7 enzyme, and in the skin where it is photochemically converted to provitamin-D_3. 7-DHC is distinct from vitamin D, and all other lipids in fact, in that it has the highest radical propagation rate constant known for any lipid. This fact makes 7-DHC incredibly important in several pathological disorders that involve free radical oxidation, especially SLOS, and even cancer.

Given that the biologically active form of vitamin D, calcitriol seems to be an ineffective cancer therapeutic due to the inherent toxicities associated with administering the high doses required, attention should be focused on 7-DHC moving forward. On that note, the question of how we can utilize the high radical propagation rate and the antiproliferative properties of 7-DHC, especially those involved with lipid radical propagation and oxidative stress to create a possible cancer therapeutic still remain.

Overview of the following chapters

The following three chapters will provide an in-depth analysis of the development of a novel nanoparticle platform to increase the efficacy of external beam radiation therapy in colorectal cancer models. In Chapter 2, we aim to take advantage of the high radical propagation rate of 7-DHC, and exploit it to increase oxidative stress within the cell. Due to the inherent hydrophobicity of 7-DHC, encapsulating it inside an FDA-approved polymeric nanoparticle affords facile delivery to cancer cells. We were successful in encapsulating 7-DHC with high efficiency and with a desirable, slow release profile of the drug with minimal leakage at physiological pH. We then show that when this nanoparticle formulation, which on its own is

nontoxic, is presented to tumor cells, the drug is released and naturally accumulates in lipid membranes of both the mitochondria and plasma membranes. Upon exposure to ionizing external beam radiation (IR), we show that compared to IR alone, the particle + IR causes a dramatic increase in ROS levels, increased lipid peroxidation byproducts, extensive DNA damage, and ultimately very efficient cell death via intrinsic mitochondrial apoptosis pathways. This formulation further decreases cell clonogenicity in CT26 cells, thereby solidifying this formulation as a very efficient radiosensitizer *in vitro*. Chapter 3 then utilizes this same nanoplatform *in vivo*, and demonstrates that within 4 h post intravenous injection, and upon exposure to IR, animal tumor volume is hampered, and survival increases dramatically. Serum calcium, as well as tissue and tumor histological analyses confirmed our hypothesis that this formulation is safe, efficient, and causes no significant side effects. Finally, Chapter 4 summarizes future endeavors, as well as describes preliminary work on engineering a synthetic low density lipoprotein (sLDL)-like formulation to not only increase the loading of 7-DHC within the nanoparticle, but also increase its delivery efficacy. sLDL would take advantage of targeting the neurotensin (NT) receptor overexpressed on H1299 non-small cell lung carcinoma cells, thereby bypassing the need for the more passive approach of the enhanced permeability and retention (EPR) effect that is utilized in Chapters 2 and 3.

CHAPTER 2

INCREASING CELLULAR OXIDATIVE STRESS *IN VITRO* AMPLIFIES RADIATION-INDUCED CELL DAMAGE[1]

[1] Ian Delahunty, Wen Jiang, Jianwen Li, Chaebin Lee, Xueyuan Yang, Anil Kumar, Amy Li, Pakteema Tong, Libin Xu, Weizhong Zhang, Jin Xie. A polymeric nanoparticle radiosensitizer based on 7-dehydrocholesterol. To be submitted to *ACS Nano*, 2021.

Abstract

Radiation therapy remains a mainstay treatment modality for cancer, but its dose and efficacy is limited by normal tissue toxicity. Pro-drugs that can be selectively activated under radiation to enhance radiotherapy are desirable. Herein, we investigate the potential of 7-dehydrocholesterol (7-DHC), a cholesterol and vitamin D analog and precursor, as a pro-drug for radiosensitization. 7-DHC is highly susceptible to radical oxidization, and has the highest propagation rate among known lipid molecules for free radical chain oxidation. 7-DHC can react with radicals generated during radiation, undergoing autoxidation and catalyzing the oxidation of other biomolecules, in turn amplifying radiation-induced cell damage. *In vitro* studies with CT26 cells confirmed this postulation, finding significantly elevated oxidative stress, lipid peroxidation, DNA damage, and mitochondrial depolarization in treated cancer cells. For efficient delivery, 7-DHC was encapsulated into poly(lactide-co-glycolic)-*block*-poly(ethylene glycol) nanoparticles (7-DHC@PLGA NPs). Finally, this formulation showed a significant decrease in cell clonogenicity, thereby establishing 7-DHC@PLGA NPs as an efficient radiosensitizer for colorectal cancer *in vitro*.

Introduction

Radiation therapy (RT) remains a mainstream treatment option for cancer, with nearly 50% patients receiving it at least once during the treatment course.[1, 2] Despite technological advances such as stereotactic body radiotherapy, intensity-modulated radiation therapy, and image-guided radiation therapy, the efficacy of RT is limited by normal tissue toxicities.[3,4] To improve cancer management, chemotherapeutic radiosensitizers can be administered during RT,

i.e. chemo-radiotherapy.[5-8] However, chemo-radiotherapy is often associated with higher rates of systemic morbidities, which frequently cause a delay or interruption in either chemotherapy or radiotherapy, leading to worse prognoses.[9] Therefore, there is an unmet clinical need for new radiosensiziting agents that are effective but also more tolerated by patients.

A biosynthetic precursor of cholesterol, 7-dehydrocholesterol (7-DHC) is converted in the serum by 7-dehydrocholesterol reductase (DHCR7) to produce cholesterol, and is photochemically oxidized in the skin to produce previtamin-D_3. 7-DHC is an excellent H-atom donor, and highly susceptible to free radical oxidation. In fact, 7-DHC has the highest known propagation rate constant towards free radical chain oxidation among lipid molecules (2260 $M^{-1}s^{-1}$, compared to 11 $M^{-1}s^{-1}$ for cholesterol).[10-19] DHCR7 dysregulation or dysfunction would cause an accumulation of 7-DHC inside cells, therefore leading to lipid peroxidation. This is observed in patients with Smith-Lemli-Opitz syndrome (SLOS), characterized by a mutation in the DHCR7 gene. SLOS patients suffer from phenotypes such as multiple congenital malformations and mental retardation, which are linked to 7-DHC-induced toxicities to the midbrain and cortex.[11, 20-27]

Herein we explore 7-DHC as a potential radiosensitizing agent, capitalizing on its high propensity to promote free radical chain reactions. 7-DHC structurally resembles cholesterol and, similar to the latter, is enriched in cell lipid layers of the plasma membrane, endoplasmic reticulum, endosomes/lysosomes, and mitochondria.[28-30] We hypothesize that under radiation, 7-DHC is radicalized by either directly interacting with high energy photons or reacting with radiation-induced reactive oxygen species (ROS). The resulting radicals and/or their peroxyl derivatives are expected to rapidly react with adjacent sterols and polyunsaturated fatty acids (PUFAs), propagating free radical chain reactions down the membranes to cause extensive lipid

peroxidation. Moreover, 7-DHC autoxidation produces toxic oxysterols such as 3β,5α-dihydroxycholest-7-en-6-one (DHCEO),[10, 31] whereas PUFA oxidation yields reactive aldehydes such as malondialdehyde (MDA).[32] We anticipate that these intermediates, which are highly reactive towards cell lipids, proteins, and DNAs, will synergize with the lipid damage to sensitize cancer cells to RT.

However, free 7-DHC is poorly soluble in water.[33] For efficient delivery, we encapsulated 7-DHC into poly(lactide-co-glycolic)-*block*-poly(ethylene glycol) (PLGA-*b*-PEG) nanoparticles, which afford a long circulation half-life and can accumulate in tumors through the enhanced permeability and retention (EPR) effect.[34-36] We speculate that 7-DHC can be released in a controlled manner from the particles and, as a hydrophobic molecule, efficiently enter cancer cells and populate their plasma/organelle membranes, in turn enhancing RT-induced cell damage. We anticipate minimal side effects as 7-DHC-falicilated lipid peroxidation mainly takes place under irradiation, which is delivered uniformly to tumors in modern RT. In normal tissues, 7-DHC is efficiently converted to cholesterol or cholecalciferol,[37] thus posing minimal risk for systemic toxicities.

Herein, we tested these hypotheses *in vitro* with CT26 cells (a murine colon cancer cell line). Colon cancer is the third most prevalent cancer type among both men and women in the United States,[38] and, as of 2020, is the second leading cause of cancer-related death worldwide according to the World Health Organization (WHO). While surgery is the primary treatment regimen for localized colon cancer, it is only viable among patients with early stage disease.[5] The majority of patients rely on RT as their primary treatment method. While fractionated (~2-3 Gy per dose) RT is a viable and effective option for treating early to mid stage colorectal cancer, radiation may induce unintended morbidities include rectal irritation, scarring, fibrosis, and

sexual issues, limiting a lifetime dose to ~60 Gy.[39] Therefore, the importance of enhancing radiation efficacy with a nontoxic and radiation-activatable radiosensitizer cannot be overemphasized.

Results and Discussion

Synthesis of 7-DHC@PLGA NPs

7-DHC was encapsulated into PLGA-*b*-PEG-OH (Mn: 6000 Da for PLGA and 1000 Da for PEG) through nanoprecipitation. Uv-vis spectroscopy found a drug loading rate of 7.1% and an encapsulation efficiency (%EE) of 21.9%. Transmission electron microscopy (TEM) with uranyl acetate negative staining revealed that the resulting nanoparticles, hereafter referred to as 7-DHC@PLGA NPs, were 88.0 ± 3.2 nm in diameter (Figure 2.1a). This agrees with the dynamic light scattering (DLS) data, finding a hydrodynamic size of ~90 nm and a polydispersity index (PDI) of 0.100 (Figure 2.1b). The surface zeta potential is –13.9 mV in PBS (Figure 2.1c). The nanoparticles were well dispersed in aqueous solutions, showing minimal size change over a 5-day incubation in PBS (Figure S2.1). 7-DHC release was evaluated in buffer solutions at pH 5.5, 6.5 and 7.4. While less than 16% of 7-DHC was released within 48 h at pH 7.4, much faster 7-DHC release was observed in acidic solutions (Figure 2.1d).

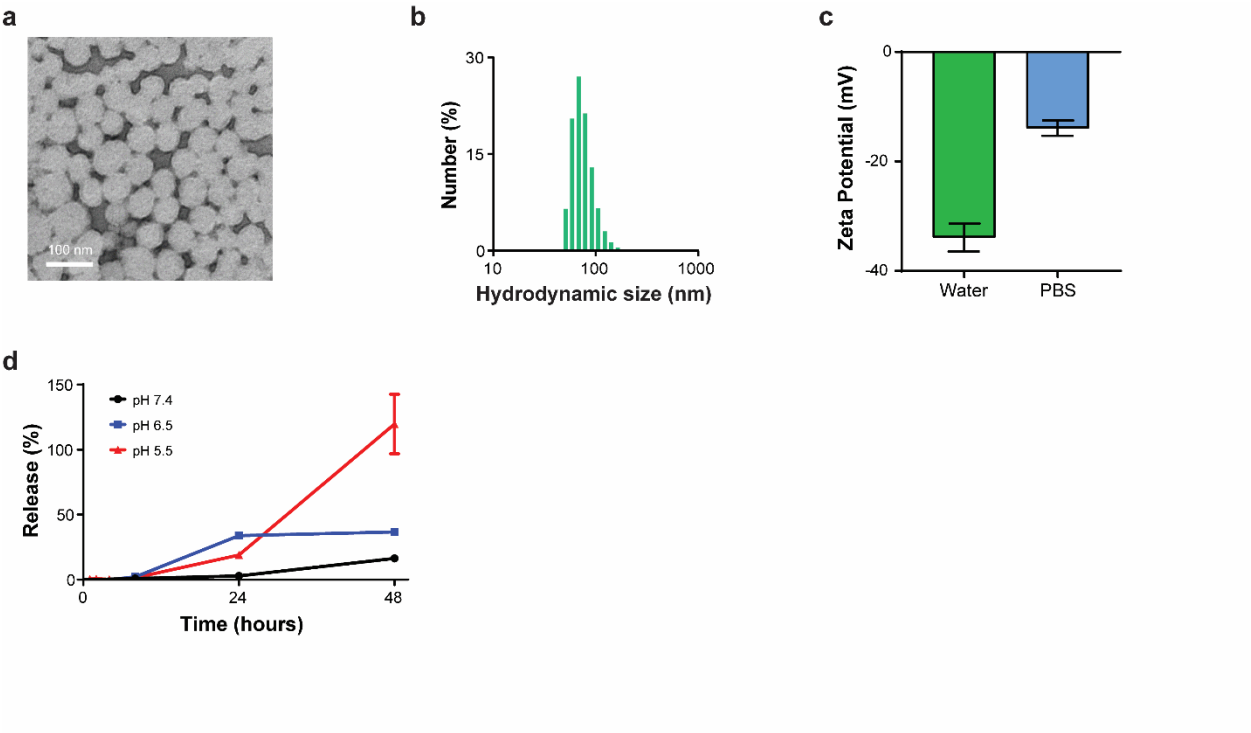

Figure 2.1. Physicochemical characterizations of 7-DHC@PLGA NPs. (a) Negative staining TEM image of 7-DHC@PLGA NPs. Scale bar, 100 nm. (b) DLS analysis of 7-DHC@PLGA NPs in water. (c) Zeta potential of 7-DHC@PLGA NPs in PBS and water. (d) 7-DHC release from 7-DHC@PLGA NPs, tested over 48 h in solutions of pH 7.4, 6.5, and 5.5, respectively.

In vitro studies to examine radiosensitizing effects of 7-DHC@PLGA NPs

We then assessed the cytotoxicity of 7-DHC and 7-DHC@PLGA NPs *in vitro* with CT26 cells. Both 7-DHC and 7-DHC@PLGA NPs showed minimal toxicity when the drug concentration was below 12.5 μg/mL. Similar results were observed using an ATP bioluminescence assay (Figure 2.2a,b). Between the two, 7-DHC@PLGA NPs showed a slightly higher toxicity (IC_{50} 52.0 μg/mL, compared to 71.4 μg/mL for free 7-DHC), which is likely

attributed to an increased cell uptake of the sterol with the nanoparticulate formulation. Confocal laser scanning microscopy found a positive overlay between the lysosome and nanoparticle, indicating a positive level of nanoparticle endocytosis (Figure S2.2). As a control, endocytosis was inhibited at 4^{o}C, confirming our postulation that the nanoparticles enter the cell through endocytosis. However, the solution 7-DHC release data suggests that most of the 7-DHC molecules can be released from the nanoparticle in the acidic tumor microenvironment (Figure 2.1d) and enter cells as a free molecule.[28] Further confocal microscopy data suggests that once internalized, 7-DHC@PLGA NP can accumulate within the mitochondria as previously hypothesized (Figure S2.3). These data are further supported by LC/MS analysis (Figure S2.4).

We then investigated the impact of 7-DHC@PLGA NPs on cell function and survival. Briefly, we incubated 7-DHC@PLGA NPs (5 µg/mL) with CT26 cells for 24 h, followed by irradiation at 5 Gy. As aforementioned, 7-DHC is expected to be enriched in lipid membranes and radicalized under irradiation to cause extensive oxidation of lipid molecules. This was confirmed by both the Image-iT Lipid Peroxidation assay (Figure 2.2c) and TBARS assay. In the latter case, a remarkable increase of MDA levels by 216.0% was observed, compared to a 56.2% increase in cells treated with IR only (Figure 2.2d.)

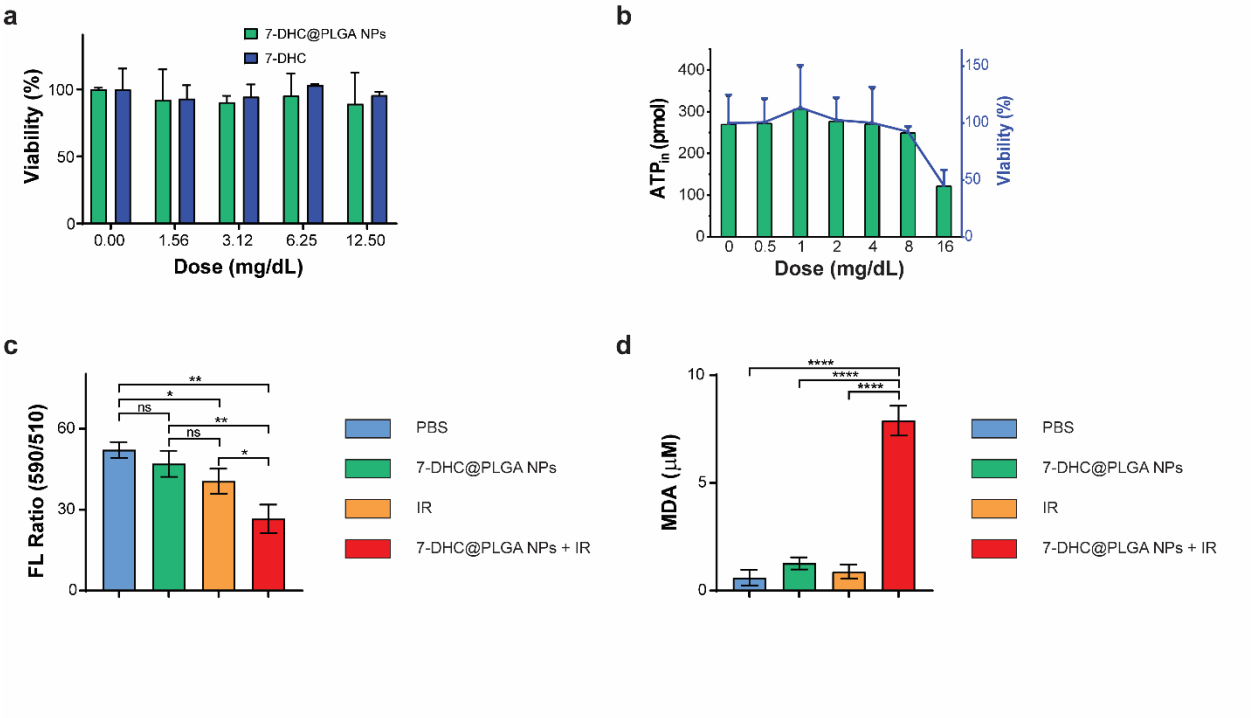

Figure 2.2. Impact of 7-DHC@PLGA NPs on cell lipid peroxidation and viability, tested in CT26 cells. (a) Cell viability in the absence of radiation, measured by MTT assays at 24 h. Both 7-DHC@PLGA NPs and free 7-DHC showed minimal toxicity below 12.5 μg/mL. (b) Cell viability in the absence of radiation, measured by ATP bioluminescence at 24 h. c, d) Impact on cell lipid peroxidation, tested with 7-DHC@PLGA NPs (5 μg/mL concentration) in the presence of radiation (5 Gy). PBS, 7-DHC@PLGA NPs, and irradiation alone (IR) were tested as controls. c) BODIPY lipid peroxidation assay results from 24 h. A decrease in the 590/510 nm fluoresce intensity ratio indicates an increase in lipid peroxidation. d) MDA secretion, measured by TBARS assay. *P < 0.05; **P < 0.01; ***P < 0.001; ****P < 0.0001; ns, no significant difference.

In particular, 7-DHC@PLGA NPs enhance radiation-induced damage to mitochondria, where sterols and oxygen are enriched.[40] Relative to ionizing radiation (IR) alone, 7-

DHC@PLGA NPs plus irradiation (7-DHC@PLGA NPs + IR) caused a 42.6% decrease in the mitochondrial membrane potential (Ψ_m), compared to a decrease of 28.7% by IR alone (Figure 2.3a). Notably, cyanide *m*-chlorophenyl hydrazone (CCCP), which disrupts the proton gradient across the mitochondrial inner membrane[41, 42] was tested as a positive control in the study, only caused a drop of 36.5% in Ψ_m (Figure 2.3a). A depolarized mitochondrial membrane would impair the electron transport chain, thereby elevating ROS in the mitochondria.[43] This is supported by the finding that the mitochondrial superoxide dismutase (MnSOD) activity was significantly increased in cells treated with 7-DHC@PLGA NPs + IR (Figure 2.3c). Meanwhile, dihydroethidium (DHE, which was responsive to superoxide) and cytosolic SOD analysis confirmed that the intracellular ROS level was also markedly elevated in cells treated with 7-DHC@PLGA NPs during radiation (Figure 2.3c&d). Such an increase in oxidative stress causes extensive destruction to cell organelles. These include, unsurprisingly, mitochondrial damage. Cytochrome c and mitochondrial complex Vα double staining found an extensive release of cytochrome c into the cytosol (Figure 2.3b and S2.5), which is an indicator of the activation of the intrinsic apoptosis pathway.[44] Indeed, compared to IR alone, caspase-3 activity was elevated by 24.3% in cells treated with 7-DHC@PLGA NPs + IR (Figure 2.3f). This damage is further manifested in severe double-strand DNA damage, as evidenced by γH2AX staining which found an increase of foci number by 557.9% in cells treated with 7-DHC@PLGA NPs + IR relative to IR alone (Figures 2.3e and S2.6). Lastly, a significant viability drop over irradiation was also confirmed by MTT assays at different nanoparticle concentrations (Figure 2.3g).

Meanwhile, lipid peroxidation products of PUFA oxidation may produce reactive aldehydes and oxysterols. For instance, DHCEO, one of the main oxysterols identified in SLOS patients, is much more toxic to CT26 cells than 7-DHC (Figure S2.7). As previously mentioned,

solution LC/MS data suggests the oxidation of 7-DHC yields a variety of oxysterol derivatives (Figure S2.3) including DHCEO. Liquid chromatography revealed numerous new peaks, presumably oxysterols ranging from 4-10 minutes. Accordingly, the mass spectrum at 8.5 minutes revealed the key m/z peaks for DHCEO. Further preliminary *in vitro* data also suggests the oxidation to DHCEO, as well as other highly reactive oxysterols, 7-keto-8-DHC and Cpd2B. (Figure S2.8).

In addition to promoting lipid peroxidation, 7-DHC may enhance toxicity by producing toxic lipid peroxidation derivatives. To investigate, carnosine (40 mM), which inhibits the formation of alpha-beta unsaturated aldehydes,[45] was added to the culturing medium as a negative control. Carnosine significantly mitigated toxicity caused by 7-DHC@PLGA NPs + IR, supporting a role of lipid peroxidation products in the radiosensitization (Figure 2.3g).

Last but not least, the radiosensitizing effects were measured by the clonogenic assay. Relative to IR alone, 7-DHC@PLGA NPs + IR significantly reduced cell reproduction across a range of radiation doses. The data was fit into the linear-quadratic (LQ) model $S = e^{-(\alpha D+\beta D^2)}$. Based on the data fitting, the dose required for 10% survival (D_{10}) was 2.916 Gy for 7-DHC@PLGA NPs + IR, compared to 4.531 Gy for IR alone. The dose modifying factor based on survival fraction at 2 Gy (SF_2) was 0.209 for 7-DHC@PLGA NPs + IR, and the dose modifying factor based required for 10% survival ($DMF_{10\%}$) was 1.554 for 7-DHC@PLGA NP +IR) . (Figure 2.3h).

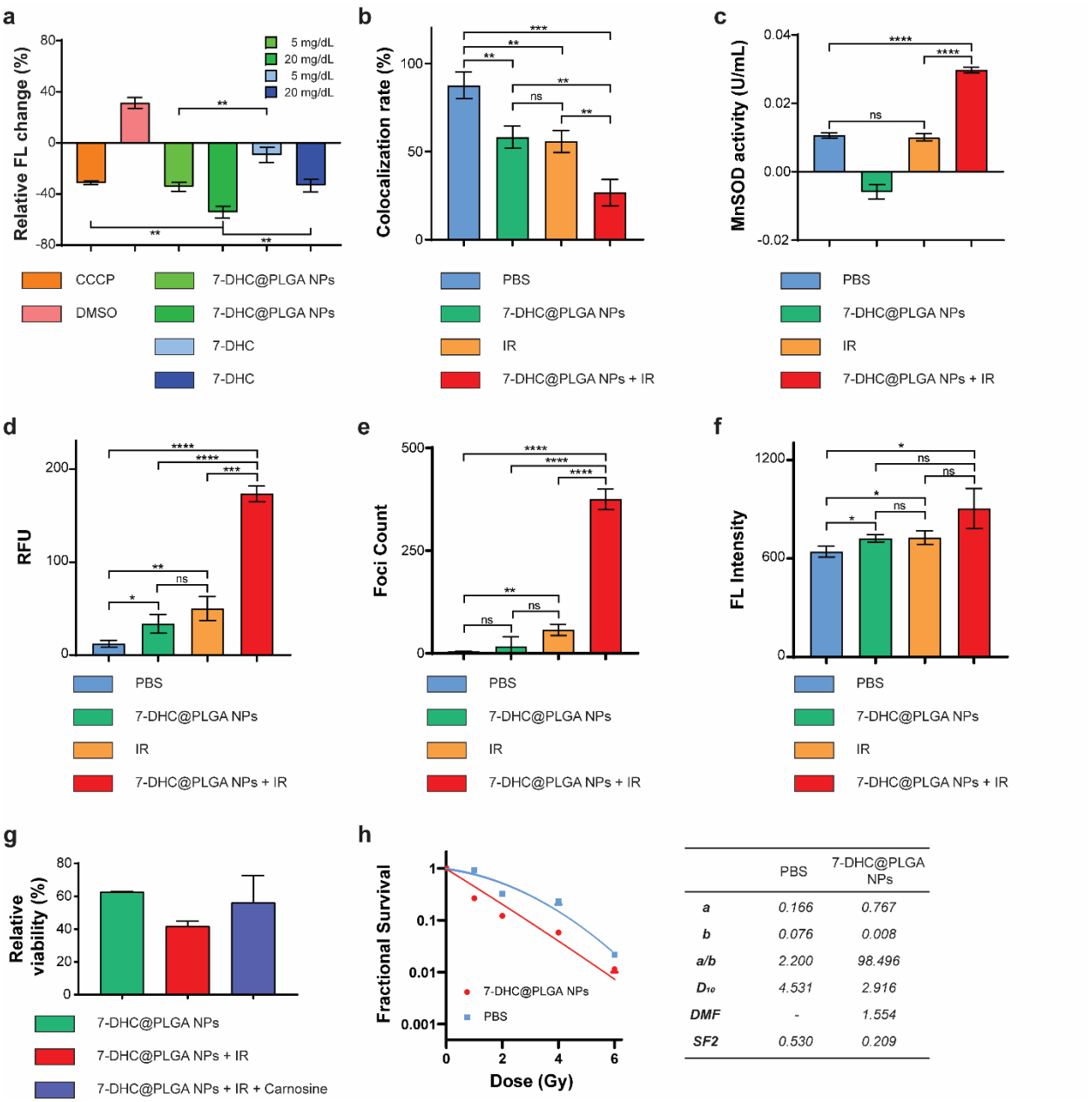

	PBS	7-DHC@PLGA NPs
a	*0.166*	*0.767*
b	*0.076*	*0.008*
a/b	*2.200*	*98.496*
D_{10}	*4.531*	*2.916*
DMF	-	*1.554*
SF2	*0.530*	*0.209*

Figure 2.3. Impact of 7-DHC@PLGA NPs on mitochondria and other organelles. 7-DHC@PLGA NPs were incubated with CT26 cells, followed by 5-Gy irradiation at 24 h (7-DHC@PLGA NPs+IR). PBS, irradiation (IR), and 7-DHC@PLGA NPs only were tested as a comparison unless specified otherwise. (a) Ψ_m changes, measured by JC-1 assay. 7-DHC@PLGA NPs led to a concentration dependent reduction of Ψ_m in the presence of irradiation. DMSO and CCCP were tested as negative and positive controls, respectively. (b)

Cytochrome c release, assessed by anti-cytochrome c and mitochondrial complex Vα double staining. Percent colocalization was evaluated by ImageJ. A decreased colocalization indicates increased level of cytochrome c release. c,d) Impact of 7-DHC@PLGA NPs on cellular oxidative stress under irradiation, measured by SOD activity and DHE superoxide assays. The presence of 7-DHC@PLGA NPs significantly elevated MnSOD activity (c) and cytosolic superoxide (d) under irradiation. (e) DNA double-strand breaks, measured by counting foci numbers using ImageJ. (f) Caspase 3 activity, measured by FAM-FLICA Caspase 3/7 assay. (g) Cell viability, evaluated by MTT assays at 24 h. Carnosine, which inhibits the formation of alpha-beta unsaturated aldehydes, was added to incubation medium and tested as a comparison. (h) Clonogenic assay, tested with PBS + irradiation (IR), and 7-DHC@PLGA NPs plus irradiation (7-DHC@PLGA NPs+IR). Survival fractions relative to the PBS control were fit into the linear quadratic (LQ) model. *, $P < 0.05$; **, $P < 0.01$; ***, $P < 0.001$; ****, $P < 0.0001$; ns, no significant difference.

Conclusion

The outlined studies demonstrate a facile synthesis of a novel polymeric nanoparticle, 7-DHC@PLGA NP, that affords high loading of the vitamin D prodrug 7-DHC. Further, under physiological pH, little to no 7-DHC is released from the particle. However, under acidic conditions similar to those found in the tumor microenvironment, all of the drug is released within 48 h, giving this formulation a desirable circulation half life and drug release properties. Once incubated with CT26 cells, 7-DHC@PLGA NP shows little to no toxicity in the absence of radiation which is ideal for a radiosensitizer. However, once IR is applied to the cells following endocytosis of the released 7-DHC, the toxicity is increased dramatically. The application of IR

hydrolyzes water in the cells creating toxic free radical species such as the hydroxide and superoxide radicals. These such radicals cause not only the auto-oxidation of 7-DHC to very toxic oxysterol derivatives, but also allows 7-DHC to facilitate the free radical propagation reactions in the lipid and mitochondrial membranes of the cell. These reactions in turn generate lipid peroxidation byproducts such as 4-HNE from the oxidation of PUFAs, but also the most mutagenic product, malondialdehyde. Such species in turn cause extensive DNA damage and mitochondrial damage, all leading to very efficient cell death via the intrinsic mitochondrial apoptotic pathway. Lastly, a colony forming assay demonstrated reduced clonogenicity with CT26 cells treated with 7-DHC@PLGA NPs, proving that this formulation is an efficient and effective radiosensitizer *in vitro*. Effects of this nanoparticle formulation will be evaluated *in vivo* in the following chapter.

CHAPTER 3

MEMBRANE LIPID OXIDATION BYPRODUCTS INHANCE THERAPEUTIC EFFICACY *IN VIVO*[2]

[2] Ian Delahunty, Wen Jiang, Jianwen Li, Chaebin Lee, Xueyuan Yang, Anil Kumar, Amy Li, Pakteema Tong, Libin Xu, Weizhong Zhang, Jin Xie. A polymeric nanoparticle radiosensitizer based on 7-dehydrocholesterol. To be submitted to *ACS Nano*, 2021.

Abstract

Our prior studies have illustrated the radiosensitizing capabilities of 7-DHC@PLGA NPs *in vitro* when incubated with CT26 cells. However, these models do not demonstrate a clear therapeutic benefit, as cells in culture generally do not harbor any immune component, as would be evident *in vivo*, in immunocompetent animals. Therefore, the previous studies were expanded and tested in small animal models. When tested *in vivo*, 7-DHC@PLGA NPs significantly enhanced radiotherapy, resulting in 40% eradication of the tumors and extended animal survival with a single around of treatment. Importantly, the nanoparticles caused no detectable tissue or hematological toxicities, nor hypercalcemia, a toxic side effect of administration of high doses of vitamin D. Our studies suggest the promise of 7-DHC as an efficient, safe, and activatable radiosensitizer.

Introduction

Cancer radiosensitizers are intended to enhance radiation-induced tumor cell damage while accruing minimal damage to normal, healthy tissue. Traditional radiosensitizers specifically target different physiological characteristics of the tumor, specifically those characteristics that cause radioresistance.[1] In a wide array of tumors, radioresistance is brought about by severe hypoxic conditions deep within the tumor. As such, agents that can restore oxygenated conditions to the tumor may help overcome the radioresistance.[2] Such agents include, unsurprisingly, oxygen and nitric oxide.[3] Additional materials include electron-affinic chemicals that react with DNA free radicals such as nimorazole, which has been shown to be clinically effective. In principle, many drugs can be delivered selectively to hypoxic tumors

using either reductase enzymes or radiation-produced free radicals to activate drug release from electron-affinic prodrugs and thereby enhancing radiotherapy by restoring normoxic conditions to the tumor.

However, in the majority of these traditional radiosensitizers, the radiation simply promotes the release of potentially toxic drugs into the tumor. Our approach as outlined *in vitro* in Chapter 2, utilizes a non-toxic, radiation-activatable pro-drug, which is unique among radiosensitizers and ideal for radiation therapy. This approach activates 7-DHC such that it promotes free radical oxidation, leading to downstream cytotoxic effects. These events significantly enhanced radiotherapy *in vivo*, while causing no detectable systemic toxicity to the animals.

Results and Discussion

In vivo therapy studies to evaluate the benefits of 7-DHC@PLGA NPs for radiotherapy

Therapy studies were conducted in CT26 tumor bearing, immunocompetent balb/c mice (Figure 3.1a). When the tumor size reached ~100 mm^3, 7-DHC@PLGA NPs (10 mg/kg, based on 7-DHC) were intravenously (i.v.) injected, followed by the application of beam radiation (320 kV, 5 Gy) to tumors at 4 h post-injection, with the rest of the body shielded by lead (7-DHC@PLGA NPs + IR; n=5). For comparison, radiation only (IR), 7-DHC@PLGA NPs only (7-DHC@PLGA), and carrier only (PBS) were tested (n=5). 7-DHC@PLGA NPs + IR significantly retarded tumor growth, causing a remarkable inhibition rate of 98.4% on Day 26 relative to the PBS control (Figure 3.1b). By the end of the study on Day 43, 60% of the animals in the 7-DHC@PLGA NPs + IR group remained alive (Figure 3.1c). As a comparison all

animals in the groups, including the IR only control, had died or reached a humane endpoint by Day 43 (Figure 3.1c).

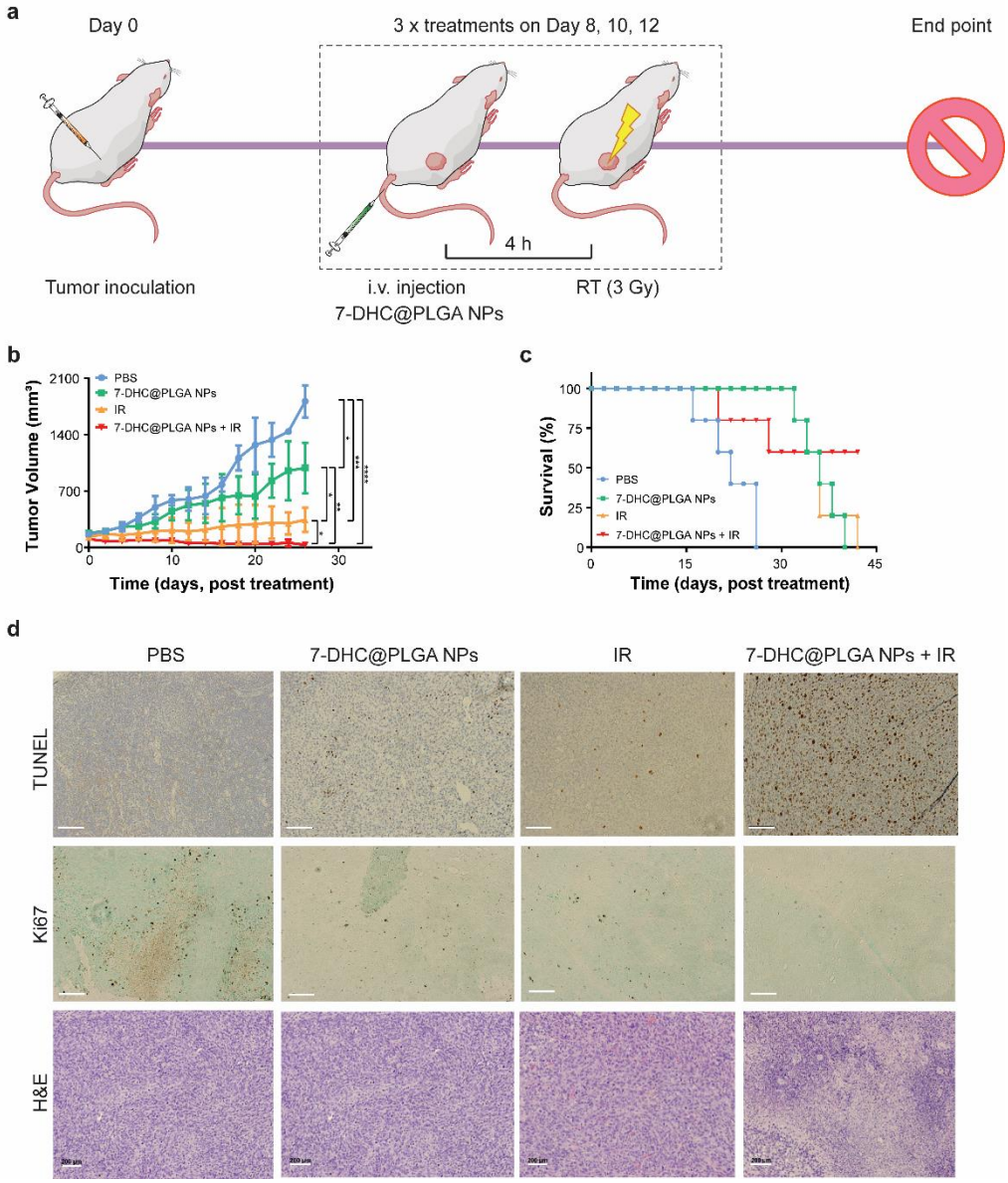

Figure 3.1. *In vivo* therapy study studies. Experiments were conducted in CT26 tumor bearing balb/c mice. 7-DHC@PLGA NPs were intravenously (i.v.) injected, followed by beam radiation (3 Gy) applied to tumors at 4 h (7-DHC@PLGA NPs + IR; n=5). Three doses of treatment were given two days apart. Irradiation only (IR), 7-DHC@PLGA NPs only (7-

DHC@PLGA NPs), and carrier only (PBS) were tested (n=5). a) Scheme showing the treatment plans. b) Tumor volume curves. 7-DHC@PLGA NPs + IR caused effective tumor regression, with 30% of the animals being tumor-free on Day 43. *, $P < 0.05$; **, $P < 0.01$; ***, $P < 0.001$; ****, $P < 0.0001$; ns, no significant difference. c) Animal survival. Sixty percent of the animals in the 7-DHC@PLGA NPs+ IR group were alive on Day 43, while all animals in the control groups had either died or reached a humane endpoint by that date. d) TUNEL, Ki67, and H&E staining tumor samples from different treatment groups. Scale bars, 200 nm.

Tumor tissues were harvested for pathology analysis (Figure 3.1d). H&E staining found a significantly reduced density of cancer cells in samples from the 7-DHC@PLGA NPs + IR group. Ki67 and TUNEL staining also displayed reduced proliferation and elevated apoptosis, confirming effective tumor suppression. Meanwhile, no animal body weight drop was observed throughout the study (Figure 3.2a). Normal tissue histology studies also detected no signs of toxicity (Figure 3.2c). In a separate study, we injected 7-DHC@PLGA NPs at the same dose into healthy mice and collected blood on Day 14. All complete blood count (CBC) indices and alanine aminotransferase (ALT) levels were all within normal ranges according to published standards (Table 3.1).

Table 3.1. CBC analysis demonstrating normal blood cell count for all indices measured, indicating no systemic toxicity due to intravenous injection of 7-DHC@PLGA NPs.

Complete Blood Count

Test	Result	Units	Reference Interval
WBC	8.1	10^3/ul	.8-10.6
Neu#	1.59	10^3/ul	0.23-3.6
Lym#	5.99	10^3/ul	0.6-8.9
Mon#	0.32	10^3/ul	0.04-1.4
Eos#	0.13	10^3/ul	0.0-0.51
Bas#	0.02	10^3/ul	0.0-0.12
Neu%	19.7	%	6.5-50.0
Lym%	74.4	%	40-92
Mon%	4	%	0.9-18.0
Eos%	1.7	%	0.0-7.5
Bas%	0.2	%	0.0-1.5
RBC	11.18	10^6/ul	6.5-11.5
Hgb	17.7	g/dl	11-16.5
Hct	50.6	%	35-55
MCV	45.3	fl	41-55
MCH	15.8	pg	13-18
MCHC	35	g/dl	30-36
RDW%	13.2	%	12.0-19.0.
Platelet	240	10^3/ul	400-1600
MPV	5.7	Fl	4-6.2
ALT	9.06	U/mL	15-84

Potential side effects of 7-DHC@PLGA NPs

In addition to being a cholesterol precursor in the serum, 7-DHC may also accumulate in the skin, where it is photochemically converted to vitamin D_3. The latter is metabolized to calcidiol in the liver, and finally to the biologically active form, calcitriol, in the proximal tubule of the kidneys. Calcitriol is an important regulator for serum calcium, posing potential risks of hypercalcemia. Indeed, i.v. injection of calcitriol at 200 μg/kg drastically elevated the serum calcium to 17.5 mg/dl, which is almost twice the maximum tolerated level (8.0-11.5 mg/dl for mice[4]). As a comparison, 7-DHC@PLGA NPs at a much higher does (1 mg/kg) had a minimal impact on the calcium level (Figure 3.2b).

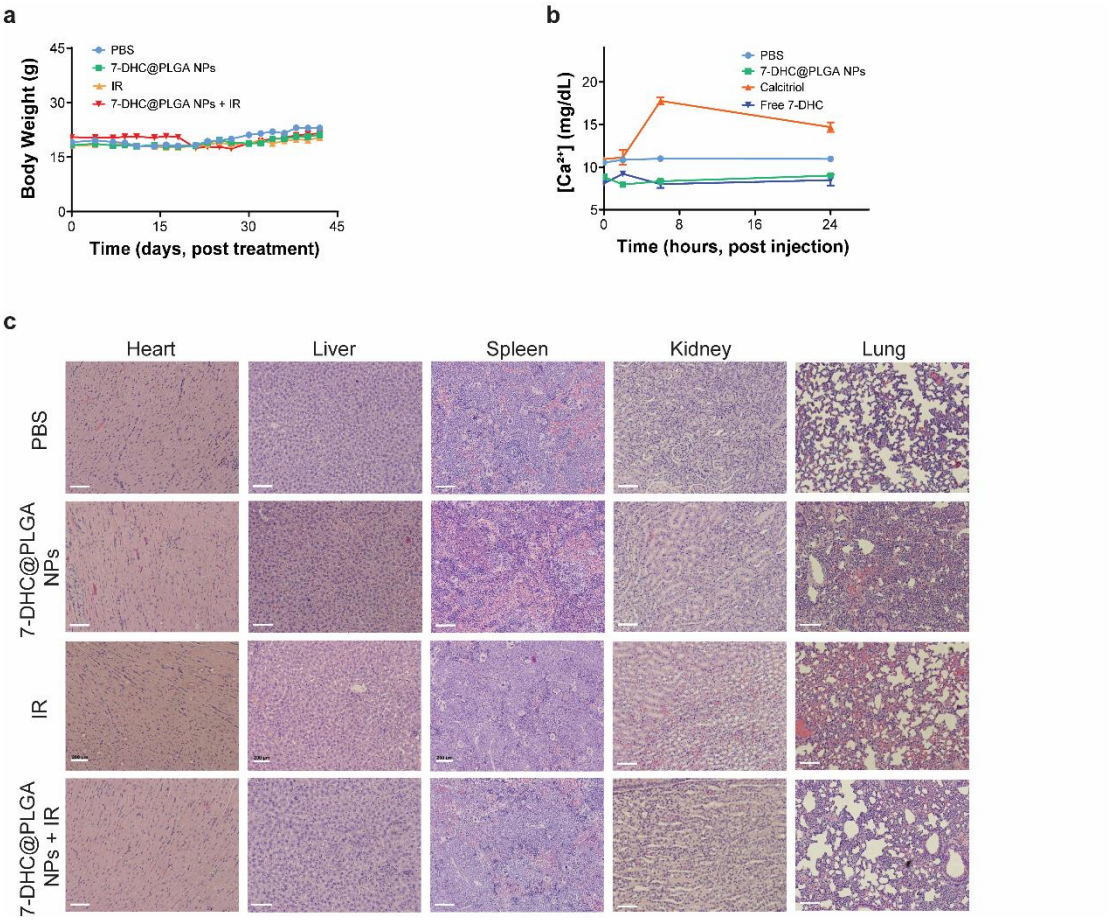

Figure 3.2. Potential side effects of 7-DHC@PLGA NPs plus irradiation. (a) Body weight change. No significant body weight drop was observed throughout the therapy study. (b) Serum

calcium level change. 7-DHC@PLGA NPs (1 mg/kg), calcitriol (200 μg/kg), 7-DHC (200 μg/kg), and PBS were intraperitoneally injected into healthy balb/c mice (n=3). Blood samples were collected at 0, 2, 6, and 24 h for analysis. No calcium level increase was observed in animals injected with 7-DHC@PLGA NPs. (c) H&E staining of normal tissues harvested post mortem. No signs of toxicity were observed. Scale bars, 200 μm.

Conclusion

Our studies suggest a great promise of 7-DHC@PLGA NPs as an effective and safe radiosensitizer. The exploration was inspired by observations from patients with SLOS, who harbor a deficiency in DHCR7 thus experiencing accumulation of 7-DHC in cholesterol-rich tissues, such as the brain. The buildup of 7-DHC over time elevates cellular ROS, which then react with the sterol. This forms a positive feedback loop that eventually causes extensive lipid peroxidation and tissue damage. In our strategy, 7-DHC is delivered to tumors by a nanoparticle carrier and activated under radiation to enhance radiation-induced toxicities. This makes our formulation a radiation-activatable one, which is unique among radiosensitizers and ideal for RT. It is interesting to note that many human colon cancer cells, including CT26, have a reduced expression of DHCR7 compared to normal tissue.[5] This phenomenon may add another level of selectivity to our approach, as 7-DHC tends to stay as 7-DHC in cancer cells instead of being metabolized to relatively non-toxic cholesterol. This may explain why 7-DHC@PLGA NPs alone caused a certain degree of tumor suppression (Figure 3.1b) but no toxicity to normal tissues (Figure 3.2c). Meanwhile, the kinetics for nanoparticle delivery and reductase conversion may have an impact on the amount of 7-DHC inside cancer cells at the time of radiation, in turn influencing IR efficacy. It will be interesting to investigate the impact of drug-radiation interval

on sterol homeostasis in tumors and identify optimal conditions for therapy. The related studies are underway.

CHAPTER 4

CONCLUSION AND FUTURE PLANS

Introduction and the Enhanced Permeability and Retention Effect

Up to this point, the 7-DHC@PLGA NP delivery system was based solely on the enhanced permeability and retention (EPR) effect. First discovered by Matsumura and Maeda in 1986, the EPR effect is a phenomenon caused by the inherent leaky vasculature that supplies the tumor.[1] Unlike the vasculature of normal tissue, which has an organized and regular branching order, the vasculature in and around the hypoxic and acidic tumor microenvironment is highly disorganized and lacks the conventional hierarchy of blood vessels as shown in Figure 4.1. Conventional vessels such as arterioles, capillaries, and venules are not identifiable as such, and instead, vessels are enlarged and poorly interconnected.[2-5] These abnormalities are caused by an imbalance in the expression of angiogenic factors and inhibitors.[6] One consequence of the heterogeneous formation of these blood vessels is the endothelial lining of the vessels often has very large gaps, upwards of several hundred nanometers. The end result is that nanosized agents with long circulation times such as our 7-DHC@PLGA NP, leak preferentially into tumor tissue through this permeable tumor vasculature and are then retained in the tumor bed due to the reduced lymphatic drainage. This is illustrated in Figure 4.2.

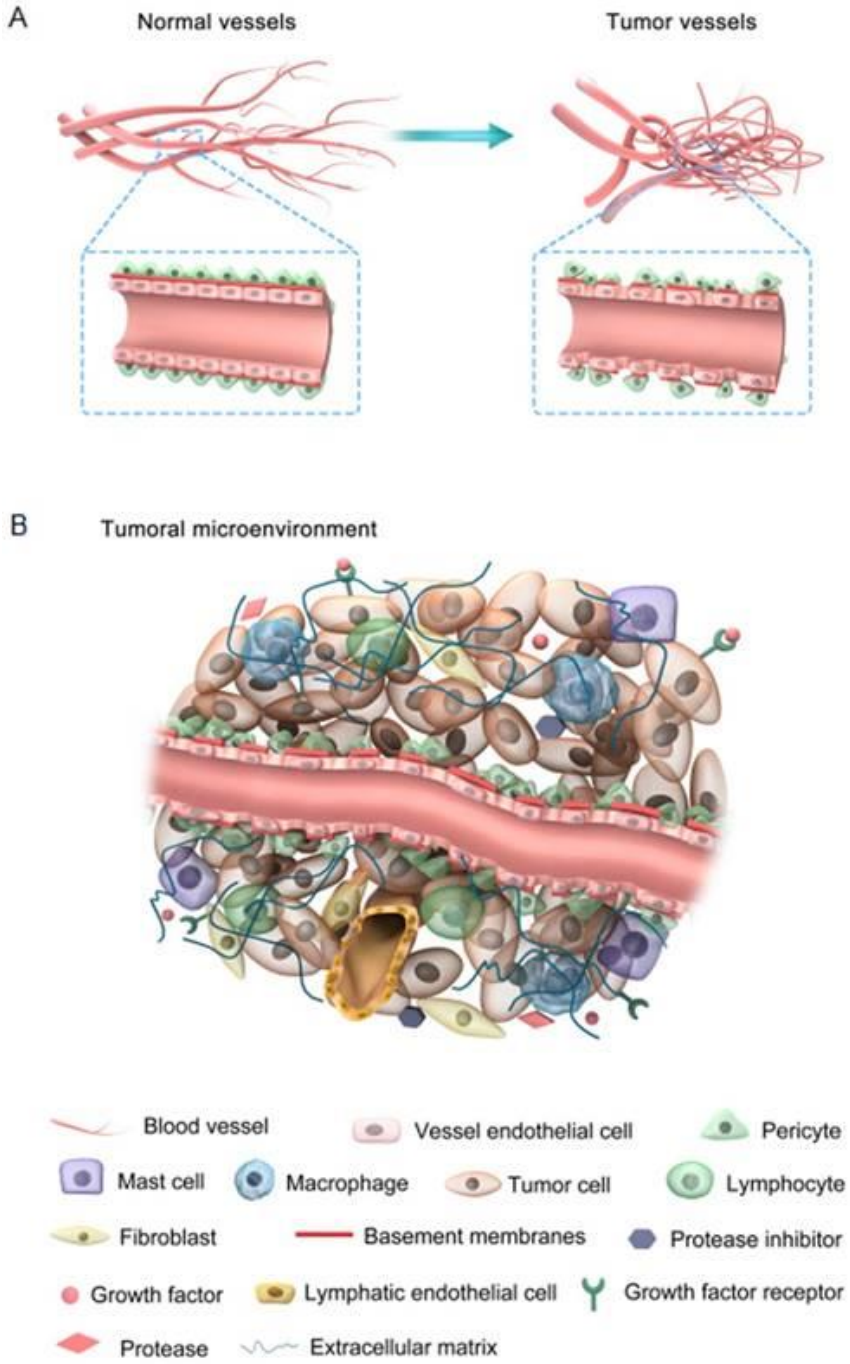

Figure 4.1. Complex irregularities between normal and tumor vessels. a) Comparison between normal and tumor vessels; b) Characteristic features of the tumor microenvironment. Reprinted with permission.[7]

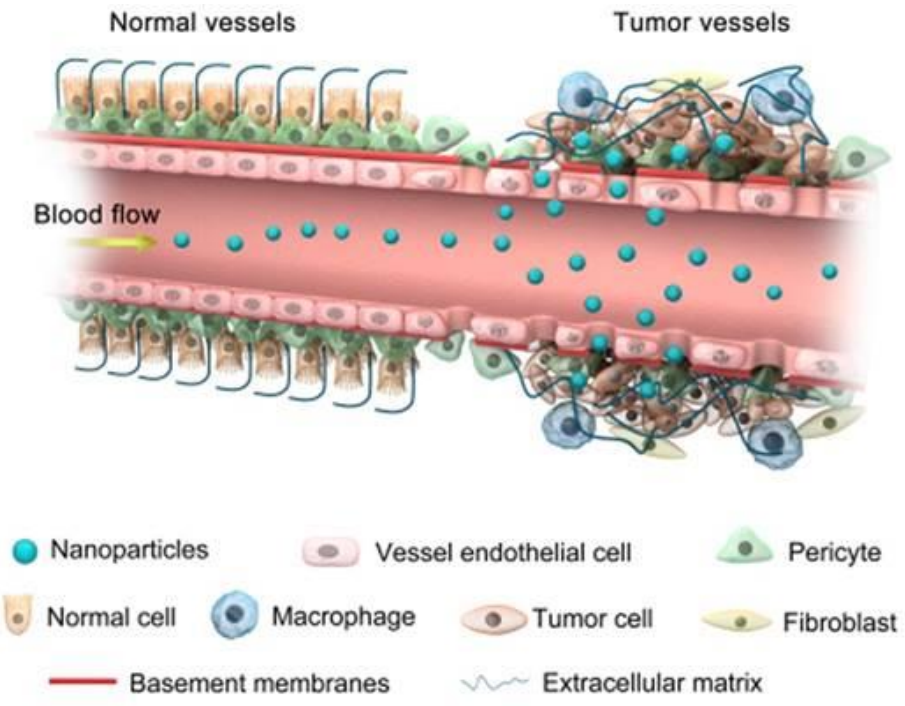

Figure 4.2. Irregularities in the endothelial lining of vessels that supply tumors. Due to the inherent leaky vasculature, nanoparticles accumulate preferentially in the tumor bed and are retained there. Reprinted with permission.[7]

While this phenomenon is incredibly useful, it is a highly controversial and hotly debated topic throughout the literature.[8-10] The reason for the controversy is, while EPR effect is widely held to improve delivery of nanodrugs to tumors, it in fact offers less than a 2-fold increase in nanodrug delivery compared with critical normal organs, resulting in drug concentrations that are not sufficient for curing most cancers. Some researchers argue in fact, that the percent of initial injected dose (%ID) that actually reaches the tumor is anywhere from 1-10%. For example, Andrew Wong and coworkers measured the %ID of Doxil to reach the tumor following intravenous injection to range from 0.01-10%.[11] Further, the relevance of the EPR effect in humans has also been debated recently.[12-14] In small animal xenograft tumor models where the tumors grow at a rate far surpassing that of human tumor growth, the EPR effect is more

pronounced. Further, recent evidence has revealed that the mechanism by which nanoparticles enter solid tumors is more complex than previously thought (potentially going beyond simple extravasation through gaps in the endothelial lining),[15] and that immune cells in the tumor microenvironment play important roles in nanomedicines' accumulation, retention and intratumoral distribution. It should be noted, however, that accumulation of nanocarriers in human tumors certainly does occur, but the extent to which varies heavily between patients and tumor types.[16] The latter point seems to severely limit the clinical use of nanomaterials designed to utilize the EPR effect for delivery. It is to this end that most clinically relevant nanomaterials utilize active targeting for tumor homing. Tumor targeting ligands include antibodies, fragments of antibodies (e.g. nanobodies) and peptides.

While our 7-DHC@PLGA formulation afforded a long circulation half life, a desirable toxicity profile, and good tumor suppression, efforts to increase not only the drug loading of 7-DHC, but also increase the amount of 7-DHC delivered to the tumor are underway. The following section highlights the design and preliminary work on a new nanoformulation based on a synthetic low density lipoprotein (sLDL). This formulation is designed to target the neurotensin receptor overexpressed on H1299 lung cancer cells and deliver 7-DHC in very high quantities.

A synthetic LDL approach to tumor radiosensitization

Low-density lipoprotein is one of the five major groups of lipoprotein which transport all fat molecules around the body, making fats available to body cells for receptor-mediated endocytosis. As a general class of liposome, which can afford increased efficacy and therapeutic index, increased stability, reduced toxicity, improved pharmacokinetics, and selective targeting,

synthetic lipoproteins seem highly advantageous for tumor targeting. In general, lipoproteins contain upwards of 100 proteins per particle, with LDL only containing 1: Apolipoprotein B. Traditionally thought of as "bad" cholesterol, LDL is implicated in atherosclerosis due to the fact that it causes a buildup of cholesterol in the arteries. However, it should be noted that due to the fact that the job of LDL is to transport cholesterol from the liver to the rest of the body, it is able to encapsulate extremely large quantities of cholesterol within its lipid membrane.[17, 18] Furthermore, in recent years, cholesterol has received increasing attention due its role in carcinogenesis. Clinical and experimental evidence supports that changes in cholesterol metabolism are implicated in cancer development do to the tumor's increased demand for cholesterol involved in membrane synthesis.[19] On this note, we hypothesize that instead of utilizing cholesterol, we can use a similar liposomal approach to deliver 7-DHC to tumors. Specifically, by designing an LDL-like liposome and incorporating, instead of apolipoprotein B, a small peptide containing the binding motif for neurotensin, which is overexpressed on H1299 non-small cell lung carcinoma cells, we can deliver high quantities of 7-DHC to the tumor for efficient radiosensitization in a similar mechanism to our 7-DHC@PLGA NPs.

Preliminary Results and Discussion

Synthesis of sLDL NPs

The liposomal nanoparticle was synthesized following previously established thin film hydration protocols with modifications.[20-22] Briefly, phosphatidyl choline, triolein, and 7-DHC were mixed. The lipid mixture was then dried under N_2, hydrated above the phase transition temperature of the lipids, and extruded through an Avanti Lipid Extruder. Following the synthesis, UV-vis spectroscopy found a 7-DHC drug loading rate of 9.4% and an encapsulation

efficiency (%EE) of 57.5%, almost a 3-fold increase from the 7-DHC@PLGA formulation. Transmission electron microscopy (TEM) with uranyl acetate negative staining revealed that the resulting nanoparticles, were 98.0 ± 4.6 nm in diameter (Figure 4.3a). This agrees with the dynamic light scattering (DLS) data, finding a hydrodynamic size of 106.0 nm and a polydispersity index (PDI) of 0.394 (Figure 4.3b). The surface zeta potential is –48.9 mV in water, -8.78 mV in PBS, and -37.8 mV in Tris buffer (Figure 4.3c). 7-DHC release was evaluated in buffer solutions at pH 5.5, 6.5 and 7.4. In a similar manner to the 7-DHC@PLGA NP formulation, a much faster 7-DHC release was observed in acidic solutions, with nearly all drug being released within 48 h (Figure 4.3d).

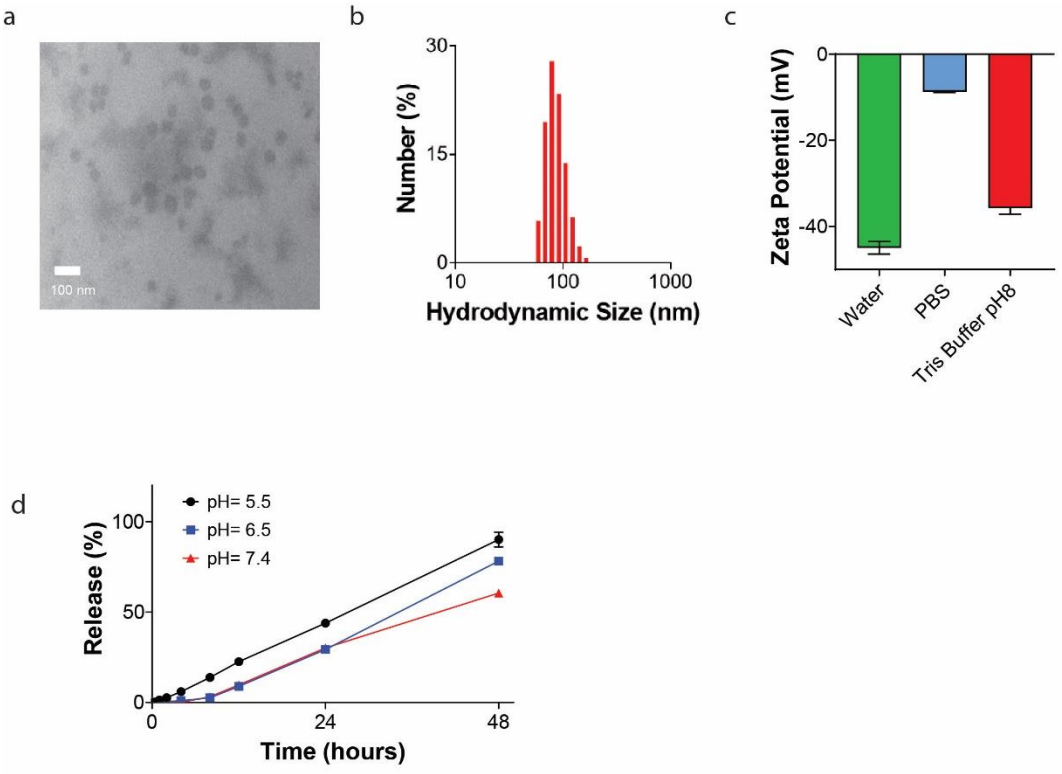

Figure 4.3. Physicochemical characterizations of 7-DHC@PLGA NPs. (a) Negative staining TEM image of sLDL NPs. Scale bar, 100 nm. (b) DLS analysis of sLDL NPs in Tris buffer. (c)

Zeta potential of sLDL NPs in Water, PBS, and Tris buffer. (d) 7-DHC release from sLDL NPs, tested over 48 h in solutions of pH 7.4, 6.5, and 5.5, respectively.

Conclusion and Future Directions

The investigations into designing new radiosensitizers have only just begun. Utilizing highly reactive compounds, whose pro-drug form are non-toxic, represent a new class of highly efficient radiosensitizers in that they're activatable by the radiation itself. Despite technological advances in radiation therapy such as stereotactic body radiotherapy, intensity-modulated radiation therapy, and image-guided radiation therapy, the efficacy of RT is limited by normal tissue toxicities. Therefore, there is an unmet need for new radiosensitizing agents that are effective but also more tolerated by patients. As such, we have designed and successfully tested a new radiosensitizer that is not only highly effective both *in vitro* in CT26 colon carcinoma cells, but also *in vivo* in CT26 tumor-bearing mice. Encapsulating high quantities of 7-DHC, our formulation shows increased efficacy over radiation alone, inhibiting tumor volume by nearly 2-fold, and extending survival time by nearly the same amount. Further, 7-DHC@PLGA NPs exhibited no observed systemic toxicity in all blood indices assessed, as well as causing no detectable hypercalcemia nor hematological toxicity to normal tissues.

Further, as illustrated in the final section(s) of this chapter, we illuminated on a newer formulation, a sLDL-like liposomal nanoparticle designed to be actively targeted to the tumor while delivering substantially higher quantities of 7-DHC. In the future, we aim to expand on this sLDL formulation, testing its radiosensitizing capabilities both *in vitro* and *in vivo* and expect to see an even higher therapeutic outcome compared to our already successful 7-DHC@PLGA NP formulation. Additionally, the kinetics for nanoparticle delivery and 7-DHC

reductase (DHCR7) conversion may have an impact on the amount of 7-DHC inside cancer cells at the time of radiation, in turn influencing IR efficacy. It will be interesting to investigate the impact of drug-radiation interval on sterol homeostasis in tumors and identify optimal conditions for therapy. The related studies are underway, as are efforts to determine the identities of all the various oxysterol derivatives and their quantities that are present in vitro following radiation. It is interesting to note that the addition of drugs such as vitamin D_3, which can selectively block the enzymatic activity of DHCR7, thereby increasing the amount of 7-DHC available for oxidation can also be incorporated into the sLDL formulation to further increase the therapeutic outcome. These studies will also be heavily investigated in the future.

References

Chapter 1:

1. Wimalawansa, S. J., Vitamin D Deficiency: Effects on Oxidative Stress, Epigenetics, Gene Regulation, and Aging. *Biology (Basel)* **2019,** *8* (2).

2. Qin, X.; Wang, X., Role of vitamin D receptor in the regulation of CYP3A gene expression. *Acta Pharm Sin B* **2019,** *9* (6), 1087-1098.

3. Pike, J. W.; Meyer, M. B., The vitamin D receptor: new paradigms for the regulation of gene expression by 1,25-dihydroxyvitamin D3. *Rheum Dis Clin North Am* **2012,** *38* (1), 13-27.

4. Holick, M. F., Vitamin D deficiency. *N Engl J Med* **2007,** *357* (3), 266-81.

5. Galitzer, H.; Ben-Dov, I.; Lavi-Moshayoff, V.; Naveh-Many, T.; Silver, J., Fibroblast growth factor 23 acts on the parathyroid to decrease parathyroid hormone secretion. *Curr Opin Nephrol Hypertens* **2008,** *17* (4), 363-7.

6. Bergwitz, C.; Jüppner, H., Regulation of phosphate homeostasis by PTH, vitamin D, and FGF23. *Annu Rev Med* **2010,** *61*, 91-104.

7. Jeon, S. M.; Shin, E. A., Exploring vitamin D metabolism and function in cancer. *Exp Mol Med* **2018,** *50* (4), 20.

8. Buchtele, N.; Lobmeyr, E.; Cserna, J.; Zauner, C.; Heinz, G.; Sengolge, G.; Sperr, W. R.; Staudinger, T.; Schellongowski, P.; Wohlfarth, P., Prevalence and Impact of Vitamin D Deficiency in Critically Ill Cancer Patients Admitted to the Intensive Care Unit. *Nutrients* **2020,** *13* (1).

9. Rasmussen, L. S.; Yilmaz, M. K.; Falkmer, U. G.; Poulsen, L. O.; Bogsted, M.; Christensen, H. S.; Bojesen, S. E.; Jensen, B. V.; Chen, I. M.; Johansen, A. Z.; Hansen, C. P.; Hasselby, J. P.; Hollander, N.; Nielsen, S. E.; Andersen, F.; Bjerregaard, J. K.; Pfeiffer, P.; Johansen, J. S., Pre-treatment serum vitamin D deficiency is associated with increased inflammatory biomarkers and short overall survival in patients with pancreatic cancer. *Eur J Cancer* **2020,** *144*, 72-80.

10. Sajo, E. A.; Okunade, K. S.; Olorunfemi, G.; Rabiu, K. A.; Anorlu, R. I., Serum vitamin D deficiency and risk of epithelial ovarian cancer in Lagos, Nigeria. *Ecancermedicalscience* **2020,** *14*, 1078.

11. McFarland, D. C.; Fernbach, M.; Breitbart, W. S.; Nelson, C., Prognosis in metastatic lung cancer: vitamin D deficiency and depression-a cross-sectional analysis. *BMJ Support Palliat Care* **2020**.

12. Bochen, F.; Balensiefer, B.; Korner, S.; Bittenbring, J. T.; Neumann, F.; Koch, A.; Bumm, K.; Marx, A.; Wemmert, S.; Papaspyrou, G.; Zuschlag, D.; Kuhn, J. P.; Al Kadah, B.; Schick, B.; Linxweiler, M., Vitamin D deficiency in head and neck cancer patients - prevalence, prognostic value and impact on immune function. *Oncoimmunology* **2018,** *7* (9), e1476817.

13. Zhao, J.; Wang, H.; Zhang, Z.; Zhou, X.; Yao, J.; Zhang, R.; Liao, L.; Dong, J., Vitamin D deficiency as a risk factor for thyroid cancer: A meta-analysis of case-control studies. *Nutrition* **2019,** *57*, 5-11.

14. Apperly, F. L., The relation of solar radiation to cancer mortality in North America. *Cancer Research* **1941,** *1* (3), 191-195.

15. Grant, W. B., Roles of Solar UVB and Vitamin D in Reducing Cancer Risk and Increasing Survival. *Anticancer Res* **2016,** *36* (3), 1357-1370.

16. Hsiao, W. C.; Sung, S. Y.; Liao, C. H.; Wu, H. C.; Hsieh, C. L., Vitamin D3-inducible mesenchymal stem cell-based delivery of conditionally replicating adenoviruses effectively targets renal cell carcinoma and inhibits tumor growth. *Mol Pharm* **2012,** *9* (5), 1396-408.

17. O'Kelly, J.; Uskokovic, M.; Lemp, N.; Vadgama, J.; Koeffler, H. P., Novel Gemini-vitamin D3 analog inhibits tumor cell growth and modulates the Akt/mTOR signaling pathway. *J Steroid Biochem Mol Biol* **2006,** *100* (4-5), 107-16.

18. Kalkunte, S.; Brard, L.; Granai, C. O.; Swamy, N., Inhibition of angiogenesis by vitamin D-binding protein: characterization of anti-endothelial activity of DBP-maf. *Angiogenesis* **2005,** *8* (4), 349-60.

19. Malafa, M. P.; Fokum, F. D.; Smith, L.; Louis, A., Inhibition of angiogenesis and promotion of melanoma dormancy by vitamin E succinate. *Ann Surg Oncol* **2002,** *9* (10), 1023-32.

20. Fujioka, T.; Hasegawa, M.; Ishikura, K.; Matsushita, Y.; Sato, M.; Tanji, S., Inhibition of tumor growth and angiogenesis by vitamin D3 agents in murine renal cell carcinoma. *J Urol* **1998,** *160* (1), 247-51.

21. Oikawa, T.; Hirotani, K.; Ogasawara, H.; Katayama, T.; Nakamura, O.; Iwaguchi, T.; Hiragun, A., Inhibition of angiogenesis by vitamin D3 analogues. *Eur J Pharmacol* **1990,** *178* (2), 247-50.

22. Mathiasen, I. S.; Lademann, U.; Jaattela, M., Apoptosis induced by vitamin D compounds in breast cancer cells is inhibited by Bcl-2 but does not involve known caspases or p53. *Cancer Res* **1999,** *59* (19), 4848-56.

23. Kang, Z.; Wang, C.; Tong, Y.; Li, Y.; Gao, Y.; Hou, S.; Hao, M.; Han, X.; Wang, B.; Wang, Q.; Zhang, C., Novel Nonsecosteroidal Vitamin D Receptor Modulator Combined

with Gemcitabine Enhances Pancreatic Cancer Therapy through Remodeling of the Tumor Microenvironment. *J Med Chem* **2021,** *64* (1), 629-643.

24. Liu, W.; Zhang, L.; Xu, H. J.; Li, Y.; Hu, C. M.; Yang, J. Y.; Sun, M. Y., The Anti-Inflammatory Effects of Vitamin D in Tumorigenesis. *Int J Mol Sci* **2018,** *19* (9).

25. Fleet, J. C.; DeSmet, M.; Johnson, R.; Li, Y., Vitamin D and cancer: a review of molecular mechanisms. *Biochem J* **2012,** *441* (1), 61-76.

26. Giammanco, M.; Di Majo, D.; La Guardia, M.; Aiello, S.; Crescimannno, M.; Flandina, C.; Tumminello, F. M.; Leto, G., Vitamin D in cancer chemoprevention. *Pharm Biol* **2015,** *53* (10), 1399-434.

27. Al-Azhri, J.; Zhang, Y.; Bshara, W.; Zirpoli, G.; McCann, S. E.; Khoury, T.; Morrison, C. D.; Edge, S. B.; Ambrosone, C. B.; Yao, S., Tumor Expression of Vitamin D Receptor and Breast Cancer Histopathological Characteristics and Prognosis. *Clin Cancer Res* **2017,** *23* (1), 97-103.

28. Brożyna, A. A.; Jozwicki, W.; Janjetovic, Z.; Slominski, A. T., Expression of vitamin D receptor decreases during progression of pigmented skin lesions. *Hum Pathol* **2011,** *42* (5), 618-31.

29. Zhang, Y.; Guo, Q.; Zhang, Z.; Bai, N.; Liu, Z.; Xiong, M.; Wei, Y.; Xiang, R.; Tan, X., VDR status arbitrates the prometastatic effects of tumor-associated macrophages. *Mol Cancer Res* **2014,** *12* (8), 1181-91.

30. Lopes, N.; Sousa, B.; Martins, D.; Gomes, M.; Vieira, D.; Veronese, L. A.; Milanezi, F.; Paredes, J.; Costa, J. L.; Schmitt, F., Alterations in Vitamin D signalling and metabolic pathways in breast cancer progression: a study of VDR, CYP27B1 and CYP24A1 expression in benign and malignant breast lesions. *BMC Cancer* **2010,** *10*, 483.

31. Thill, M.; Fischer, D.; Kelling, K.; Hoellen, F.; Dittmer, C.; Hornemann, A.; Salehin, D.; Diedrich, K.; Friedrich, M.; Becker, S., Expression of vitamin D receptor (VDR), cyclooxygenase-2 (COX-2) and 15-hydroxyprostaglandin dehydrogenase (15-PGDH) in benign and malignant ovarian tissue and 25-hydroxycholecalciferol (25(OH2)D3) and prostaglandin E2 (PGE2) serum level in ovarian cancer patients. *J Steroid Biochem Mol Biol* **2010,** *121* (1-2), 387-90.

32. Hendrickson, W. K.; Flavin, R.; Kasperzyk, J. L.; Fiorentino, M.; Fang, F.; Lis, R.; Fiore, C.; Penney, K. L.; Ma, J.; Kantoff, P. W.; Stampfer, M. J.; Loda, M.; Mucci, L. A.; Giovannucci, E., Vitamin D receptor protein expression in tumor tissue and prostate cancer progression. *J Clin Oncol* **2011,** *29* (17), 2378-85.

33. Matusiak, D.; Benya, R. V., CYP27A1 and CYP24 expression as a function of malignant transformation in the colon. *J Histochem Cytochem* **2007,** *55* (12), 1257-64.

34. Horváth, H. C.; Lakatos, P.; Kósa, J. P.; Bácsi, K.; Borka, K.; Bises, G.; Nittke, T.; Hershberger, P. A.; Speer, G.; Kállay, E., The candidate oncogene CYP24A1: A potential biomarker for colorectal tumorigenesis. *J Histochem Cytochem* **2010,** *58* (3), 277-85.

35. Cross, H. S.; Bises, G.; Lechner, D.; Manhardt, T.; Kállay, E., The Vitamin D endocrine system of the gut--its possible role in colorectal cancer prevention. *J Steroid Biochem Mol Biol* **2005,** *97* (1-2), 121-8.

36. Brozek, W.; Manhardt, T.; Kállay, E.; Peterlik, M.; Cross, H. S., Relative Expression of Vitamin D Hydroxylases, CYP27B1 and CYP24A1, and of Cyclooxygenase-2 and Heterogeneity of Human Colorectal Cancer in Relation to Age, Gender, Tumor Location, and Malignancy: Results from Factor and Cluster Analysis. *Cancers (Basel)* **2012,** *4* (3), 763-76.

37. Mercer, P. F.; Chambers, R. C., Coagulation and coagulation signalling in fibrosis. *Biochimica et Biophysica Acta (BBA) - Molecular Basis of Disease* **2013,** *1832* (7), 1018-1027.

38. Liu, Y.-M.; Nepali, K.; Liou, J.-P., Idiopathic Pulmonary Fibrosis: Current Status, Recent Progress, and Emerging Targets. *Journal of Medicinal Chemistry* **2017,** *60* (2), 527-553.

39. Hu, L.; Xia, L.; Zhou, H.; Wu, B.; Mu, Y.; Wu, Y.; Yan, J., TF/FVIIa/PAR2 promotes cell proliferation and migration via PKCalpha and ERK-dependent c-Jun/AP-1 pathway in colon cancer cell line SW620. *Tumour Biol* **2013,** *34* (5), 2573-81.

40. Guo, D.; Zhou, H.; Wu, Y.; Zhou, F.; Xu, G.; Wen, H.; Zhang, X., Involvement of ERK1/2/NF-kappaB signal transduction pathway in TF/FVIIa/PAR2-induced proliferation and migration of colon cancer cell SW620. *Tumour Biol* **2011,** *32* (5), 921-30.

41. Martinez-Moreno, J. M.; Herencia, C.; Montes de Oca, A.; Muñoz-Castañeda, J. R.; Rodríguez-Ortiz, M. E.; Díaz-Tocados, J. M.; Peralbo-Santaella, E.; Camargo, A.; Canalejo, A.; Rodriguez, M.; Velasco-Gimena, F.; Almaden, Y., Vitamin D modulates tissue factor and protease-activated receptor 2 expression in vascular smooth muscle cells. *Faseb j* **2016,** *30* (3), 1367-76.

42. Tang, J.; Zhou, R.; Luger, D.; Zhu, W.; Silver, P. B.; Grajewski, R. S.; Su, S. B.; Chan, C. C.; Adorini, L.; Caspi, R. R., Calcitriol suppresses antiretinal autoimmunity through inhibitory effects on the Th17 effector response. *J Immunol* **2009,** *182* (8), 4624-32.

43. Pichler, J.; Gerstmayr, M.; Szépfalusi, Z.; Urbanek, R.; Peterlik, M.; Willheim, M., 1 alpha,25(OH)2D3 inhibits not only Th1 but also Th2 differentiation in human cord blood T cells. *Pediatr Res* **2002,** *52* (1), 12-8.

44. Matheu, V.; Bäck, O.; Mondoc, E.; Issazadeh-Navikas, S., Dual effects of vitamin D-induced alteration of TH1/TH2 cytokine expression: enhancing IgE production and decreasing airway eosinophilia in murine allergic airway disease. *J Allergy Clin Immunol* **2003,** *112* (3), 585-92.

45. Xystrakis, E.; Kusumakar, S.; Boswell, S.; Peek, E.; Urry, Z.; Richards, D. F.; Adikibi, T.; Pridgeon, C.; Dallman, M.; Loke, T. K.; Robinson, D. S.; Barrat, F. J.; O'Garra, A.; Lavender, P.; Lee, T. H.; Corrigan, C.; Hawrylowicz, C. M., Reversing the defective induction of IL-10-secreting regulatory T cells in glucocorticoid-resistant asthma patients. *J Clin Invest* **2006,** *116* (1), 146-55.

46. Fischer, K. D.; Agrawal, D. K., Erratum to: Vitamin D regulating TGF-β induced epithelial-mesenchymal transition. *Respir Res* **2015,** *16*, 139.

47. Bonventre, J. V., Antifibrotic vitamin D analogs. *J Clin Invest* **2013,** *123* (11), 4570-3.

48. Huang, L. S.; Natarajan, V., Sphingolipids in pulmonary fibrosis. *Adv Biol Regul* **2015,** *57*, 55-63.

49. Meng, X. M.; Nikolic-Paterson, D. J.; Lan, H. Y., TGF-β: the master regulator of fibrosis. *Nat Rev Nephrol* **2016,** *12* (6), 325-38.

50. Meng, X. M.; Tang, P. M.; Li, J.; Lan, H. Y., TGF-β/Smad signaling in renal fibrosis. *Front Physiol* **2015,** *6*, 82.

51. Wang, J.; Chen, L.; Chen, B.; Meliton, A.; Liu, S. Q.; Shi, Y.; Liu, T.; Deb, D. K.; Solway, J.; Li, Y. C., Chronic Activation of the Renin-Angiotensin System Induces Lung Fibrosis. *Sci Rep* **2015,** *5*, 15561.

52. Jiang, J. S.; Lang, Y. D.; Chou, H. C.; Shih, C. M.; Wu, M. Y.; Chen, C. M.; Wang, L. F., Activation of the renin-angiotensin system in hyperoxia-induced lung fibrosis in neonatal rats. *Neonatology* **2012,** *101* (1), 47-54.

53. Lang, Y. D.; Hung, C. L.; Wu, T. Y.; Wang, L. F.; Chen, C. M., The renin-angiotensin system mediates hyperoxia-induced collagen production in human lung fibroblasts. *Free Radic Biol Med* **2010,** *49* (1), 88-95.

54. Ferder, M.; Inserra, F.; Manucha, W.; Ferder, L., The world pandemic of vitamin D deficiency could possibly be explained by cellular inflammatory response activity induced by the renin-angiotensin system. *Am J Physiol Cell Physiol* **2013,** *304* (11), C1027-39.

55. Wang, Z.; Zhang, H.; Sun, X.; Ren, L., The protective role of vitamin D3 in a murine model of asthma via the suppression of TGF-beta/Smad signaling and activation of the Nrf2/HO-1 pathway. *Mol Med Rep* **2016,** *14* (3), 2389-96.

56. Ito, I.; Waku, T.; Aoki, M.; Abe, R.; Nagai, Y.; Watanabe, T.; Nakajima, Y.; Ohkido, I.; Yokoyama, K.; Miyachi, H.; Shimizu, T.; Murayama, A.; Kishimoto, H.; Nagasawa, K.; Yanagisawa, J., A nonclassical vitamin D receptor pathway suppresses renal fibrosis. *J Clin Invest* **2013,** *123* (11), 4579-94.

57. Zerr, P.; Vollath, S.; Palumbo-Zerr, K.; Tomcik, M.; Huang, J.; Distler, A.; Beyer, C.; Dees, C.; Gela, K.; Distler, O.; Schett, G.; Distler, J. H. W., Vitamin D receptor regulates TGF-β signalling in systemic sclerosis. *Annals of the Rheumatic Diseases* **2015,** *74* (3), e20.

58. Shany, S.; Sigal-Batikoff, I.; Lamprecht, S., Vitamin D and Myofibroblasts in Fibrosis and Cancer: At Cross-purposes with TGF-β/SMAD Signaling. *Anticancer Res* **2016,** *36* (12), 6225-6234.

59. Sahai, E.; Astsaturov, I.; Cukierman, E.; DeNardo, D. G.; Egeblad, M.; Evans, R. M.; Fearon, D.; Greten, F. R.; Hingorani, S. R.; Hunter, T.; Hynes, R. O.; Jain, R. K.; Janowitz, T.; Jorgensen, C.; Kimmelman, A. C.; Kolonin, M. G.; Maki, R. G.; Powers, R. S.; Puré, E.; Ramirez, D. C.; Scherz-Shouval, R.; Sherman, M. H.; Stewart, S.; Tlsty, T. D.; Tuveson, D. A.; Watt, F. M.; Weaver, V.; Weeraratna, A. T.; Werb, Z., A framework for advancing our understanding of cancer-associated fibroblasts. *Nature Reviews Cancer* **2020,** *20* (3), 174-186.

60. Ferrer-Mayorga, G.; Gómez-López, G.; Barbáchano, A.; Fernández-Barral, A.; Peña, C.; Pisano, D. G.; Cantero, R.; Rojo, F.; Muñoz, A.; Larriba, M. J., Vitamin D receptor expression and associated gene signature in tumour stromal fibroblasts predict clinical outcome in colorectal cancer. *Gut* **2017,** *66* (8), 1449-1462.

61. Sherman, M. H.; Yu, R. T.; Engle, D. D.; Ding, N.; Atkins, A. R.; Tiriac, H.; Collisson, E. A.; Connor, F.; Van Dyke, T.; Kozlov, S.; Martin, P.; Tseng, T. W.; Dawson, D. W.; Donahue, T. R.; Masamune, A.; Shimosegawa, T.; Apte, M. V.; Wilson, J. S.; Ng, B.; Lau, S. L.; Gunton, J. E.; Wahl, G. M.; Hunter, T.; Drebin, J. A.; O'Dwyer, P. J.; Liddle, C.; Tuveson, D. A.; Downes, M.; Evans, R. M., Vitamin D receptor-mediated stromal reprogramming suppresses pancreatitis and enhances pancreatic cancer therapy. *Cell* **2014,** *159* (1), 80-93.

62. COLSTON, K.; COLSTON, M. J.; FELDMAN, D., 1,25-DIHYDROXYVITAMIN D3 AND MALIGNANT MELANOMA: THE PRESENCE OF RECEPTORS AND INHIBITION OF CELL GROWTH IN CULTURE. *Endocrinology* **1981,** *108* (3), 1083-1086.

63. Campbell, M. J.; Gombart, A. F.; Kwok, S. H.; Park, S.; Koeffler, H. P., The anti-proliferative effects of 1α,25(OH)2D3 on breast and prostate cancer cells are associated with induction of BRCA1 gene expression. *Oncogene* **2000,** *19* (44), 5091-5097.

64. Samuel, S.; Sitrin, M. D., Vitamin D's role in cell proliferation and differentiation. *Nutrition Reviews* **2008,** *66* (suppl_2), S116-S124.

65. Massagué, J., TGFbeta in Cancer. *Cell* **2008,** *134* (2), 215-30.

66. Chen, A.; Davis, B. H.; Sitrin, M. D.; Brasitus, T. A.; Bissonnette, M., Transforming growth factor-beta 1 signaling contributes to Caco-2 cell growth inhibition induced by 1,25(OH)(2)D(3). *Am J Physiol Gastrointest Liver Physiol* **2002,** *283* (4), G864-74.

67. Daniel, C.; Schroder, O.; Zahn, N.; Gaschott, T.; Steinhilber, D.; Stein, J. M., The TGFβ/Smad 3-signaling pathway is involved in butyrate-mediated vitamin D receptor (VDR)-expression. *Journal of Cellular Biochemistry* **2007,** *102* (6), 1420-1431.

68. Koli, K.; Keski-Oja, J., 1,25-Dihydroxyvitamin D₃ Enhances the Expression of Transforming Growth Factor β1 and Its Latent Form Binding Protein in Cultured Breast Carcinoma Cells. *Cancer Research* **1995,** *55* (7), 1540.

69. Tu, H.; Flanders, W. D.; Ahearn, T. U.; Daniel, C. R.; Gonzalez-Feliciano, A. G.; Long, Q.; Rutherford, R. E.; Bostick, R. M., Effects of calcium and vitamin D3 on transforming growth factors in rectal mucosa of sporadic colorectal adenoma patients: A randomized controlled trial. *Molecular Carcinogenesis* **2015,** *54* (4), 270-280.

70. Bizzarri, M.; Cucina, A.; Valente, M. G.; Tagliaferri, F.; Borrelli, V.; Stipa, F.; Cavallaro, A., Melatonin and vitamin D3 increase TGF-β1 release and induce growth inhibition in breast cancer cell cultures. *Journal of Surgical Research* **2003,** *110* (2), 332-337.

71. Yang, L.; Yang, J.; Venkateswarlu, S.; Ko, T.; Brattain, M. G., Autocrine TGFβ signaling mediates vitamin D3 analog-induced growth inhibition in breast cells. *Journal of Cellular Physiology* **2001,** *188* (3), 383-393.

72. Giammanco, M.; Di Majo, D.; La Guardia, M.; Aiello, S.; Crescimannno, M.; Flandina, C.; Tumminello, F. M.; Leto, G., Vitamin D in cancer chemoprevention. *Pharmaceutical Biology* **2015,** *53* (10), 1399-1434.

73. Mantovani, A.; Allavena, P.; Sica, A.; Balkwill, F., Cancer-related inflammation. *Nature* **2008,** *454* (7203), 436-44.

74. Nonn, L.; Peng, L.; Feldman, D.; Peehl, D. M., Inhibition of p38 by vitamin D reduces interleukin-6 production in normal prostate cells via mitogen-activated protein kinase phosphatase 5: implications for prostate cancer prevention by vitamin D. *Cancer Res* **2006,** *66* (8), 4516-24.

75. Hidaka, M.; Wakabayashi, I.; Takeda, Y.; Fukuzawa, K., Vitamin D_3 derivatives increase soluble CD14 release through ERK1/2 activation and decrease IL-8 production in intestinal epithelial cells. *Eur J Pharmacol* **2013,** *721* (1-3), 305-12.

76. Wang, Q.; He, Y.; Shen, Y.; Zhang, Q.; Chen, D.; Zuo, C.; Qin, J.; Wang, H.; Wang, J.; Yu, Y., Vitamin D inhibits COX-2 expression and inflammatory response by targeting thioesterase superfamily member 4. *J Biol Chem* **2014,** *289* (17), 11681-94.

77. Olson, K. C.; Kulling, P. M.; Olson, T. L.; Tan, S.-F.; Rainbow, R. J.; Feith, D. J.; Loughran, T. P., Jr., Vitamin D decreases STAT phosphorylation and inflammatory cytokine output in T-LGL leukemia. *Cancer Biol Ther* **2017,** *18* (5), 290-303.

78. Liu, W.; Zhang, L.; Xu, H.-J.; Li, Y.; Hu, C.-M.; Yang, J.-Y.; Sun, M.-Y., The Anti-Inflammatory Effects of Vitamin D in Tumorigenesis. *International journal of molecular sciences* **2018,** *19* (9), 2736.

79. Jeon, S.-M.; Shin, E.-A., Exploring vitamin D metabolism and function in cancer. *Experimental & molecular medicine* **2018,** *50* (4), 20-20.

80. Nagpal, S.; Na, S.; Rathnachalam, R., Noncalcemic actions of vitamin D receptor ligands. *Endocr Rev* **2005,** *26* (5), 662-87.

81. Jin, T.; Guo, Y.; Huang, Z.; Zhang, Q.; Huang, Z.; Zhang, Y.; Huang, Z., Vitamin D inhibits the proliferation of Oral Squamous Cell Carcinoma by suppressing lncRNA LUCAT1 through the MAPK pathway. *J Cancer* **2020,** *11* (20), 5971-5981.

82. Thill, M.; Woeste, A.; Reichert, K.; Fischer, D.; Rody, A.; Friedrich, M.; Koster, F., Vitamin D inhibits ovarian cancer cell line proliferation in combination with celecoxib and suppresses cyclooxygenase-2 expression. *Anticancer Res* **2015,** *35* (2), 1197-203.

83. Consiglio, M.; Destefanis, M.; Morena, D.; Foglizzo, V.; Forneris, M.; Pescarmona, G.; Silvagno, F., The vitamin D receptor inhibits the respiratory chain, contributing to the metabolic switch that is essential for cancer cell proliferation. *PLoS One* **2014,** *9* (12), e115816.

84. Pilon, C.; Urbanet, R.; Williams, T. A.; Maekawa, T.; Vettore, S.; Sirianni, R.; Pezzi, V.; Mulatero, P.; Fassina, A.; Sasano, H.; Fallo, F., 1alpha,25-Dihydroxyvitamin D(3) inhibits the human H295R cell proliferation by cell cycle arrest: a model for a protective role of vitamin D receptor against adrenocortical cancer. *J Steroid Biochem Mol Biol* **2014,** *140*, 26-33.

85. Tang, J. Y.; Xiao, T. Z.; Oda, Y.; Chang, K. S.; Shpall, E.; Wu, A.; So, P. L.; Hebert, J.; Bikle, D.; Epstein, E. H., Jr., Vitamin D3 inhibits hedgehog signaling and proliferation in murine Basal cell carcinomas. *Cancer Prev Res (Phila)* **2011,** *4* (5), 744-51.

86. Blauer, M.; Rovio, P. H.; Ylikomi, T.; Heinonen, P. K., Vitamin D inhibits myometrial and leiomyoma cell proliferation in vitro. *Fertil Steril* **2009,** *91* (5), 1919-25.

87. Sutton, A. L.; Zhang, X.; Ellison, T. I.; Macdonald, P. N., The 1,25(OH)2D3-regulated transcription factor MN1 stimulates vitamin D receptor-mediated transcription and inhibits osteoblastic cell proliferation. *Mol Endocrinol* **2005,** *19* (9), 2234-44.

88. Szabo, A.; Merke, J.; Beier, E.; Mall, G.; Ritz, E., 1,25(OH)2 vitamin D3 inhibits parathyroid cell proliferation in experimental uremia. *Kidney Int* **1989,** *35* (4), 1049-56.

89. Dusso, A. S.; Brown, A. J.; Slatopolsky, E., Vitamin D. *Am J Physiol Renal Physiol* **2005,** *289* (1), F8-28.

90. Masuda, S.; Jones, G., Promise of vitamin D analogues in the treatment of hyperproliferative conditions. *Mol Cancer Ther* **2006,** *5* (4), 797-808.

91. Banerjee, P.; Chatterjee, M., Antiproliferative role of vitamin D and its analogs--a brief overview. *Mol Cell Biochem* **2003,** *253* (1-2), 247-54.

92. Samuel, S.; Sitrin, M. D., Vitamin D's role in cell proliferation and differentiation. *Nutr Rev* **2008,** *66* (10 Suppl 2), S116-24.

93. Larriba, M. J.; González-Sancho, J. M.; Barbáchano, A.; Niell, N.; Ferrer-Mayorga, G.; Muñoz, A., Vitamin D Is a Multilevel Repressor of Wnt/b-Catenin Signaling in Cancer Cells. *Cancers (Basel)* **2013,** *5* (4), 1242-60.

94. Pendás-Franco, N.; García, J. M.; Peña, C.; Valle, N.; Pálmer, H. G.; Heinäniemi, M.; Carlberg, C.; Jiménez, B.; Bonilla, F.; Muñoz, A.; González-Sancho, J. M., DICKKOPF-4 is induced by TCF/beta-catenin and upregulated in human colon cancer, promotes tumour cell invasion and angiogenesis and is repressed by 1alpha,25-dihydroxyvitamin D3. *Oncogene* **2008,** *27* (32), 4467-77.

95. An, B. S.; Tavera-Mendoza, L. E.; Dimitrov, V.; Wang, X.; Calderon, M. R.; Wang, H. J.; White, J. H., Stimulation of Sirt1-regulated FoxO protein function by the ligand-bound vitamin D receptor. *Mol Cell Biol* **2010,** *30* (20), 4890-900.

96. Alvarez-Díaz, S.; Larriba, M. J.; López-Otín, C.; Muñoz, A., Vitamin D: Proteases, protease inhibitors and cancer. *Cell Cycle* **2010,** *9* (1), 32-7.

97. Lopez-Lopez, N.; Gonzalez-Curiel, I.; Trevino-Santa Cruz, M. B.; Rivas-Santiago, B.; Trujillo-Paez, V.; Enciso-Moreno, J. A.; Serrano, C. J., Expression and vitamin D-mediated regulation of matrix metalloproteinases (MMPs) and tissue inhibitors of metalloproteinases (TIMPs) in healthy skin and in diabetic foot ulcers. *Arch Dermatol Res* **2014,** *306* (9), 809-21.

98. Koli, K.; Keski-Oja, J., 1alpha,25-dihydroxyvitamin D3 and its analogues down-regulate cell invasion-associated proteases in cultured malignant cells. *Cell Growth Differ* **2000,** *11* (4), 221-9.

99. Bao, B. Y.; Yeh, S. D.; Lee, Y. F., 1alpha,25-dihydroxyvitamin D3 inhibits prostate cancer cell invasion via modulation of selective proteases. *Carcinogenesis* **2006,** *27* (1), 32-42.

100. Díaz, G. D.; Paraskeva, C.; Thomas, M. G.; Binderup, L.; Hague, A., Apoptosis is induced by the active metabolite of vitamin D3 and its analogue EB1089 in colorectal adenoma and carcinoma cells: possible implications for prevention and therapy. *Cancer Res* **2000,** *60* (8), 2304-12.

101. Salvesen, G. S.; Dixit, V. M., Caspases: intracellular signaling by proteolysis. *Cell* **1997,** *91* (4), 443-6.

102. Cory, S.; Adams, J. M., The Bcl2 family: regulators of the cellular life-or-death switch. *Nat Rev Cancer* **2002,** *2* (9), 647-56.

103. Liu, X.; Kim, C. N.; Yang, J.; Jemmerson, R.; Wang, X., Induction of apoptotic program in cell-free extracts: requirement for dATP and cytochrome c. *Cell* **1996,** *86* (1), 147-57.

104. Smith, D. W.; Lemli, L.; Opitz, J. M., A newly recognized syndromeof multiple congenital anomalies. *The Journal of Pediatrics* **1964,** *64* (2), 210-217.

105. Björkhem, I.; Starck, L.; Andersson, U.; Lütjohann, D.; von Bahr, S.; Pikuleva, I.; Babiker, A.; Diczfalusy, U., Oxysterols in the circulation of patients with the Smith-Lemli-Opitz syndrome: abnormal levels of 24S- and 27-hydroxycholesterol. *J Lipid Res* **2001,** *42* (3), 366-71.

106. Batta, A. K.; Tint, G. S.; Shefer, S.; Abuelo, D.; Salen, G., Identification of 8-dehydrocholesterol (cholesta-5,8-dien-3 beta-ol) in patients with Smith-Lemli-Opitz syndrome. *Journal of Lipid Research* **1995,** *36* (4), 705-713.

107. Griffiths, W. J.; Abdel-Khalik, J.; Crick, P. J.; Ogundare, M.; Shackleton, C. H.; Tuschl, K.; Kwok, M. K.; Bigger, B. W.; Morris, A. A.; Honda, A.; Xu, L.; Porter, N. A.; Björkhem, I.; Clayton, P. T.; Wang, Y., Sterols and oxysterols in plasma from Smith-Lemli-Opitz syndrome patients. *The Journal of Steroid Biochemistry and Molecular Biology* **2017,** *169*, 77-87.

108. Goyal, S.; Xiao, Y.; Porter, N. A.; Xu, L.; Guengerich, F. P., Oxidation of 7-dehydrocholesterol and desmosterol by human cytochrome P450 46A1. *J Lipid Res* **2014,** *55* (9), 1933-43.

109. Xu, L.; Korade, Z.; Rosado, D. A., Jr.; Mirnics, K.; Porter, N. A., Metabolism of oxysterols derived from nonenzymatic oxidation of 7-dehydrocholesterol in cells. *J Lipid Res* **2013,** *54* (4), 1135-43.

110. Shinkyo, R.; Xu, L.; Tallman, K. A.; Cheng, Q.; Porter, N. A.; Guengerich, F. P., Conversion of 7-dehydrocholesterol to 7-ketocholesterol is catalyzed by human cytochrome P450 7A1 and occurs by direct oxidation without an epoxide intermediate. *J Biol Chem* **2011,** *286* (38), 33021-8.

111. Xu, L.; Korade, Z.; Rosado, D. A., Jr.; Liu, W.; Lamberson, C. R.; Porter, N. A., An oxysterol biomarker for 7-dehydrocholesterol oxidation in cell/mouse models for Smith-Lemli-Opitz syndrome. *J Lipid Res* **2011,** *52* (6), 1222-33.

112. Xu, L.; Korade, Z.; Porter, N. A., Oxysterols from free radical chain oxidation of 7-dehydrocholesterol: product and mechanistic studies. *J Am Chem Soc* **2010,** *132* (7), 2222-32.

113. Brown, A. J.; Jessup, W., Oxysterols: Sources, cellular storage and metabolism, and new insights into their roles in cholesterol homeostasis. *Mol Aspects Med* **2009,** *30* (3), 111-22.

114. Kulig, W.; Cwiklik, L.; Jurkiewicz, P.; Rog, T.; Vattulainen, I., Cholesterol oxidation products and their biological importance. *Chem Phys Lipids* **2016,** *199*, 144-160.

115. Appukuttan, A.; Kasseckert, S. A.; Kumar, S.; Reusch, H. P.; Ladilov, Y., Oxysterol-induced apoptosis of smooth muscle cells is under the control of a soluble adenylyl cyclase. *Cardiovasc Res* **2013,** *99* (4), 734-42.

116. Miah, S.; Zadeh, S. N.; Yuan, X. M.; Li, W., Expression of Egr1 and p53 in human carotid plaques and apoptosis induced by 7-oxysterol or p53. *Exp Toxicol Pathol* **2013,** *65* (5), 677-82.

117. Liu, H.; Zhang, C.; Huang, K., Lanthanum chloride suppresses oxysterol-induced ECV-304 cell apoptosis via inhibition of intracellular Ca(2+) concentration elevation, oxidative stress, and activation of ERK and NF-kappaB signaling pathways. *J Biol Inorg Chem* **2011,** *16* (5), 671-81.

118. Huang, Z. Y.; Liu, Q. P.; Li, W. Z.; Wang, R. J.; Chi, Y.; Liu, Y. Y.; Zhang, Q. M., [The apoptosis of mouse macrophage J774A.1 induced by oxysterol depend on NF-kappaB activation]. *Xi Bao Yu Fen Zi Mian Yi Xue Za Zhi* **2009,** *25* (10), 879-82.

119. Perales, S.; Alejandre, M. J.; Palomino-Morales, R.; Torres, C.; Iglesias, J.; Linares, A., Effect of oxysterol-induced apoptosis of vascular smooth muscle cells on experimental hypercholesterolemia. *J Biomed Biotechnol* **2009,** *2009*, 456208.

120. Freeman-Anderson, N. E.; Pickle, T. G.; Netherland, C. D.; Bales, A.; Buckley, N. E.; Thewke, D. P., Cannabinoid (CB2) receptor deficiency reduces the susceptibility of macrophages to oxidized LDL/oxysterol-induced apoptosis. *J Lipid Res* **2008,** *49* (11), 2338-46.

121. Nakazawa, T.; Xui, N.; Hesong, Z.; Kinoshita, M.; Chiba, T.; Kaneko, E.; Yui, K.; Shimokado, K., Danshen inhibits oxysterol-induced endothelial cell apoptosis in vivo. *J Atheroscler Thromb* **2005,** *12* (3), 132-7.

122. Freeman, N. E.; Rusinol, A. E.; Linton, M.; Hachey, D. L.; Fazio, S.; Sinensky, M. S.; Thewke, D., Acyl-coenzyme A:cholesterol acyltransferase promotes oxidized LDL/oxysterol-induced apoptosis in macrophages. *J Lipid Res* **2005,** *46* (9), 1933-43.

123. Miyashita, Y.; Ozaki, H.; Koide, N.; Otsuka, M.; Oyama, T.; Itoh, Y.; Mastuzaka, T.; Shirai, K., Oxysterol-induced apoptosis of vascular smooth muscle cells is reduced by HMG-CoA reductase inhibitor, pravastatin. *J Atheroscler Thromb* **2002,** *9* (1), 65-71.

124. Panini, S. R.; Sinensky, M. S., Mechanisms of oxysterol-induced apoptosis. *Curr Opin Lipidol* **2001,** *12* (5), 529-33.

125. Aupeix, K.; Weltin, D.; Mejia, J. E.; Christ, M.; Marchal, J.; Freyssinet, J. M.; Bischoff, P., Oxysterol-induced apoptosis in human monocytic cell lines. *Immunobiology* **1995,** *194* (4-5), 415-28.

126. Bakos, J. T.; Johnson, B. H.; Thompson, E. B., Oxysterol-induced cell death in human leukemic T-cells correlates with oxysterol binding protein occupancy and is independent of glucocorticoid-induced apoptosis. *J Steroid Biochem Mol Biol* **1993,** *46* (4), 415-26.

127. Kang, K. A.; Chae, S.; Lee, K. H.; Park, M. T.; Lee, S. J.; Lee, Y. S.; Hyun, J. W., Cytotoxic effect of 7beta-hydroxycholesterol on human NCI-H460 lung cancer cells. *Biol Pharm Bull* **2005,** *28* (8), 1377-80.

128. Lee, T.; Chau, L., Fas/Fas ligand-mediated death pathway is involved in oxLDL-induced apoptosis in vascular smooth muscle cells. *Am J Physiol Cell Physiol* **2001,** *280* (3), C709-18.

129. Xu, L.; Korade, Z.; Porter, N. A., Oxysterols from Free Radical Chain Oxidation of 7-Dehydrocholesterol: Product and Mechanistic Studies. *Journal of the American Chemical Society* **2010,** *132* (7), 2222-2232.

130. Porter, N. A.; Caldwell, S. E.; Mills, K. A., Mechanisms of free radical oxidation of unsaturated lipids. *Lipids* **1995,** *30* (4), 277-90.

131. Yin, H.; Porter, N. A., New insights regarding the autoxidation of polyunsaturated fatty acids. *Antioxid Redox Signal* **2005,** *7* (1-2), 170-84.

132. Barrera, G., Oxidative stress and lipid peroxidation products in cancer progression and therapy. *ISRN Oncol* **2012,** *2012*, 137289-137289.

133. Lü, J. M.; Lin, P. H.; Yao, Q.; Chen, C., Chemical and molecular mechanisms of antioxidants: experimental approaches and model systems. *J Cell Mol Med* **2010,** *14* (4), 840-60.

134. Weisiger, R. A.; Fridovich, I., Superoxide dismutase. Organelle specificity. *J Biol Chem* **1973,** *248* (10), 3582-92.

135. Wu, W. S., The signaling mechanism of ROS in tumor progression. *Cancer Metastasis Rev* **2006,** *25* (4), 695-705.

136. Allen, C.; Her, S.; Jaffray, D. A., Radiotherapy for Cancer: Present and Future. *Adv Drug Deliv Rev* **2017,** *109*, 1-2.

137. Zou, Z.; Chang, H.; Li, H.; Wang, S., Induction of reactive oxygen species: an emerging approach for cancer therapy. *Apoptosis* **2017,** *22* (11), 1321-1335.

138. Kim, W.; Lee, S.; Seo, D.; Kim, D.; Kim, K.; Kim, E.; Kang, J.; Seong, K. M.; Youn, H.; Youn, B., Cellular Stress Responses in Radiotherapy. *Cells* **2019,** *8* (9), 1105.

139. Yin, H.; Xu, L.; Porter, N. A., Free radical lipid peroxidation: mechanisms and analysis. *Chem Rev* **2011,** *111* (10), 5944-72.

140. Cadenas, E.; Muller, A.; Brigelius, R.; Esterbauer, H.; Sies, H., Effects of 4-hydroxynonenal on isolated hepatocytes. Studies on chemiluminescence response, alkane production and glutathione status. *Biochem J* **1983,** *214* (2), 479-87.

141. Esterbauer, H.; Cheeseman, K. H.; Dianzani, M. U.; Poli, G.; Slater, T. F., Separation and characterization of the aldehydic products of lipid peroxidation stimulated by ADP-Fe2+ in rat liver microsomes. *Biochem J* **1982,** *208* (1), 129-40.

142. Benedetti, A.; Fulceri, R.; Ferrali, M.; Ciccoli, L.; Esterbauer, H.; Comporti, M., Detection of carbonyl functions in phospholipids of liver microsomes in CCl4- and BrCCl3-poisoned rats. *Biochim Biophys Acta* **1982,** *712* (3), 628-38.

143. Curzio, M.; Torrielli, M. V.; Giroud, J. P.; Esterbauer, H.; Dianzani, M. U., Neutrophil chemotactic responses to aldehydes. *Res Commun Chem Pathol Pharmacol* **1982,** *36* (3), 463-76.

144. Benedetti, A.; Esterbauer, H.; Ferrali, M.; Fulceri, R.; Comporti, M., Evidence for aldehydes bound to liver microsomal protein following CCl4 or BrCCl3 poisoning. *Biochim Biophys Acta* **1982,** *711* (2), 345-56.

145. Negro, F.; Curzio, M.; Torrielli, M. V.; Esterbauer, H.; Dianzani, M. U., [Preliminary data on the influence of 4-hydroxyalkenals on the phagocytic activity polymorphonuclear leukocytes in the rat]. *Boll Soc Ital Biol Sper* **1981,** *57* (24), 2472-8.

146. Benedetti, A.; Comporti, M.; Esterbauer, H., Identification of 4-hydroxynonenal as a cytotoxic product originating from the peroxidation of liver microsomal lipids. *Biochim Biophys Acta* **1980,** *620* (2), 281-96.

147. Esterbauer, H.; Schaur, R. J.; Zollner, H., Chemistry and biochemistry of 4-hydroxynonenal, malonaldehyde and related aldehydes. *Free Radic Biol Med* **1991,** *11* (1), 81-128.

148. Pizzimenti, S.; Ciamporcero, E.; Daga, M.; Pettazzoni, P.; Arcaro, A.; Cetrangolo, G.; Minelli, R.; Dianzani, C.; Lepore, A.; Gentile, F.; Barrera, G., Interaction of aldehydes derived from lipid peroxidation and membrane proteins. *Front Physiol* **2013,** *4*, 242.

149. Traverso, N.; Menini, S.; Maineri, E. P.; Patriarca, S.; Odetti, P.; Cottalasso, D.; Marinari, U. M.; Pronzato, M. A., Malondialdehyde, a lipoperoxidation-derived aldehyde, can bring about secondary oxidative damage to proteins. *J Gerontol A Biol Sci Med Sci* **2004,** *59* (9), B890-5.

150. Niedernhofer, L. J.; Daniels, J. S.; Rouzer, C. A.; Greene, R. E.; Marnett, L. J., Malondialdehyde, a product of lipid peroxidation, is mutagenic in human cells. *J Biol Chem* **2003,** *278* (33), 31426-33.

151. Marnett, L. J., Lipid peroxidation-DNA damage by malondialdehyde. *Mutat Res* **1999,** *424* (1-2), 83-95.

152. Miyake, T.; Reese, J.; Loch, C. M.; Auble, D. T.; Li, R., Genome-wide Analysis of ARS (Autonomously Replicating Sequence) Binding Factor 1 (Abf1p)-mediated Transcriptional Regulation in Saccharomyces cerevisiae*. *Journal of Biological Chemistry* **2004,** *279* (33), 34865-34872.

153. Demple, B.; Harrison, L., Repair of oxidative damage to DNA: enzymology and biology. *Annu Rev Biochem* **1994,** *63*, 915-48.

154. Ramanathan, B.; Jan, K. Y.; Chen, C. H.; Hour, T. C.; Yu, H. J.; Pu, Y. S., Resistance to paclitaxel is proportional to cellular total antioxidant capacity. *Cancer Res* **2005,** *65* (18), 8455-60.

155. Niture, S. K.; Jaiswal, A. K., Nrf2 protein up-regulates antiapoptotic protein Bcl-2 and prevents cellular apoptosis. *J Biol Chem* **2012,** *287* (13), 9873-86.

156. Hour, T. C.; Huang, C. Y.; Lin, C. C.; Chen, J.; Guan, J. Y.; Lee, J. M.; Pu, Y. S., Characterization of molecular events in a series of bladder urothelial carcinoma cell lines with progressive resistance to arsenic trioxide. *Anticancer Drugs* **2004,** *15* (8), 779-85.

Chapter 2:

1. Delaney, G.; Jacob, S.; Featherstone, C.; Barton, M., The role of radiotherapy in cancer treatment: estimating optimal utilization from a review of evidence-based clinical guidelines. *Cancer* **2005,** *104* (6), 1129-37.

2. Begg, A. C.; Stewart, F. A.; Vens, C., Strategies to improve radiotherapy with targeted drugs. *Nat Rev Cancer* **2011,** *11* (4), 239-53.

3. McKelvey, K. J.; Hudson, A. L.; Prasanna Kumar, R.; Eade, T.; Clarke, S. J.; Wheeler, H. R.; Diakos, C. I.; Howell, V. M., Sub-acute Toxicity in Non-cancerous Tissue and Immune-Related Adverse Events of a Novel Combination Therapy for Cancer. *Front Oncol* **2019,** *9*, 1504.

4. Burbach, J. P.; den Harder, A. M.; Intven, M.; van Vulpen, M.; Verkooijen, H. M.; Reerink, O., Impact of radiotherapy boost on pathological complete response in patients with locally advanced rectal cancer: a systematic review and meta-analysis. *Radiother Oncol* **2014,** *113* (1), 1-9.

5. Gustavsson, B.; Carlsson, G.; Machover, D.; Petrelli, N.; Roth, A.; Schmoll, H. J.; Tveit, K. M.; Gibson, F., A review of the evolution of systemic chemotherapy in the management of colorectal cancer. *Clin Colorectal Cancer* **2015,** *14* (1), 1-10.

6. Engstrom, P. F.; Arnoletti, J. P.; Benson, A. B., 3rd; Chen, Y. J.; Choti, M. A.; Cooper, H. S.; Covey, A.; Dilawari, R. A.; Early, D. S.; Enzinger, P. C.; Fakih, M. G.; Fleshman, J., Jr.; Fuchs, C.; Grem, J. L.; Kiel, K.; Knol, J. A.; Leong, L. A.; Lin, E.; Mulcahy, M. F.; Rao, S.; Ryan, D. P.; Saltz, L.; Shibata, D.; Skibber, J. M.; Sofocleous, C.;

Thomas, J.; Venook, A. P.; Willett, C.; National Comprehensive Cancer, N., NCCN Clinical Practice Guidelines in Oncology: colon cancer. *J Natl Compr Canc Netw* **2009,** *7* (8), 778-831.

7. Babaei, M.; Jansen, L.; Balavarca, Y.; Sjovall, A.; Bos, A.; van de Velde, T.; Moreau, M.; Liberale, G.; Goncalves, A. F.; Bento, M. J.; Ulrich, C. M.; Schrotz-King, P.; Lemmens, V.; Glimelius, B.; Brenner, H., Neoadjuvant Therapy in Rectal Cancer Patients With Clinical Stage II to III Across European Countries: Variations and Outcomes. *Clin Colorectal Cancer* **2018,** *17* (1), e129-e142.

8. Beppu, N.; Yanagi, H.; Tomita, N., A review of preoperative chemoradiotherapy for lower rectal cancer. *J Anus Rectum Colon* **2017,** *1* (3), 65-73.

9. Restivo, A.; Delrio, P.; Deidda, S.; Spolverato, G.; Rega, D.; Cerci, M.; Barina, A.; Perin, A.; Pace, U.; Zorcolo, L.; Pucciarelli, S., Predictors of Early Distant Relapse in Rectal Cancer Patients Submitted to Preoperative Chemoradiotherapy. *Oncol Res Treat* **2020,** *43* (4), 146-152.

10. Xu, L.; Korade, Z.; Porter, N. A., Oxysterols from Free Radical Chain Oxidation of 7-Dehydrocholesterol: Product and Mechanistic Studies. *Journal of the American Chemical Society* **2010,** *132* (7), 2222-2232.

11. Korade, Z.; Xu, L.; Mirnics, K.; Porter, N. A., Lipid biomarkers of oxidative stress in a genetic mouse model of Smith-Lemli-Opitz syndrome. *J Inherit Metab Dis* **2013,** *36* (1), 113-22.

12. Korade, Z.; Xu, L.; Shelton, R.; Porter, N. A., Biological activities of 7-dehydrocholesterol-derived oxysterols: implications for Smith-Lemli-Opitz syndrome. *J Lipid Res* **2010,** *51* (11), 3259-69.

13. Lamberson, C. R.; Muchalski, H.; McDuffee, K. B.; Tallman, K. A.; Xu, L.; Porter, N. A., Propagation rate constants for the peroxidation of sterols on the biosynthetic pathway to cholesterol. *Chem Phys Lipids* **2017,** *207* (Pt B), 51-58.

14. Porter, N. A., A perspective on free radical autoxidation: the physical organic chemistry of polyunsaturated fatty acid and sterol peroxidation. *J Org Chem* **2013,** *78* (8), 3511-24.

15. Valencia, A.; Rajadurai, A.; Carle, A. B.; Kochevar, I. E., 7-Dehydrocholesterol enhances ultraviolet A-induced oxidative stress in keratinocytes: roles of NADPH oxidase, mitochondria, and lipid rafts. *Free Radic Biol Med* **2006,** *41* (11), 1704-18.

16. Xu, L.; Davis, T. A.; Porter, N. A., Rate constants for peroxidation of polyunsaturated fatty acids and sterols in solution and in liposomes. *J Am Chem Soc* **2009,** *131* (36), 13037-44.

17. Xu, L.; Korade, Z.; Porter, N. A., Oxysterols from free radical chain oxidation of 7-dehydrocholesterol: product and mechanistic studies. *J Am Chem Soc* **2010,** *132* (7), 2222-32.

18. Xu, L.; Porter, N. A., Reactivities and products of free radical oxidation of cholestadienols. *J Am Chem Soc* **2014,** *136* (14), 5443-50.

19. Xu, L.; Porter, N. A., Free radical oxidation of cholesterol and its precursors: Implications in cholesterol biosynthesis disorders. *Free Radic Res* **2015,** *49* (7), 835-49.

20. Xu, L.; Korade, Z.; Rosado, D. A., Jr.; Liu, W.; Lamberson, C. R.; Porter, N. A., An oxysterol biomarker for 7-dehydrocholesterol oxidation in cell/mouse models for Smith-Lemli-Opitz syndrome. *J Lipid Res* **2011,** *52* (6), 1222-33.

21. Xu, L.; Liu, W.; Sheflin, L. G.; Fliesler, S. J.; Porter, N. A., Novel oxysterols observed in tissues and fluids of AY9944-treated rats: a model for Smith-Lemli-Opitz syndrome. *J Lipid Res* **2011,** *52* (10), 1810-20.

22. Xu, L.; Sheflin, L. G.; Porter, N. A.; Fliesler, S. J., 7-Dehydrocholesterol-derived oxysterols and retinal degeneration in a rat model of Smith-Lemli-Opitz syndrome. *Biochim Biophys Acta* **2012,** *1821* (6), 877-83.

23. Windsor, K.; Genaro-Mattos, T. C.; Kim, H. Y.; Liu, W.; Tallman, K. A.; Miyamoto, S.; Korade, Z.; Porter, N. A., Probing lipid-protein adduction with alkynyl surrogates: application to Smith-Lemli-Opitz syndrome. *J Lipid Res* **2013,** *54* (10), 2842-50.

24. Meljon, A.; Watson, G. L.; Wang, Y.; Shackleton, C. H.; Griffiths, W. J., Analysis by liquid chromatography-mass spectrometry of sterols and oxysterols in brain of the newborn Dhcr7(Delta3-5/T93M) mouse: a model of Smith-Lemli-Opitz syndrome. *Biochem Pharmacol* **2013,** *86* (1), 43-55.

25. Xu, L.; Korade, Z.; Rosado, D. A., Jr.; Mirnics, K.; Porter, N. A., Metabolism of oxysterols derived from nonenzymatic oxidation of 7-dehydrocholesterol in cells. *J Lipid Res* **2013,** *54* (4), 1135-43.

26. Liu, W.; Xu, L.; Lamberson, C. R.; Merkens, L. S.; Steiner, R. D.; Elias, E. R.; Haas, D.; Porter, N. A., Assays of plasma dehydrocholesteryl esters and oxysterols from Smith-Lemli-Opitz syndrome patients. *J Lipid Res* **2013,** *54* (1), 244-53.

27. Shinkyo, R.; Xu, L.; Tallman, K. A.; Cheng, Q.; Porter, N. A.; Guengerich, F. P., Conversion of 7-dehydrocholesterol to 7-ketocholesterol is catalyzed by human cytochrome P450 7A1 and occurs by direct oxidation without an epoxide intermediate. *J Biol Chem* **2011,** *286* (38), 33021-8.

28. Feigin, A. M., Selective modification of sterol composition of hepatomas: new opportunities for chemotherapy. *Med Hypotheses* **1999,** *52* (5), 383-8.

29. Szlasa, W.; Zendran, I.; Zalesinska, A.; Tarek, M.; Kulbacka, J., Lipid composition of the cancer cell membrane. *J Bioenerg Biomembr* **2020,** *52* (5), 321-342.

30. Martin, L. A.; Kennedy, B. E.; Karten, B., Mitochondrial cholesterol: mechanisms of import and effects on mitochondrial function. *J Bioenerg Biomembr* **2016,** *48* (2), 137-51.

31. Korade, Z.; Xu, L.; Shelton, R.; Porter, N. A., Biological activities of 7-dehydrocholesterol-derived oxysterols: implications for Smith-Lemli-Opitz syndrome. *J Lipid Res* **2010,** *51* (11), 3259-3269.

32. Ayala, A.; Muñoz, M. F.; Argüelles, S., Lipid peroxidation: production, metabolism, and signaling mechanisms of malondialdehyde and 4-hydroxy-2-nonenal. *Oxid Med Cell Longev* **2014,** *2014*, 360438-360438.

33. Sun, F.; Ju, C.; Chen, J.; Liu, S.; Liu, N.; Wang, K.; Liu, C., Nanoparticles based on hydrophobic alginate derivative as nutraceutical delivery vehicle: vitamin D3 loading. *Artif Cells Blood Substit Immobil Biotechnol* **2012,** *40* (1-2), 113-9.

34. Acharya, S.; Sahoo, S. K., PLGA nanoparticles containing various anticancer agents and tumour delivery by EPR effect. *Advanced drug delivery reviews* **2011,** *63* (3), 170-83.

35. Wei, J.; Wang, H.; Zhu, M.; Ding, D.; Li, D.; Yin, Z.; Wang, L.; Yang, Z., Janus nanogels of PEGylated Taxol and PLGA-PEG-PLGA copolymer for cancer therapy. *Nanoscale* **2013,** *5* (20), 9902-7.

36. Locatelli, E.; Comes Franchini, M., Biodegradable PLGA-b-PEG polymeric nanoparticles: synthesis, properties, and nanomedical applications as drug delivery system. *Journal of Nanoparticle Research* **2012,** *14* (12), 1316.

37. Prabhu, A. V.; Luu, W.; Sharpe, L. J.; Brown, A. J., Cholesterol-mediated Degradation of 7-Dehydrocholesterol Reductase Switches the Balance from Cholesterol to Vitamin D Synthesis. *J Biol Chem* **2016,** *291* (16), 8363-8373.

38. Center, M. M.; Jemal, A.; Ward, E., International Trends in Colorectal Cancer Incidence Rates. *Cancer Epidemiology Biomarkers & Prevention* **2009,** *18* (6), 1688-1694.

39. Bentzen, S. M., Preventing or reducing late side effects of radiation therapy: radiobiology meets molecular pathology. *Nature Reviews Cancer* **2006,** *6* (9), 702-713.

40. Martin, L. A.; Kennedy, B. E.; Karten, B., Mitochondrial cholesterol: mechanisms of import and effects on mitochondrial function. *Journal of Bioenergetics and Biomembranes* **2016,** *48* (2), 137-151.

41. Kane, M. S.; Paris, A.; Codron, P.; Cassereau, J.; Procaccio, V.; Lenaers, G.; Reynier, P.; Chevrollier, A., Current mechanistic insights into the CCCP-induced cell survival response. *Biochem Pharmacol* **2018,** *148*, 100-110.

42. de Graaf, A. O.; van den Heuvel, L. P.; Dijkman, H. B.; de Abreu, R. A.; Birkenkamp, K. U.; de Witte, T.; van der Reijden, B. A.; Smeitink, J. A.; Jansen, J. H., Bcl-2 prevents loss of mitochondria in CCCP-induced apoptosis. *Exp Cell Res* **2004,** *299* (2), 533-40.

43. Zorova, L. D.; Popkov, V. A.; Plotnikov, E. Y.; Silachev, D. N.; Pevzner, I. B.; Jankauskas, S. S.; Babenko, V. A.; Zorov, S. D.; Balakireva, A. V.; Juhaszova, M.; Sollott, S. J.; Zorov, D. B., Mitochondrial membrane potential. *Anal Biochem* **2018,** *552*, 50-59.

44. Campos, C. B.; Paim, B. A.; Cosso, R. G.; Castilho, R. F.; Rottenberg, H.; Vercesi, A. E., Method for monitoring of mitochondrial cytochrome c release during cell death: Immunodetection of cytochrome c by flow cytometry after selective permeabilization of the plasma membrane. *Cytometry A* **2006,** *69* (6), 515-23.

45. Xie, Z.; Baba, S. P.; Sweeney, B. R.; Barski, O. A., Detoxification of aldehydes by histidine-containing dipeptides: From chemistry to clinical implications. *Chemico-Biological Interactions* **2013,** *202* (1), 288-297.

Chapter 3:

1. Wardman, P., Chemical radiosensitizers for use in radiotherapy. *Clin Oncol (R Coll Radiol)* **2007,** *19* (6), 397-417.

2. Wang, H.; Jiang, H.; Van De Gucht, M.; De Ridder, M., Hypoxic Radioresistance: Can ROS Be the Key to Overcome It? *Cancers (Basel)* **2019,** *11* (1), 112.

3. Gao, S.; Zhang, W.; Wang, R.; Hopkins, S. P.; Spagnoli, J. C.; Racin, M.; Bai, L.; Li, L.; Jiang, W.; Yang, X.; Lee, C.; Nagata, K.; Howerth, E. W.; Handa, H.; Xie, J.; Ma, Q.; Kumar, A., Nanoparticles Encapsulating Nitrosylated Maytansine To Enhance Radiation Therapy. *ACS Nano* **2020,** *14* (2), 1468-1481.

4. Smith, E. A.; Frankenburg, E. P.; Goldstein, S. A.; Koshizuka, K.; Elstner, E.; Said, J.; Kubota, T.; Uskokovic, M.; Koeffler, H. P., Effects of long-term administration of vitamin D3 analogs to mice. *Journal of Endocrinology* **2000,** *165* (1), 163-172.

5. Thul, P. J.; Åkesson, L.; Wiking, M.; Mahdessian, D.; Geladaki, A.; Ait Blal, H.; Alm, T.; Asplund, A.; Björk, L.; Breckels, L. M.; Bäckström, A.; Danielsson, F.; Fagerberg, L.; Fall, J.; Gatto, L.; Gnann, C.; Hober, S.; Hjelmare, M.; Johansson, F.; Lee, S.; Lindskog, C.; Mulder, J.; Mulvey, C. M.; Nilsson, P.; Oksvold, P.; Rockberg, J.; Schutten, R.; Schwenk, J. M.; Sivertsson, Å.; Sjöstedt, E.; Skogs, M.; Stadler, C.; Sullivan, D. P.; Tegel, H.; Winsnes, C.; Zhang, C.; Zwahlen, M.; Mardinoglu, A.; Pontén, F.; von Feilitzen, K.; Lilley, K. S.; Uhlén, M.; Lundberg, E., A subcellular map of the human proteome. *Science* **2017,** *356* (6340), eaal3321.

Chapter 4:

1. Matsumura, Y.; Maeda, H., A new concept for macromolecular therapeutics in cancer chemotherapy: mechanism of tumoritropic accumulation of proteins and the antitumor agent smancs. *Cancer Res* **1986,** *46* (12 Pt 1), 6387-92.

2. Yoshikawa, T.; Mori, Y.; Feng, H.; Phan, K. Q.; Kishimura, A.; Kang, J. H.; Mori, T.; Katayama, Y., Rapid and continuous accumulation of nitric oxide-releasing liposomes in tumors to augment the enhanced permeability and retention (EPR) effect. *Int J Pharm* **2019,** *565*, 481-487.

3. Maeda, H., Toward a full understanding of the EPR effect in primary and metastatic tumors as well as issues related to its heterogeneity. *Adv Drug Deliv Rev* **2015,** *91*, 3-6.

4. Araki, T.; Ogawara, K.; Suzuki, H.; Kawai, R.; Watanabe, T.; Ono, T.; Higaki, K., Augmented EPR effect by photo-triggered tumor vascular treatment improved therapeutic efficacy of liposomal paclitaxel in mice bearing tumors with low permeable vasculature. *J Control Release* **2015,** *200*, 106-14.

5. Stylianopoulos, T., EPR-effect: utilizing size-dependent nanoparticle delivery to solid tumors. *Ther Deliv* **2013,** *4* (4), 421-3.

6. Trédan, O.; Galmarini, C. M.; Patel, K.; Tannock, I. F., Drug resistance and the solid tumor microenvironment. *J Natl Cancer Inst* **2007,** *99* (19), 1441-54.

7. Abdalla, A. M. E.; Xiao, L.; Ullah, M. W.; Yu, M.; Ouyang, C.; Yang, G., Current Challenges of Cancer Anti-angiogenic Therapy and the Promise of Nanotherapeutics. *Theranostics* **2018,** *8* (2), 533-548.

8. Shi, Y.; van der Meel, R.; Chen, X.; Lammers, T., The EPR effect and beyond: Strategies to improve tumor targeting and cancer nanomedicine treatment efficacy. *Theranostics* **2020,** *10* (17), 7921-7924.

9. Matsumura, Y., Cancer stromal targeting therapy to overcome the pitfall of EPR effect. *Adv Drug Deliv Rev* **2020,** *154-155*, 142-150.

10. Fang, J.; Islam, W.; Maeda, H., Exploiting the dynamics of the EPR effect and strategies to improve the therapeutic effects of nanomedicines by using EPR effect enhancers. *Adv Drug Deliv Rev* **2020,** *157*, 142-160.

11. Wong, A. D.; Ye, M.; Ulmschneider, M. B.; Searson, P. C., Quantitative Analysis of the Enhanced Permeation and Retention (EPR) Effect. *PLoS One* **2015,** *10* (5), e0123461-e0123461.

12. Park, K., The beginning of the end of the nanomedicine hype. *J Control Release* **2019,** *305*, 221-222.

13. Lammers, T., Macro-nanomedicine: Targeting the big picture. *J Control Release* **2019,** *294*, 372-375.

14. Wilhelm, S.; Tavares, A. J.; Dai, Q.; Ohta, S.; Audet, J.; Dvorak, H. F.; Chan, W. C. W., Analysis of nanoparticle delivery to tumours. *Nature Reviews Materials* **2016,** *1* (5), 16014.

15. Sindhwani, S.; Syed, A. M.; Ngai, J.; Kingston, B. R.; Maiorino, L.; Rothschild, J.; MacMillan, P.; Zhang, Y.; Rajesh, N. U.; Hoang, T.; Wu, J. L. Y.; Wilhelm, S.; Zilman, A.; Gadde, S.; Sulaiman, A.; Ouyang, B.; Lin, Z.; Wang, L.; Egeblad, M.; Chan, W. C. W., The entry of nanoparticles into solid tumours. *Nat Mater* **2020,** *19* (5), 566-575.

16. Harrington, K. J.; Mohammadtaghi, S.; Uster, P. S.; Glass, D.; Peters, A. M.; Vile, R. G.; Stewart, J. S., Effective targeting of solid tumors in patients with locally advanced cancers by radiolabeled pegylated liposomes. *Clin Cancer Res* **2001,** *7* (2), 243-54.

17. Sacks, F. M.; Lichtenstein, A. H.; Wu, J. H. Y.; Appel, L. J.; Creager, M. A.; Kris-Etherton, P. M.; Miller, M.; Rimm, E. B.; Rudel, L. L.; Robinson, J. G.; Stone, N. J.; Van Horn, L. V., Dietary Fats and Cardiovascular Disease: A Presidential Advisory From the American Heart Association. *Circulation* **2017,** *136* (3), e1-e23.

18. Karney, A.; Brągoszewska, H.; Soluch, L.; Ołtarzewski, M., [Risk factors for atherosclerosis in obese children aged 6-12 years]. *Dev Period Med* **2017,** *21* (3), 259-265.

19. Silvente-Poirot, S.; Poirot, M., Cholesterol metabolism and cancer: the good, the bad and the ugly. *Curr Opin Pharmacol* **2012,** *12* (6), 673-6.

20. Nikanjam, M.; Blakely, E. A.; Bjornstad, K. A.; Shu, X.; Budinger, T. F.; Forte, T. M., Synthetic nano-low density lipoprotein as targeted drug delivery vehicle for glioblastoma multiforme. *International Journal of Pharmaceutics* **2007,** *328* (1), 86-94.

21. Nikanjam, M.; Gibbs, A. R.; Hunt, C. A.; Budinger, T. F.; Forte, T. M., Synthetic nano-LDL with paclitaxel oleate as a targeted drug delivery vehicle for glioblastoma multiforme. *Journal of Controlled Release* **2007,** *124* (3), 163-171.

22. Baillie, G.; Owens, M. D.; Halbert, G. W., A synthetic low density lipoprotein particle capable of supporting U937 proliferation in vitro. *Journal of Lipid Research* **2002,** *43* (1), 69-73.

APPENDICES

A Supporting information for Chapter 2

Materials and Methods

7-DHC@PLGA-PEG nanoparticle Synthesis

7-DHC@PLGA-PEG nanoparticles (7-DHC@PLGA NPs) were synthesized by a nanoprecipitation method following previously published protocols. Briefly, 1.5 mg of 7-DHC and 5 mg of PLGA-*b*-PEG-OH were dissolved in 1 mL CH_3CN, and the solution added to 10 mL of Mil-Q-H_2O. The reaction was stirred at room temperature for 2 hours to facilitate the evaporation of the acetonitrile, and the resulting solution was purified by multiple rounds of centrifugation at 2,800 RPM for 10 minutes. The final product was stored in PBS at 4ºC for further experiments and storage for up to 1 week.

Physicochemical Characterization of 7-DHC@PLGA NPs

Transmission electron microscopy (TEM) was carried out on a FEI TECNAI 20 transmission electron microscope at 200 kV. The zeta potential and size distribution measurements were carried out on a Malvern Zetasizer Nano ZS system (Zeta potential -13.9mV, DLS 90.0 nm). 7-DHC loading and release studies were carried out using the absorption of 7-DHC at 282 nm on a BioTek Synergy MX multi-mode microplate reader. The absorbance of 7-DHC was subtracted from the water background that of the PLGA polymer at 260 nm to account for any potential overlap in absorbance readings. The corrected absorbance was then compared to an experimentally generated standard curve to extrapolate the drug loading and encapsulation efficiency of 7-DHC within the polymer NP.

LC/MS Analysis for Oxysterol Generation

Samples were generated by mixing solutions of 10 mg/mL 7-DHC, or 5 mg/mL DHCEO in 5 mL solvent containing 4 mL CH_3CN+1 mL Mil-Q-H_2O (or 1 mL H_2O_2). Samples were treated with either PBS or 5 Gy IR followed by incubation for 24 h. Samples were then subjected to LC/MS analysis. The liquid chromatography was performed on an Applied Biosystems 140 B solvent delivery system using water with 0.1% formic acid as solvent A and acetonitrile as solvent B. The linear solvent gradient was from 70% B to 95% B over 20 minutes at a flow rate of 50 µl/min. The column used was a Thermo Hypersil-Keystone 1 x 150 mm Biobasic-4 column with 5 µm particle size and 300A pore size. The effluent was directed into a Bruker Daltonics Esquire 3000 plus ion trap mass spectrometer equipped with an atmospheric pressure chemical ionization (APCI) source. The instrument was scanned in enhanced mode from 340 - 500 m/z with the capillary at 4 KV. The dry as temperature was held at 300 degrees C at a flow rate of 4 l/min nitrogen. The nebulizer was at 15 PSI of nitrogen. The vaporizer temperature was held at 380 degrees C. The obtained chromatogram and subsequent mass spectra were analyzed for the elution time of DHCEO and other oxysterols, as well as the key M/Z mass signatures for DHCEO.

Physical stability of 7-DHC@PLGA NPs (7-DHC release)

The 7-DHC@PLGA NPs were incubated in 2 mL PBS at different pH values (pH=5.5, 6.5, and 7.2) to test the stability of the nanoparticle and the drug release. The samples were kept in an incubating shaker at 37 °C in a 10k MWCO dialysis tube. At each time point (0, 0.25, 0.5, 1, 2, 4, 8, 12 and 24, 48 hours), aliquots of the samples were collected and centrifuged using a micro filter unit (MWCO: 10k; Amicon® Cat# UFC800308). The solution's absorbance was analyzed using

BioTek Synergy MX multi-mode microplate reader, and once again compared to an experimentally generated standard curve to determine the amount of free 7-DHC in the lower portion of the dialysis tube. This absorbance corresponded to the quantity of drug released from the nanoparticle at the given time point.

Cell culture

CT26, a murine colorectal carcinoma cell line, was cultured following the protocol provided by the ATCC. A complete growth medium was prepared by adding 50 mL fetal bovine serum (FBS; Atlanta Biologicals, Cat#S11150) and 5 mL penicillin-streptomycin (Corning Cat# 30-002-CI) to 450 mL of RPMI 1640 medium (Corning, Cat# 10-104-CV). The cells were sub-cultured every three days and stored in a Thermo Scientific Heracell 150i incubator at 37 °C and 5% CO_2. A day before the experiment, the cells were washed with PBS and collected by trypsinization (37 °C, 2 min) followed by neutralization with cell culture medium and centrifugation (1200 rpm, 5 min). The supernatant was removed, and cells were dispersed in new cell culture medium. Then, the cell density was counted using a hemocytometer (Hausser Scientific, Cat# 3200) to seed the desired number of cells on the experimental plate(s).

Reactive Oxygen Species Generation

Specific Reactive Oxygen Species: Superoxide (O_2^-) generation was tested using a Dihydroethidium assay kit (DHE, ThermoFisher™, Cat# D11347). Briefly, 7-DHC@PLGA NPs at a concentration of 5 µg/mL and 5 µM DHE were prepared in cell culture medium. 100 µL of 7-DHC@PLGA NP solution and 100 µL of sensor solution were added to a black 96-well-plate (Corning Costar, Cat# 3614). The initial fluorescence was measured using a microplate reader

(Synergy Mx, BioTeK) at excitation and emission wavelengths of 518/605 nm/nm respectively. Subsequently, the wells containing 7-DHC@PLGA NPs were irradiated with 5 Gy using a 50 kV X-ray generator and the fluorescence was measured again. The fluorescence was then compared to the initial fluorescence reading to evaluate the superoxide radical generation.

Cell uptake study (Lysosome and Mitochondria targeting) using fluorescence imaging

The 7-DHC@PLGA NP colocalization in the lysosome and mitochondria were tested using LysoTracker™ Green DND-26 (ThermoFisher, Cat# L7526) and MitoTracker™ Green FM (ThermoFisher, Cat# M7514), respectively. Briefly, 1×10^5 CT26 cells were seeded on a 2-chamber glass slide (Nunc™ Lab-Tek™ II Chamber Slide™ System, ThermoFisher) and incubated for 24 h. Then 7-DHC@PLGA-Cy5 were added to the cells and incubated for an additional 24 h at 37 °C. After the cells were washed with PBS 3 times, 90 nM LysoTracker or 148 nM MitoTracker was added to stain the lysosome or the mitochondria for 60 min or 4 h, respectively. The cells were fixed with 4% paraformaldehyde, and cell nuclei were stained with DAPI. The fluorescence image was taken using a Zess LSM 710 Confocal Microscope with 40x magnification for lysosome imaging, and 20x for mitochondrial imaging.

Cytotoxicity

The cell viability was studied with CT26 cells using the standard MTT assays. Briefly, CT26 cells (10,000 cells per well) were seeded on clear 96-well plates (Corning Costar, Cat#3599). When the cells adhered to the bottom, 0 – 100 μg/mL of 7-DHC@PLGA NPs were added to the cells and incubated for 24 h. 20 μL of 10 mg/mL 3-(4,5-Dimethylthiazolyl-2)-2,5-diphenyltetrazolium bromide (MTT) solution was added into each well. After 4 h incubation at 37°C and 5% CO_2, the

solution was discarded from each well, and 100 µL of DMSO was added to each well resulting in purple suspensions. The absorbance at 570 nm was measured using a BioTek Synergy MX multi-mode microplate reader.

Intracellular ATP

CT26 cells at density of 10,000 cells (100 µL) per well were plated in white 96-well plates (Corning Costar, Cat# 3610) and incubated at 37 °C for 24 h. Then, 100 µL of particle solutions prepared in cell culture medium, 7-DHC@PLGA (5 µg/mL), 7-DHC@PLGA NPs+IR (5 µg/mL), IR alone, or PBS were added to the cells and incubated for another 24 h followed by 5 Gy irradiation in the IR respective groups. The IR groups were then incubated at 37 °C for 30 minutes, followed by incubation at room temperature for 30 minutes. Subsequently, the supernatant from each well was removed completely. Then, 100 uL ATPLite (PerkinElmer Cat# 016943) solution was added following the manufacturers protocol. The plate was then shaken in the dark for 10 minutes, and the luminescence was read using a microplate reader (Synergy Mx, BioTeK). The result was compared to the standard curve prepared according to the manufacture's protocol.

Mitochondrial electric membrane potential ($\Delta\Psi_m$)

The change of mitochondrial membrane potential was measured by a JC-1 mitochondrial membrane potential detection kit (Biotium, Cat# 30001). The JC-1 working solution was prepared by adding 10 µL of the concentrated dye to 1 mL of FBS free RPMI medium. 200 µL of cell culture medium containing Carbonyl Cyanide Chlorophenylhydrazone, (CCCP, positive control), DMSO (negative control), free 7-DHC (5 or 20 µg/mL) or 7-DHC@PLGA NPs (5 or 20 µg/mL) was incubated with cells for 4 h, then irradiated with 5 Gy. The medium was removed and replaced

with the JC-1 working solution to incubate for another 15 min. The fluorescence signal from the stained cells were detected using microplate reader (Synergy Mx, BioTeK; Green: ex/em 510/527 nm; Red: ex/em 585/590nm). Then, the green to red fluorescence ratios were calculated to evaluate mitochondrial membrane depolarization.

Cytochrome c release

Cytochrome *c* release induced by 7-DHC@PLGA NPs was tested using ApoTrack™ Cytochrome *c* Apoptosis ICC Antibody Kit (Abcam, Cat# ab110417). On the first day, 1×10^5 CT26 cells were seeded in a 2-well chamber glass slide (Nunc™ Lab-Tek™ II Chamber Slide™ System, ThermoFisher, Cat# 154461PK). The cells were incubated with PBS or 7-DHC@PLGA NPs (5μg/mL) for 4 h. Then, the cells were irradiated with 5 Gy and incubated for 24 h. Then, ApoTrack™ Cytochrome c Apoptosis ICC Antibody was added following manufacture's protocol. Confocal images were taken at 40× magnification on a Zeiss LSM 710 Confocal Microscope to evaluate the fluorescence colocalization. The percent colocalization of the red and green fluorescent signals was subsequently quantified using ImageJ.

Caspase 3 activity

CT26 cells were seeded in a black 96-well-plate (Corning Costar, Cat# 3614) at a cell density of 8,000 cells per well and incubated overnight. Then the cells were incubated with PBS, IR alone, 7-DHC@PLGA alone (5 μg/mL) or 7-DHC@PLGA NPs (5 μg/mL) for 4 h followed by 5 Gy irradiation. The cells were incubated another 24 h, and the Caspase 3 activity was evaluated using FAM-FLICA® Caspase-3/7 kit (Immunochemistry, Cat# 94) following the manufacturer's protocol. Briefly, the medium was replaced with 96.7 μL of cell culture medium and 3.3 μL of

FAM-FLICA working solution. After 1 h of incubation at 37 °C, FAM-FLICA working solution containing cell culture medium was replaced with 1× Apoptosis Wash Buffer three times to remove any unbound FAM-FLICA. Then, the wash buffer was replaced with 100 μL PBS. The caspase 3 activity was evaluated by measuring the fluorescence (ex/em 488nm/530nm) using a microplate reader (Synergy Mx, BioTeK).

Superoxide Dismutase (SOD) assay

CT26 cells at a density of 1.5×10^5 cells per dish were seeded in a 6 well cell culture plate (Corning, Cat# 3516) and incubated at 37 °C overnight. The cell culture medium was removed, and the cells were incubated for another 24 h with 1.5 mL of cell culture medium containing PBS, 7-DHC@PLGA NPs (5 μg/mL), or IR only, or 7-DHC@PLGA NPs NPs+IR (5 μg/mL). Then, each IR group was irradiated with 5 Gy and incubated for an additional 1 h. The cells were washed with PBS 3 times and collected using a cell scraper followed by centrifugation (1200 rpm, 5 min). Next, the cells were dispersed in 1 mL PBS and lysed using a probe sonicator in an ice bath (30% amplitude, 5 min, 10 seconds on 10 seconds off). The supernatant was collected by centrifugation (1500 x g, 5 min) and analyzed using the Superoxide Dismutase Assay Kit (Cayman Chemical, Cat# 706002) following the manufacture's protocol. The absorbance at 450 nm was obtained using a microplate reader (Synergy Mx, BioTeK).

Lipid peroxidation Assay

Image-iT Lipid Peroxidation Kit (Abcam, Cat# ab118970) was used to test lipid damage. Cells were seeded in a black 96-well-plate (Corning Costar, Cat# 3614, 8000 cells per well) and stored in an incubator overnight. Then, the cell culture medium was refreshed with 200 μL culture

medium containing either 7-DHC@PLGA NPs (5 μg/mL,), PBS (30 μg/mL), or 7-DHC@PLGA NPs+IR (5 μg/mL) and incubated at 37 °C. After 24 h, excess particles were removed, and fresh medium was added. The cells were irradiated by X-ray (5 Gy), and incubated for another 24 h. The cell culture medium was removed and 200 μL of image-iT Lipid peroxidation sensor (30 μM) dispersed in cell culture medium was added to the cells. After incubation for 30 minutes at 37 °C, the medium was removed, and the cells were washed with PBS three times. The fluorescence at two separate wavelengths (ex/em at 581/591 nm and ex/em at 488/510 nm) were read using a microplate reader (Synergy Mx, BioTeK). The ratio of the emission fluorescence intensities at 590 nm to 510 nm was evaluated to analyze lipid peroxidation in cells.

TBARS Assay

TBARS Assay Kit (Cayman Chemical, Cat# 100009055) was used to test for the production of MDA. Cells were seeded 100 mm cell culture dishes (Corning, Cat# 353003, 10^6 cells per dish) and stored in an incubator overnight. Then, the cell culture medium was refreshed with 10 mL culture medium containing either 7-DHC@PLGA NPs (5 μg/mL,), PBS, or 7-DHC@PLGA NPs+IR (5 μg/mL) and incubated at 37 °C. After 24 h, excess particles were removed, and fresh medium was added. The cells were irradiated by X-ray (5 Gy), and incubated for another 24 h. The cells were then collected using a cell scraper, and each treatment group was suspended in 1 mL PBS. The cells were then lysed on ice using a probe sonicator. (30% amplitude, 5 min, 10 seconds on 10 seconds off). The assay was then performed following the manufacturers protocol. Briefly, 100 μl of either the sample or the standard was added to a 15 mL centrifuge tube. 100 μl SDS solution was added to each tube, as well as 4 mL of the provided color reagent. All tubes were then boiled for 1 h, then placed in an ice bath to stop the reaction. Each sample was then

centrifuged at 4ºC for 10 minutes at 1600 x g. Each sample or standard was then loaded onto a clear 96-well plate (Corning, Cat#3599) in triplicate and the absorbance at 530 nm was read using a microplate reader (Synergy Mx, BioTeK). The absorbance readings for each experimental group were then averaged and compared to an experimentally generated standard curve, and the MDA concentrations were determined.

γH2AX Assay

The DNA damage was studied using anti-γH2AX (Alexa 647) antibody (Millipore Sigma, Cat# 07-164-AF647). CT26 Cells ($1x10^6$) were seeded in a 4-chamber glass slide (Nunc™ Lab-Tek™ II Chamber Slide™ System, ThermoFisher) and incubated overnight. Then, the cell culture medium was refreshed with 1.5 mL medium with 7-DHC@PLGA NPs (5 μg/mL), PBS, or 7-DHC@PLGA NPs+IR (5 μg/mL). After 4 h of incubation, X-ray radiation at 5 Gy was delivered to the IR only, and 7-DHC@PLGA NP+IR groups, and cells were incubated for another 1 h at 37 °C. The cells were collected, fixed, permeabilized, and stained with anti-γH2AX antibody according to the protocol from the manufacturer. The presence of γH2AX protein was analyzed using a Zeiss LSM 710 Confocal Microscope and analyzed by ImageJ to evaluate and quantify the red fluorescence and the foci number for each group.

Clonogenic Assay

To evaluate the therapeutic effect of 7-DHC@PLGA, a clonogenic assay was performed. Briefly, $1×10^6$ CT26 cells in 1.5 mL cell culture medium were seeded in a 35 mm cell culture dish (Corning, Cat# 430165) and stored in a 37 ºC incubator overnight. Then, the cell culture medium was refreshed with 7-DHC@PLGA NPs at 12.5 μg/mL or PBS for 24 h. Then, the cells were collected

and 100-10,000 cells were seeded on a 100 mm cell culture plate (Corning, Cat# 353003) in triplicate. The cells were irradiated with the corresponding dose using a 300 kV X-ray generator and cultured for 14 days. The colonies were stained with crystal violet, counted, and a survival fraction was evaluated by the linear quadratic (LQ) model: $S = e^{-(\alpha D + \beta D^2)}$.

Statistical analysis

The means and standard errors were calculated from at least three repeated groups in all the experiments. Statistical significance between groups was determined with the Student's t test where $P < 0.05$ was considered to be statistically significant between two groups. *P < 0.05; **P < 0.01; ***P < 0.001; ****P <0.0001; ns, no significant difference.

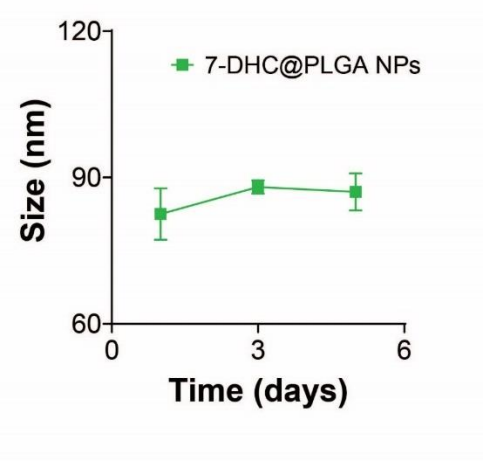

Figure S2.1. DLS over 5 d in PBS showing little size change in 7-DHC@PLGA NPs. Minimal size change represents good stability over the 5 d study.

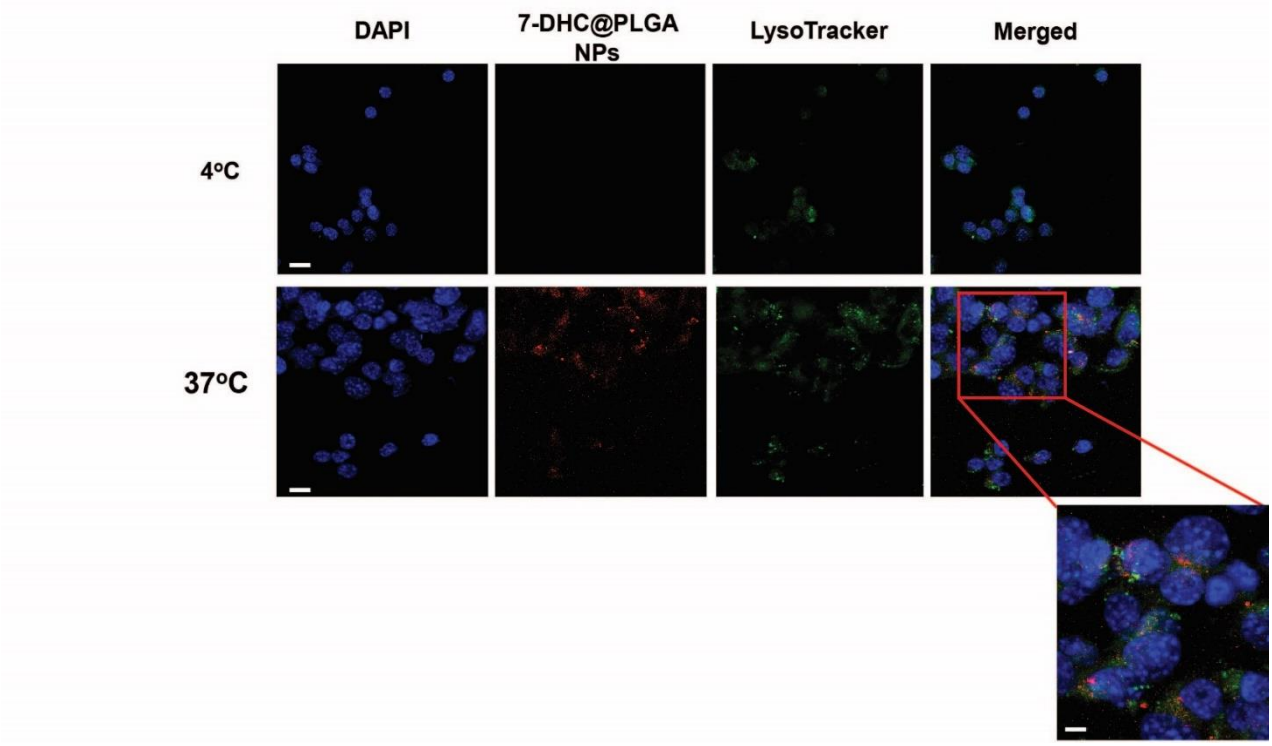

Figure S2.2. Cellular internalization of 7-DHC@PLGA NPs. Confocal scanning laser microscope images demonstrating that 7-DHC@PLGA NPs are internalized via endocytosis within 1 h incubation at 37°C (lower panel). The NPs were labeled with Cy5, whose fluorescent signal overlays well with the lysotracker dye (inset image). Endocytosis is inhibited at 4°C (top panel), indicating that endocytosis does in fact occur at 37°C. Scale bar, 20 μm

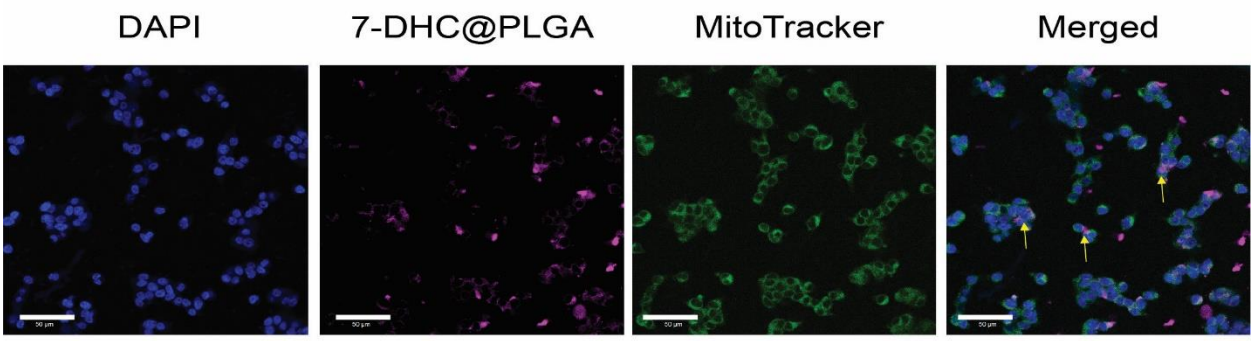

Figure S2.3. Mitochondrial accumulation of 7-DHC@PLGA NPs. Confocal scanning laser microscope images demonstrating that 7-DHC@PLGA NPs can accumulate within the

mitochondria at 4 h incubation at 37°C. The NPs were labeled with Cy5, whose fluorescent signal overlays well with the MitoTracker dye (Yellow arrows). Scale bar, 50 µm

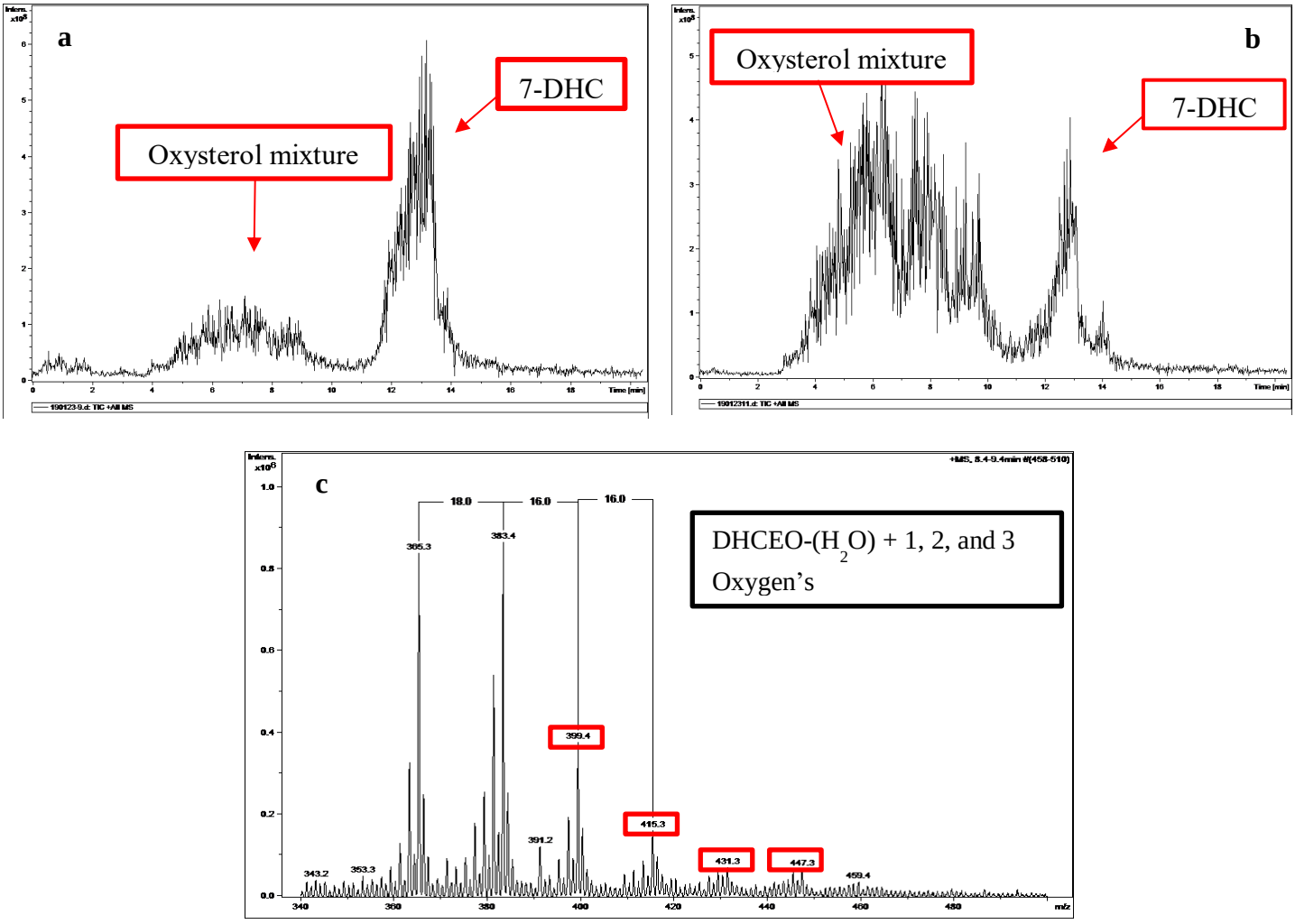

Figure S2.4. LC/MS data in solution. (a) solution of 7-DHC oxidized in the presence of 5 Gy irradiation. (b) solution of 7-DHC oxidized in the presence of H_2O_2. (c) mass spectrum indicating key M/Z peaks for DHCEO (dehydrated DHCEO, M/Z = 399.4, DHCEO + 1, 2, or 3 Oxygen's, M/Z = 416.3, 431.3, or 447.3, respectively).

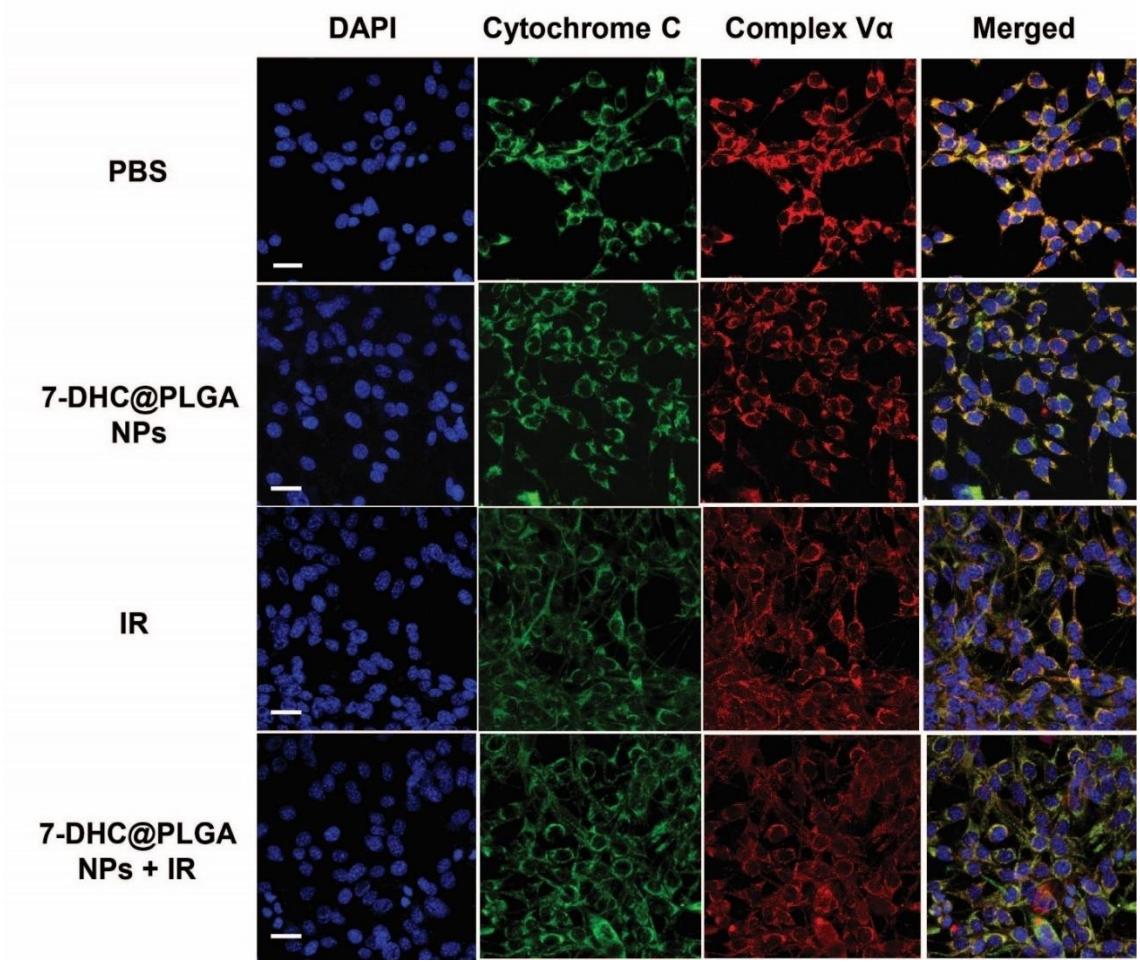

Figure S2.5. Cytochrome C release from complex Vα of the mitochondria in CT26 cells. Confocal scanning laser microscope images demonstrating that 7-DHC@PLGA NPs +IR cause a significant decrease in the colocalization of the green and red fluorescent signals compared to IR alone. Cytochrome C that is still localized within the mitochondria shows a yellow-orange fluorescent signal in the merged images. Released Cytochrome C shows more bright green signals in the merged images as seen in 7-DHC@PLGA + IR treated cells. Scale bar, 20 μm

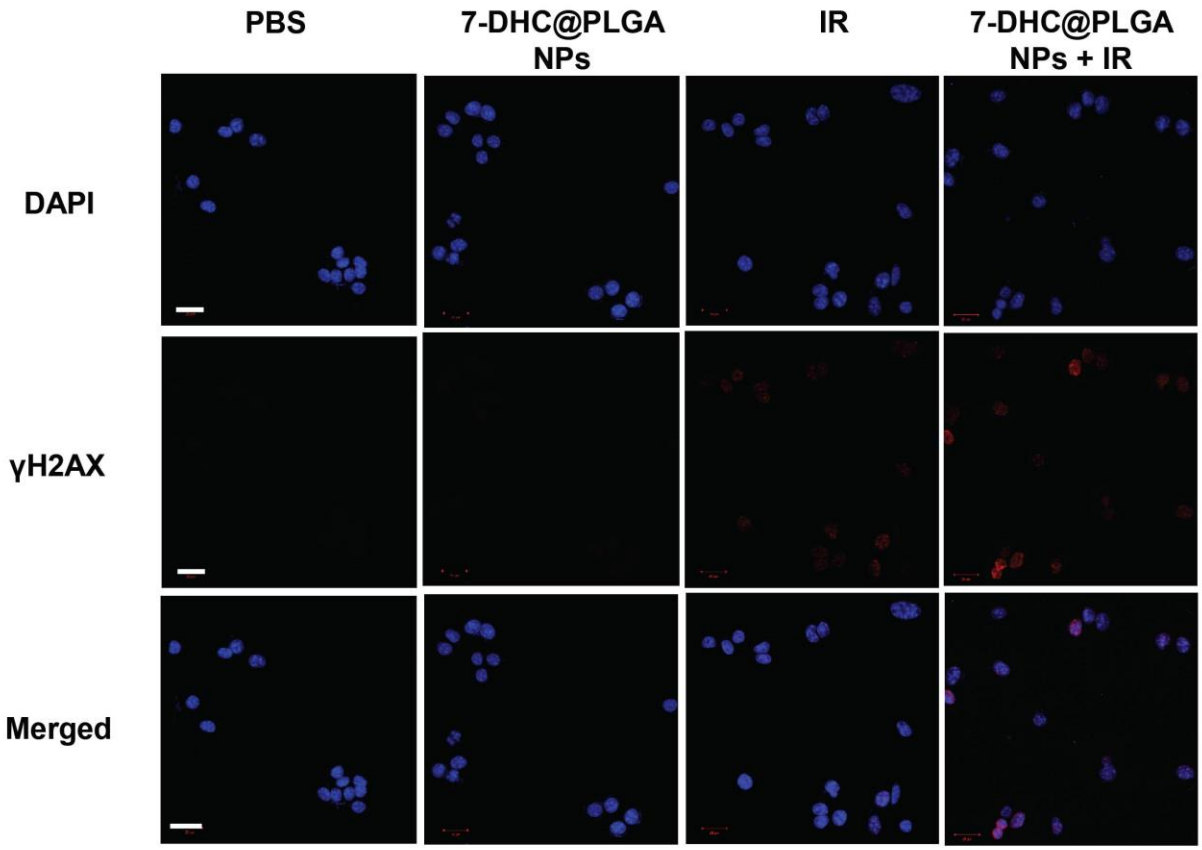

Figure S2.6. Confocal scanning laser microscope images showing DNA double strand breaks (DSBs). DSBs were probed using a fluorescent antibody for γH2AX, (anti-γH2AX, AF-647). Compared to IR alone, CT26 cells treated with 7-DHC@PLGA + IR caused a drastic increase in the red fluorescent foci. Each focus represents a DNA DSB. Scale bar, 20 μm.

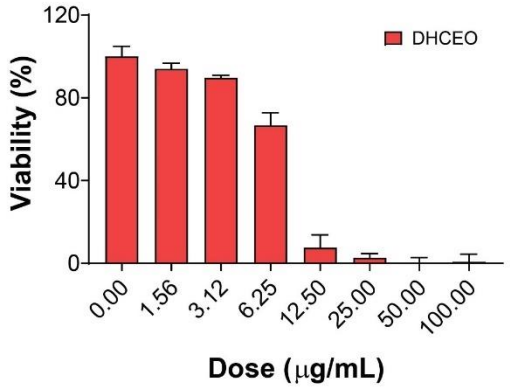

Figure S2.7. MTT assay showing toxicity associated with 3β,5α-dihydroxycholest-7-en-6-one (DHCEO). IC_{50} value, 7.54 μg/mL.

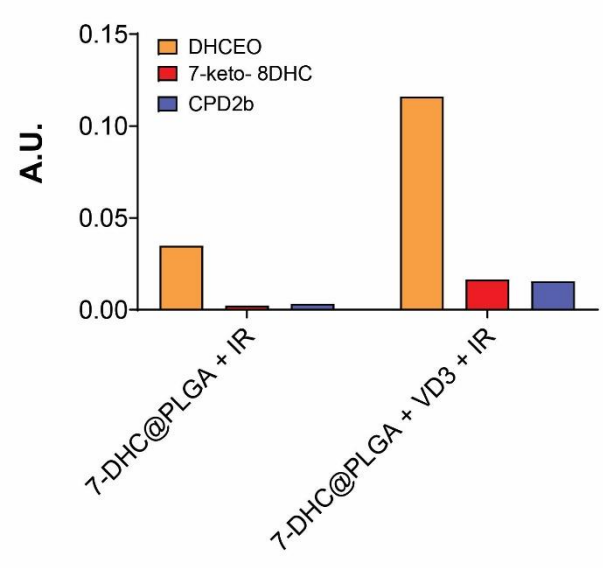

Figure S2.8. Preliminary *in vitro* oxysterol generation. The production of DHCEO as well as 7-keto-8-DHC and Cpd2B following irradiation of 7-DHC@PLGA NPs with and without vitamin D_3 (VD3) is observed. VD3 blocks the DHCR7 enzyme, thereby allowing more 7-DHC to be oxidized to oxysterols.

B Supporting information for Chapter 3

Materials and Methods

Small animal models

For therapy as well as associated toxicity studies, a CT26 subcutaneous mouse model was used. The animal model was established by subcutaneously inoculating 1 million CT26 cells onto the right hind leg of 4 week old female balb/c mice (Charles River). All the animal studied were performed according to a protocol approved by the Institutional Animal Care and Use Committee (IACUC) of University of Georgia.

In vivo radiation therapy

An *in vivo* therapy study was performed using 20 4-week old female Balb/c mice purchased from Charles River. The mice were cared for by following the Animal Use Protocol (AUP). The tumor model was developed by subcutaneous injection of 2×10^6 CT26 cells into the right flank of each animal. When the tumor size reached 100 mm^3, the mice were randomly divided into four groups (PBS, PBS+RT, and 7-DHC@PLGA NPs, 7-DHC@PLGA NPs+RT). The materials (10 mg/kg, 125 μL) were delivered by tail vein injection, and the tumors were irradiated with 5 Gy at 4 h after the injection, with the remainder of the body shielded by lead. The therapy was delivered every 48 h, for a total of 3 doses. The tumor size was measured every 2 days with calipers, and the tumor volume was calculated using the equation: $Tumor\ volume = \frac{tumor\ length\ x\ tumor\ width^2}{2}$ where tumor length ≥ tumor width. The mice were sacrificed when they reached a humane end point, including either length or width was > 1.7 cm, the weight loss was more than 20%, or any tumor

discharge was observed. The tumors and major organs such as liver, heart, lung, kidney, and spleen were collected for histological analysis using hematoxylin and eosin (H&E) staining. The tumors were also stained for Ki67, as well as using a TUNEL assay kit (Abcam, Cat# ab206386) to evaluate apoptotic cell death. Each stained tissue was examined under a digital microscope, and the most representative areas were captured and compared to see the difference between the groups.

Hematology and blood chemistry

In a separate experiment, three Balb/c mice were intravenously injected with PBS or 7-DHC@PLGA NPs (5 mg/kg). Blood samples were collected using a cardiac puncture blood collection method. 250 μL of each of the blood samples were tested for a complete blood count to evaluate the total number of each type of blood cell. Remaining blood samples were used to evaluate liver function using the Alanine Aminotransferase (ALT) kit (Abcam, Cat# ab105134).

Statistical analysis

The means and standard errors were calculated from at least three repeated groups in all the experiments. Statistical significance between groups was determined with the Student's t test where $P < 0.05$ was considered to be statistically significant between two groups. *$P < 0.05$; **$P < 0.01$; ***$P < 0.001$; ****$P < 0.0001$; ns, no significant difference.

C Supporting information for Chapter 4

sLDL nanoparticle synthesis

The synthetic low density lipoprotein nanoparticles (sLDL NPs) were synthesized by a thin film hydration method following previously published protocols with modifications. Briefly, a 3:2:1 molar ratio of phosphatidyl choline (PC), triolein (TO) and 7-DHC were dissolved in 10 mL solvent (2:1 v/v $CHCl_3$:CH_3OH). The solvent was evaporated at elevated temperature on a Buchi RII rotary evaporator, and the resulting lipid film was rehydrated at T > 41ºC in 0.01 mM Tris buffer, pH = 8 and allowed to stir for 1 h. Following hydration, the resultant NPs were subsequently extruded by multiple passes through an Avanti Lipid Extruder using a 0.01 μm polycarbonate filter. The resultant lipids were centrifuged at 10,000 RPM for 1 h, resuspended in fresh Tris buffer, and sonicated in a Branson M2800H bath sonicator for 30 minutes. The final product can be freeze dried by lyophilization, and stored at -20ºC for further experiments for up to 1 week.

Physicochemical characterizations of sLDL nanoparticles

Transmission electron microscopy (TEM) was carried out on a FEI TECNAI 20 transmission electron microscope at 200 kV. The zeta potential and size distribution measurements were carried out on a Malvern Zetasizer Nano ZS system (Zeta potential -48.9mV, DLS 106.0 nm). 7-DHC loading and release studies were carried out using the absorption of 7-DHC at 282 nm on a BioTek Synergy MX multi-mode microplate reader. The corrected absorbance was then compared to an

experimentally generated standard curve to extrapolate the drug loading and encapsulation efficiency of 7-DHC within the polymer NP.